UMinho|2012

Clarisse Marta de Oliveira Ribeiro

Processing and characterization of piezoelectric polymers for tissue engineering applications

---

Universidade do Minho
Escola de Ciências

Clarisse Marta de Oliveira Ribeiro

Processing and characterization of piezoelectric polymers for tissue engineering applications

Setembro de 2012

Universidade do Minho
Escola de Ciências

Clarisse Marta de Oliveira Ribeiro

Processing and characterization of piezoelectric polymers for tissue engineering applications

Tese de Doutoramento
Doutoramento em Ciências
Especialidade de Física

Trabalho realizado sob orientação do
Professor Doutor Senentxu Lanceros-Méndez
e do
Professor Doutor José Luis Gómez-Ribelles

Setembro de 2012

DECLARAÇÃO

Nome

Clarisse Marta de Oliveira Ribeiro

Endereço electrónico:cribeiro@fisica.uminho.pt

Número do Bilhete de Identidade: 13314172

Título dissertação ? /tese ?

Processing and characterization of piezoelectric polymers for tissue engineering applications

Orientador(es): Senentxu Lanceros-Méndez e José Luis Gómez-Ribelles

Ano de conclusão: 2012

Designação do Mestrado ou do Ramo de Conhecimento do Doutoramento: Física

DE ACORDO COM A LEGISLAÇÃO EM VIGOR, NÃO É PERMITIDA A REPRODUÇÃO DE QUALQUER PARTE DESTA TESE/TRABALHO

Universidade do Minho, 04/09/2012

Assinatura: ____

Acknowledgements

Last words to be written...

During the journey of my PhD, several people helped me and made this achievement possible. So, I cannot conclude this relevant step of my life without expressing my most sincere gratitude to all those that direct or indirectly have contributed for the development of this work throughout all these years and that helped me to grow as a researcher.

My first acknowledgments are made to my supervisor Prof. Senentxu for give me the opportunity to being a part of a fantastic research group; the scientific expertise, ideas and shared knowledge; the availability and generosity that revealed throughout these years. Thanks for the transmitted knowledge and friendship.

To my co-supervisor, José Luis Gómez Ribelles, for receiving me in his group, for their ideas and scientific knowledge provided and for his friendship during this step.

I could not avoid mentioning my colleagues/friends of Electroactive Materials group for help me along this journey, for their dynamic and friendly spirit. In particular, to Vítor Sencadas for his valuable help along this work; to Carlos Costa for his help in DSC and FTIR techniques used in this work; to Vanessa and Anabela for their support and friendship.

To all colleagues and researchers at the Centro de Biomateriales e Ingeniería Tisular (CBIT) and Laboratório de Microscopia Electrónica da UPV, I would thank the reception, help and friendliness during my stays.

I would like to thank the CEB/IBB of Minho University, for providing me excellent working facilities and possibilities to develop this work. To Susana for her valuable help along the last stage of this work and for her friendship.

I also acknowledge the INL - International Iberian Nanotechnology Laboratory for my scholarship grant. I would to acknowledge to all my co-authors for the contribution to the papers included in this thesis.

I also would like to thank to my closest friends, you know who you are!

I would thanks Luis for his friendship and help.

A very special thanks to my parents for everything you have done for me, what they do and for what I know they will do in the future, whenever I need. Thanks for your advices, support, friendship and love. This thesis would not exist without you.

To my sisters, Sylvie and Melanie, who deserve special mention, for their friendship and for the feeling of unconditional love. They are very important in my life!!!

At last but not the least, to my dear Pedro. Thank you for being who you are. Thank you for your patience, dedication, sense of humor and for your unconditional love. Love you!

I dedicate this work to

Pedro, Sylvie, Melanie and My parents,

I am thankful for their love.

Abstract

In the last decades, the biomaterials and tissue engineering interdisciplinary research fields have been two of the most dynamic ones and have attracted increasing attention by the scientific community. With the advancements in the tissue engineering field the necessity of study and develop a wide variety of biomaterials with different properties has emerged. Among the different types of materials, polymers have proved to be an excellent choice, due to their simple processing, flexibility, physical properties and due to be easy to get in different shapes. In particular, piezoelectric polymers have attracted interest since they respond to electrical and mechanical solicitations, allowing to actively stimulating tissues. Further, interesting for tissue engineering are the polymer structures in the form of micro and nanofibers.

In this work, the processing and characterization of two piezoelectric polymers, poly(L-lactic acid) (PLLA) and poly(vinylidene fluoride) (PVDF), aiming tissue engineering applications was achieved. Processing was achieved both in the form of films and fibers. PLLA and PVDF electrospun fibers morphology was controlled by changing process parameters such as applied voltage, feed rate and collector system. Regarding PVDF fibers, the processing parameters allows to change the β-phase fraction between 50% and 85% and fiber diameter from a few hundreds of nanometers to micrometers. Concerning PLLA fibers, the crystallinity was tailored between 0%, i.e. amorphous fibers, and 50%, by annealing treatment. The PLLA fibers diameter was further reduced by the introduction of poly(ethylene oxide) (PEO) polymer. In this way, electrospun membranes were prepared with tailored fiber diameter from some micrometers for pure PLLA membranes to few hundreds of nanometers by electrospinning of PLLA-PEO solution.

PLLA degradation was also studied and it was observed that the samples degradation in phosphate buffer solution (PBS) up to 20 weeks produces only a slight decrease in the sample weight. The local properties of the PLLA and PVDF individual electrospun fibers were studied by piezoelectric force microscopy (PFM) and the piezoelectric response for both polymers have been proved.

Additionally, the biological response of PLLA and PVDF membranes was also addressed.

In the case of PLLA electrospun membranes, human chondrocytes were used and it was found that proliferation of human chondrocytes cultured in the monolayer substrates is not different on aligned or non-aligned amorphous mats. However, the differentiation rate seems to be higher on the non-aligned amorphous mats. Furthermore, the crystallization of the aligned mats showed nearly suppressed proliferation and the cells had produced higher amounts of aggrecan, characteristic of the extracellular matrix of hyaline cartilage.

In relation to the PVDF, the biological response to the polarization state was studied in films. The effect of polarization on fibronectin conformation, cell adhesion and proliferation has been studied. It was observed that polarization of a PVDF modifies the conformation of adsorbed fibronectin on the material surface and therefore cell adhesion on the fibronectin-coated substrates. As a consequence, a higher number of cells on the substrate were observed in poled than in non-poled samples. These results open the possibility of developing active substrates for cell culture and tissue engineering.

Further investigations on the piezoelectric effect on cell response were performed by evaluating osteoblast growth in poled and non-poled PVDF (non-coated and coated with thin titanium layer to get a more homogeneous charge distribution) under static and dynamic conditions. The polarization and titanium layer modifies the mean roughness of PVDF films surface and therefore also modifies cell adhesion and proliferation on the samples, also, the positively charge of β-PVDF promotes higher adhesion and proliferation on osteoblast.

Finally, dynamic culture with MC3T3-E1 cells showed higher cell proliferation on "poled +" β-PVDF. Thus, results reported in this thesis have demonstrated that varying surface electrical charge (when a mechanical solicitation is applied) influences cell response and confirms the interest of electroactive polymers in cell culture and tissue engineering applications.

Resumo

Nas últimas décadas, os biomateriais e a engenharia de tecidos têm sido dos campos interdisciplinares mais dinâmicos e que têm atraído cada vez mais atenção por parte da comunidade científica. Com os avanços realizados em engenharia de tecidos, surgiu a necessidade de estudar e desenvolver uma ampla variedade de biomateriais com diferentes propriedades. Entre os diferentes tipos de materiais, os polímeros têm provado serem uma excelente escolha devido às suas várias vantagens tais como o seu simples processamento, flexibilidade, propriedades físicas e serem facilmente obtidos em diferentes formas. Em particular, os polímeros piezoelétricos têm atraído cada vez mais interesse uma vez que conseguem responder a solicitações elétricas e mecânicas, permitindo assim o estímulo ativo dos tecidos. Além disso, as estruturas poliméricas na forma de micro e nanofibras mostraram ser interessantes para engenharia de tecidos.

Neste trabalho, o processamento e a caracterização de dois polímeros piezoelétricos, o poli(L-ácido láctico) (PLLA) e o poli(fluoreto de vinilideno) (PVDF), foram realizados com o objetivo de serem utilizados para aplicações de engenharia de tecidos. O processamento foi realizado sob a forma de filmes e fibras. A morfologia das fibras de PVDF e PLLA foi controlada pela variação dos parâmetros de processamento tais como a tensão aplicada, o fluxo e o coletor. Em relação às fibras de PVDF, os parâmetros do processamento mostraram influenciar a fração de fase β entre 50% e 85% e o diâmetro das fibras desde algumas centenas de nanómetros até micrómetros. Em relação às fibras de PLLA, a cristalinidade pode ser alterada de 0%, isto é, fibras amorfas, até 50%, através de um tratamento térmico. O diâmetro das fibras de PLLA pode ainda ser reduzido através da introdução do polímero poli(óxido de etileno) (PEO). Desta forma, as membranas foram preparadas por electrospinning através de uma solução de PLLA-PEO com diâmetros de fibras desde micrómetros até algumas centenas de nanómetros.

A degradação do PLLA também foi estudada e verificou-se que a degradação até 20 semanas das amostras numa solução tampão de fosfato (PBS - *phosphate buffer solution*) produz uma ligeira diminuição de peso na amostra. As propriedades locais das fibras individuais de PLLA e PVDF foram estudadas por microscopia de força piezoelétrica (PFM) e a resposta piezoelétrica para ambos os polímeros foi verificada.

Além disso, a resposta biológica das membranas de PLLA e PVDF foi também investigada.

No caso das membranas de PLLA, os condrócitos humanos foram utilizados e verificou-se que a sua proliferação, aquando cultivados nos substratos de monocamada, é igual tanto para as membranas amorfas de fibras alinhadas como para as não-alinhadas. No entanto, a taxa de diferenciação parece ser maior nos substratos amorfos de fibras não-alinhadas. Além disso, a cristalização dos substratos amorfos de fibras alinhadas demonstraram uma supressão da proliferação, sendo que as células produziram elevadas quantidades de agrecano, característica da matriz extracelular da cartilagem hialina.

Em relação ao PVDF, a resposta biológica relativamente ao estado de polarização foi estudada em filmes. O efeito da polarização na conformação da fibronectina, adesão e proliferação celular foi estudado. Verificou-se que a polarização do PVDF tem influência na conformação da fibronectina adsorvida na superfície do material e, por conseguinte, na adesão de células em substratos revestidos com fibronectina. Como consequência, foi observado um maior número de células nos substratos polarizados relativamente aos não-polarizados. Estes resultados abrem a possibilidade de desenvolver substratos ativos para cultivo celular e para engenharia de tecidos.

Outras investigações sobre o efeito piezoelétrico na resposta celular foram realizadas sob condições estáticas e dinâmicas, através da avaliação do crescimento de osteoblastos em filmes de PVDF polarizados e não-polarizados (não revestidos e revestidos com uma camada fina de titânio para obter uma distribuição mais homogénea de carga). Além disso, verificou-se que a camada de polarização e de titânio modificam a rugosidade média da superfície dos filmes de PVDF e, portanto, também modificam a adesão e proliferação celular. Observou-se ainda que a carga positiva dos filmes β-PVDF promove uma maior adesão e proliferação de osteoblastos.

Finalmente, um estudo dinâmico realizado com as células MC3T3-E1 mostrou uma maior proliferação celular nos filmes β-PVDF com polarização positiva. Assim, os resultados observados neste trabalho demonstraram que a variação da carga elétrica na superfície (quando é aplicada uma solicitação mecânica) influencia a resposta celular e confirma o interesse dos polímeros eletroativos para cultivos celulares e aplicações em engenharia de tecidos.

Table of contents

1. Introduction 1

1.1 Tissue engineering 3

1.1.1 Biomaterials for tissue engineering applications 4

1.1.2 Design and development of membranes and scaffolds 5

1.2 Electroactive materials 8

1.2.1 Conducting polymers 9

1.2.2 Piezoelectric polymers 10

1.3 Objectives 11

1.4 Structure and methodology 12

1.5 References 14

2. Tailoring the morphology and crystallinity of poly(L-lactide acid) electrospun membranes 21

2.1 Introduction 23

2.2 Experimental 24

2.3 Results and discussion 25

2.3.1 Processing parameters 25

2.3.2 Fibrils orientation using a rotating collector 28

2.3.3 Isothermal crystallization of electrospun mats 29

2.3.4 Phase content 34

2.4 Conclusions 38

2.5 References 39

3. Fabrication of poly(lactic acid)-poly(ethylene oxide) electrospun membranes with controlled micro to nanofiber sizes.. 43

3.1 Introduction.. 45

3.2 Experimental.. 47

3.3 Results and discussion 49

3.3.1 Scanning electron microscopy.. 49

3.3.2 Thermal behavior.. 55

3.3.3 Infrared spectra 58

3.3.4 Hydrolytic degradation 59

3.4 Conclusions... 61

3.5 References... 63

4. Local piezoelectric activity of single poly(L- lactic acid) microfibers............. 67

4.1 Introduction.. 69

4.2 Experimental.. 71

4.3 Results.. 72

4.4 Conclusions... 75

4.5 References... 76

5. Influence of crystallinity on hydrophobicity and biological response of poly(L-lactide) electrospun mats.. 79

5.1 Introduction.. 81

5.2 Materials and methods 83

5.2.1 Preparation of PLLA electrospun membranes 83

5.2.2 Contact angle measurements 84

5.2.3 Substrate topography measurements 84

5.2.4 Cell culture 84

5.2.5 Cell morphology ... 85

5.2.6 Cell viability and proliferation ... 85

5.2.7 Cell differentiation ... 86

5.2.8 Statistical analysis ... 87

5.3 Results ... 87

5.3.1 Contact angle measurements ... 87

5.3.2 Substrate topography measurements ... 88

5.3.3 Cell attachment and cell morphology ... 89

5.3.4 Cell viability and proliferation ... 91

5.3.5 Cell differentiation ... 92

5.4 Discussion ... 94

5.5 Conclusions ... 98

5.6 References ... 99

6. Influence of processing conditions on polymorphism and nanofiber morphology of electroactive poly(vinylidene fluoride) electrospun membranes.. 105

6.1 Introduction ... 107

6.2 Experimental ... 108

6.3 Results and discussion ... 110

6.3.1 Influence of applied voltage ... 110

6.3.2 Influence of flow rate and needle diameter ... 115

6.3.3 Fibrils orientation using a rotating collector ... 118

6.3.4 Local piezoelectric response of a single PVDF electrospun fiber ... 120

6.4 Conclusions ... 121

6.5 References ... 123

7. Fibronectin adsorption and cell response on electroactive poly(vinylidene fluoride) films 127

7.1 Introduction 129

7.2 Materials and methods 130

7.2.1 Preparation of polymer films 130

7.2.2 Contact angle measurements 131

7.2.3 Fibronectin adsorption 131

7.2.4 Cell adhesion and overall morphology 132

7.2.5 Cell viability and proliferation 133

7.2.6 Statistical analysis 134

7.3 Results 135

7.3.1 Contact angle measurements 135

7.3.2 Surface topography 135

7.3.3 Protein adsorption 137

7.3.4 Cell attachment and cell proliferation 140

7.4 Discussion 142

7.5 Conclusions 145

7.6 References 146

8. Enhanced viability of pre-osteoblastic cells by dynamic piezoelectric stimulation 149

8.1 Introduction 151

8.2 Materials and methods 152

8.2.1 Preparation of PVDF samples 152

8.2.2 Substrate topography and contact angle measurements 153

8.2.3 Cell culture 154

8.2.4 Cell viability and proliferation 154

8.2.5 Statistical analysis 155
8.3 Results 155
8.3.1 Surface topography 155
8.3.2 Contact angle measurements 156
8.3.3 Cell viability and proliferation 157
8.4 Discussion 160
8.5 Conclusions 162
8.6 References 163

9. Conclusions and future work 167
9.1 Conclusions 169
9.2 Future work 171

List of figures

1. **Introduction**

Figure 1.1 – General process of tissue engineering. It involves seed cells on scaffold, culturing *in vitro* and implant into the patient [10]. 4
Figure 1.2 – Basic experimental electrospinning setup [34]. 7
Figure 1.3 – SEM images of PLA nanofibers produced by electrospinning: a) aligned and b) non-aligned fibers (magnification of 2000X).. 7

2. **Tailoring the morphology and crystallinity of poly(L-lactide acid) electrospun membranes**

Figure 2.1 – SEM images of PLLA mats electrospun at a traveling distance of 15 cm, a needle diameter of 0.50 mm, a flow rate of 4 $mL.h^{-1}$ and an applied voltage of a) 12 kV, b) 15 kV, c) 20 kV and d) 25 kV. The scale bar corresponds to 20 µm......................... 26
Figure 2.2 – SEM image of PLLA electrospun mats obtained at a traveling distance of 15 cm, needle diameter of 0.50 mm, applied voltage of 20 kV and a flow rate of a) 1 $mL.h^{-1}$, b) 2 $mL.h^{-1}$, c) 4 $mL.h^{-1}$ and d) 8 $mL.h^{-1}$. The scale bar corresponds to 20 µm. 27
Figure 2.3 – SEM images of PLLA nanofibers electrospun obtained at a traveling distance of 15 cm, a needle diameter of 0.50 mm, an applied voltage of 20 kV, a flow rate of 4 $mL.h^{-1}$ and a rotation speed of a) 500 rpm, b) 750 rpm, c) 1000 rpm, and d) 1500 rpm. The scale bar corresponds to 20 µm.. 28
Figure 2.4 – DSC normalized thermograms of a PLLA sample electrospun at a traveling distance of 15 cm, a needle diameter of 0.50 mm, an applied voltage of 20 kV and a flow rate of 2 $mL.h^{-1}$. Scan 1 is the first heating scan, scan 2 was recorded after heating the sample to 65 ºC followed by cooling at 40 $ºC.min^{-1}$ to 20 ºC, and scan 3 was performed after cooling the sample at 10 $ºC.min^{-1}$ from 200 ºC to 20 ºC...................... 30
Figure 2.5 – Crystalline fraction of electrospun samples annealed at different temperatures. 32
Figure 2.6 – Melting peaks of a PLLA film (black line) and an electrospun mat annealed at 140 ºC for 48 h. 33
Figure 2.7 – SEM image of PLLA mats electrospun at a traveling distance of 15 cm, a needle diameter of 0.50 mm, an applied voltage of 20 kV and a flow rate of 2 $mL.h^{-1}$: a)

as-produced, b) crystallized at 70 ºC for 48 h, c) and d) crystallized at 140 ºC for 48 h. The scale bar corresponds to 5 µm in a)-c) and to 0.5 µm in d).................................... 34

Figure 2.8 – FTIR transmission spectra of PLLA electrospun scaffolds before and after annealing at the indicated temperatures for 48 h.. 35

Figure 2.9 – FTIR transmission spectra of PLLA electrospun scaffolds before and after annealing at the indicated temperatures for 48 h.. 37

Figure 2.10 – FTIR transmission spectra of PLLA electrospun scaffolds before and after annealing at 70 ºC for the indicated times.. 38

3. Fabrication of poly(lactic acid)-poly(ethylene oxide) electrospun membranes with controlled micro to nanofiber sizes

Figure 3.1 – Morphology of the PLLA-PEO membranes before PEO removal: a) SEM image of the sample with 50% of PLLA, b) Fiber distribution for the 50/50 PLLA-PEO membrane, c) SEM image of the sample with 75% of PLLA sample, d) Fiber distribution for the 75/25 PLLA-PEO scaffold. 51

Figure 3.2 – PLLA membrane obtained for the pure polymer by electrospinning at 20 kV with a 0.5 mm inner diameter needle placed at 15 cm from the collector............... 51

Figure 3.3 – Morphology of the PLLA-PEO scaffolds after PEO removal: a) SEM image of the sample with 50% of PLLA, b) Fiber distribution for the 50/50 PLLA-PEO membrane, c) SEM image of the membrane with 75% PLLA, d) Fiber distribution for the 75/25 PLLA-PEO membrane. 53

Figure 3.4 – AFM topographic surface images of the PLLA-PEO (50/50) sample: a) before PEO removal and b) after PEO removal in water for 24 h................................. 54

Figure 3.5 – a) TGA data for pure PLLA and PEO samples, as well as for the PLLA-PEO and b) DTG curves for the obtained scaffolds. 55

Figure 3.6 – Evolution of the T_{onset} for the PLLA-PEO blends. 56

Figure 3.7 – DSC normalized thermograms of: a) electrospun PLLA and blend samples and b) first heating scan of the pure PEO mesh. 57

Figure 3.8 – Detail of FTIR spectra in the 650-2000 cm^{-1} region for the pure PLLA and for the PLLA-PEO blend membranes. 59

Figure 3.9 – SEM micrographs for the PLLA membranes with 583 nm average diameter and 45% crystallinity after different *in-vitro* degradation time: a) 2 days, b) 14 days, c) 28 days and d) 140 days... 61

4. Local piezoelectric activity of single poly(L- lactic acid) microfibers

Figure 4.1 – Design of the experimental arrangement for the measurement of the electroactive response of a single PLLA fiber. 72

Figure 4.2 – a) 3D topography image; b) detailed 3D topography image; c) cross-section topography features of the fibers: roughness (above) and dimensions (below) of a single PLLA fiber. 73

Figure 4.3 – PLLA fiber surfaces poled at a) 100 V and b) 200 V; well defined poled regions are obtained of fully poled material and c) measured hysteresis loops recorded in locations shown by x in a) and b). 74

5. Influence of crystallinity on hydrophobicity and biological response of poly(L-lactide) electrospun mats

Figure 5.1 – Evaluation of water contact angle of PLLA membranes. Values are mean ± SD. No statistically significant difference in contact angle was found between non-oriented PLLA membrane with 50% of crystallinity and oriented PLLA membrane amorphous and also between oriented PLLA membrane with 8% and 27% of crystallinity. 87

Figure 5.2 – a) Micrograph of static contact angle of non-oriented PLLA amorphous and b) Micrograph of static contact angle of oriented PLLA amorphous. 88

Figure 5.3 – AFM images of one nanofiber morphology on a) non-oriented PLLA amorphous and b) non-oriented PLLA with 50% of crystallinity. 89

Figure 5.4 – Overall cell morphology of chondrocytes on PLLA membranes analyzed by SEM. a) amorphous non-oriented PLLA membrane for 14 days; b) non-oriented PLLA membrane with 27% of crystallinity for 7 days; c) oriented PLLA membrane with 27% of crystallinity for 7 days; d) amorphous oriented PLLA membrane for 14 days. The scale bar (50 µm) is valid for all the images. 90

Figure 5.5 – Confocal fluorescence microscopy images of chondrocyte cells after 21 days of cell culture in PLLA membranes. a) non-oriented PLLA membrane amorphous; b) oriented PLLA membrane amorphous. The scale bar (10 µm) is valid for all the images (green: cytoskeleton; blue: nucleus). 91

Figure 5.6 – MTT absorbance results after cells seeded for 0, 7, 14 and 28 days on different PLLA membranes. Values are mean ± SD. *Significantly different ($p<0.05$) PLLA samples. 92

Figure 5.7 – Fluorescence micrographs of live/dead of cell culture with chondrocyte cells during 21 days in PLLA membranes. a) Non-oriented amorphous PLLA membrane; b) oriented amorphous PLLA membrane. The scale bar (100 µm) is valid for all the images. 92

Figure 5.8 – Immunocytochemical visualization of type II collagen after 21 days of chondrocytes culture in amorphous non-oriented PLLA membrane.......... 93

Figure 5.9 – Human aggrecan production in supernatant after cells seeded for 7, 14 and 28 days on different PLLA membranes. Values are mean ± SD. No statistically significant difference in concentration was found among samples after 7 and 28 days. At 14 days, significant differences between PLLA non-oriented and oriented membranes were found. 93

6. Influence of processing conditions on polymorphism and nanofiber morphology of electroactive poly(vinylidene fluoride) electrospun membranes

Figure 6.1 – Experimental setup for the measurement of the local piezoelectric response of single PVDF electrospun fibers (the fiber in the figure is a real polymer fiber)...... 109

Figure 6.2 – SEM image of PVDF electrospun nanofibers obtained from a solution of 20/80 (20% PVDF + 80% DMF by w/w) at a traveling distance of 15cm, needle diameter of 0.25 mm and flow rate of 4 mL.h^{-1}, with an applied voltage of a) 15 kV, b) 20 kV, c) 25 kV and d) 30 kV. 111

Figure 6.3 – a) Detail of the FTIR spectra for the PVDF electrospun scaffolds obtained at different applied voltages (lines indicates the absorption bands characteristics of the α- and β-phase), b) Crystalline phase content of the polymeric membranes. 112

Figure 6.4 – a) DSC thermograms for the electrospun PVDF scaffolds processed at different applied voltages and b) crystallinity degree and melting peak temperature of the obtained electrospun mats. 114

Figure 6.5 – SEM image of PVDF electrospun nanofibers obtained from a solution of 20/80 (20% PVDF + 80%DMF by w/w) at a traveling distance of 15cm, needle diameter of 0.5 mm and voltage of 20 kV, with an increase of flow rate from 0,5 to 4 mL.h^{-1} (a) 0,5 mL.h^{-1}, b) 1 mL.h^{-1}, c) 2 mL.h^{-1}, d) 4 mL.h^{-1}). The scale bar corresponds to 10 µm.......... 116

Figure 6.6 – a) Detail of the FTIR spectra for the PVDF electrospun membranes obtained at different flow rates (lines indicates the absorption bands characteristics of the α- and β-phase), b) Crystalline phase content of the polymeric membranes. 116

Figure 6.7 – a) DSC thermograms for the electrospun PVDF membranes processed at different flow rate, b) Influence of the flow rate on the crystallinity degree and melting peak temperature of the electrospun membranes. 117

Figure 6.8 – SEM image of PVDF electrospun nanofibers obtained from a solution of 25/75 (25% PVDF + 75% DMF by w/w) at a traveling distance of 15 cm, needle diameter of 0.5 mm, voltage of 20 kV and flow rate of 4 mL.h^{-1}, with an increase of rotation from 750 to 2000 rpm: a) 750 rpm, b) 1000 rpm, c) 1500 rpm, d) 2000 rpm. 118

Figure 6.9 – a) Detail of the FTIR spectra for the PVDF electrospun membranes obtained at different rotations (lines indicates the absorption bands characteristics of α- and β-phase), b) Crystalline phase content of the polymeric membranes. 119

Figure 6.10 – a) DSC thermograms for the electrospun PVDF membranes processed at different rotations, b) Influence of the applied voltage in the crystallinity degree and melting peak temperature of the electrospun membranes. 120

Figure 6.11 – PFM images of the patterns obtained for the E = 20 V: a) t = 5 s, b) t = 20 s, c) electrical response of the fiber for the different time intervals of the applied electric field, d) poled area, e) domain area as a function of the applied time and f) domain length for the different time of the applied electrical field. 121

7. Fibronectin adsorption and cell response on electroactive poly(vinylidene fluoride) films

Figure 7.1 – Evaluation of water contact angle of different PVDF films (Alfa, Beta non-poled, poled + and poled -). 135

Figure 7.2 – AFM images recorded in a 1 x 1 μm area of: a) - b) α-PVDF and c) - d) non-poled β-PVDF surfaces. a) - c) Phase and b) - d) amplitude pictures. 136

Figure 7.3 – AFM images of non-poled β-PVDF with fibronectin adsorbed form a solution with a concentration of 2 μg.mL^{-1}. a) Height, b) phase and c) amplitude magnitudes respectively. 137

Figure 7.4 – Fibronectin distribution as observed by the amplitude magnitude in AFM on the different substrates (α–PVDF, β-PVDF non-poled, “poled +” β-PVDF and "poled –" β-PVDF). Fibronectin was adsorbed for 10 min from solutions of different concentrations (1µg.mL^{-1}, 2 µg.mL^{-1}, 5µg.mL^{-1}). 138

Figure 7.5 – Monoclonal antibody binding for HFN7.1 monoclonal antibody on the different PVDF samples after FN adsorption from a solution of concentration 5 µg.mL^{-1}. * Significantly different ($p<0.05$) PVDF samples. 139

Figure 7.6 – Cell culture with pre-osteoblast cells during 2 h in negative poled β-PVDF film (DAPI stained nuclei are shown in a), vinculin expression in b) and F-actin staining in c), overlay d)) For comparison the overlay images of α-PVDF film and control glass are shown in e) and f) respectively. The scale bar (100µm) is valid for all the images. 140

Figure 7.7 – MTS absorbance results after cells seeded for 3 and 7 days on different PVDF films and control substrate. * Significantly different ($p<0.05$) PVDF samples. 141

Figure 7.8 – Cell density after for 3 and 7 days on different PVDF films and control substrate. * Significantly different ($p<0.05$) PVDF samples. 142

8. Enhanced viability of pre-osteoblastic cells by dynamic piezoelectric stimulation

Figure 8.1 – Home-made bioreactor system used for dynamic cell culture at 1 Hz: a) schematic system and b) system photography. 154

Figure 8.2 – AFM pictures recorded in a 5×5 µm area of different PVDF sample: a) non-poled; b) non-poled with titanium; c) poled + and d) poled + with titanium. 156

Figure 8.3 – Contact angle of the different PVDF films. Values are mean ± SD. 157

Figure 8.4 – LIVE/DEAD staining of MC-3T3-E1 osteoblasts a) PVDF non-poled and b) PVDF non-poled with titanium; c) PVDF poled + and d) PVDF poled + with titanium after cell culture for 3 days. The scale bar (50 µm) is valid for all the images. 158

Figure 8.5 – MTT results from proliferation assays of MC-3T3 osteoblast seeded on different PVDF samples and on the control surface under static and dynamic conditions after a) 1 day, b) 3 days and c) 5 days. * $p\leq0{,}05$ vs Glass control under static conditions; $^{\#}$ $p\leq0{,}05$ vs PVDF non-poled under static conditions; $^{\delta}$ $p\leq0{,}05$ vs PVDF non-poled under dynamic conditions. 159

List of tables

1. Introduction

Table 1.1 – Classification of electroactive polymers [53]. 9

2. Tailoring the morphology and crystallinity of poly(L-lactide acid) electrospun membranes

Table 2.1 – Literature review of the relevant infrared bands associated with different phases of PLLA. 36

3. Fabrication of poly(lactic acid)-poly(ethylene oxide) electrospun membranes with controlled micro to nanofiber sizes

Table 3.1 – Porosity of the PLLA-PEO samples for different PEO contents before and after PEO removal. 54
Table 3.2 – Evolution of average fiber diameter and porosity for the samples after 20 weeks hydrolytic degradation. 60

5. Influence of crystallinity on hydrophobicity and biological response of poly(L-lactide) electrospun mats

Table 5.1 – Specification of the PLLA samples. 83

List of symbols

∅ – Diameter

ΔC_p – Heat capacity

ΔH_{cc} – Cold-crystallization enthalpy

ΔH_m – Melting enthalpy

ΔX_c – Degree of crystallinity

Abs – Absorbance

*d*33 – Piezoelectric response

Sa – Average absolute distance from average flat surface

Sq – Root mean square from average flat surface

T_{cc} – Cold-crystallization temperature

T_g – Glass transition temperature

T_m – Melting temperature

wt.% – Weight percentage

List of abbreviations

A

AFM – Atomic force microscopy

AGG – Aggrecan

ANOVA – Analysis of variance

ATR – Attenuated total reflection

C

CG – Cationized gelatin

D

DMEM – Dulbecoo's modified eagle's medium

DMF – N,N-dimethylformamide

DMSO – Dimethyl sulfoxide

DPBS – Dulbecco's phosphate buffered saline

DSC – Differential scanning calorimetry

E

EAP – Electroactive polymer

ECM – Extra-cellular matrix

ELISA – Enzyme-linked immunosorbent assay

F

FBS – Fetal bovine serum

FDA – U.S. food and drug administration

FN – Fibronectin

FTIR – Fourier transform infrared

G

GPC – Gel permeation chromatography

I

ITS – Insulin, Transferin and Selenium

M

MC – Dichloromethane

MTS – (3-(4,5-dymethylthiazol-2-yl)-5-(3-carboxymethoxyphenyl)-2(4-sulfopheny)-2H tetrazolium)

MTT – (3-(4,5-Dimethylthiazol-2-yl)-2,5-diphenyltetrazolium bromide

MUP – Methylumbelliferyl phosphate

P

P/S – Penicillin/Streptomycin

PANI – Polyaniline

PBS – Phosphate Buffer Solution

PCL – Polycaprolactone

PDLA – Poly(D-lactic acid)

PDLLA – Poly(D,L-lactic acid)

PDMS – Polydimethylsiloxane

PEDOT – Poly(3,4-ethylenedioxythiophene)

PEG – Poly(ethylene glycol)

PEO – Poly(ethylene oxide)

PFM – Piezoresponse Force Microscopy

PGA – Poly(glycolic acid)

PLA – Poly(lactic acid)

PLGA – Poly(lactic-co-glycolic acid)

PLLA – Poly(L-lactic acid)

PPy – Polypyrrole

PT – Polythiophenes

PVDF – Poly(vinylidene fluoride)

PVDF-TrFE – Poly[(vinylidenefluoride-co-trifluoroethylene]

S

SEM – Scanning Electron Microscopy

T

TCPS – Tissue Culture Polystyrene

TGA – Thermogravimetric Analysis

TGFβ1 – Transforming Growth Factor Beta 1

W

WCA – Water Contact Angle

1. Introduction

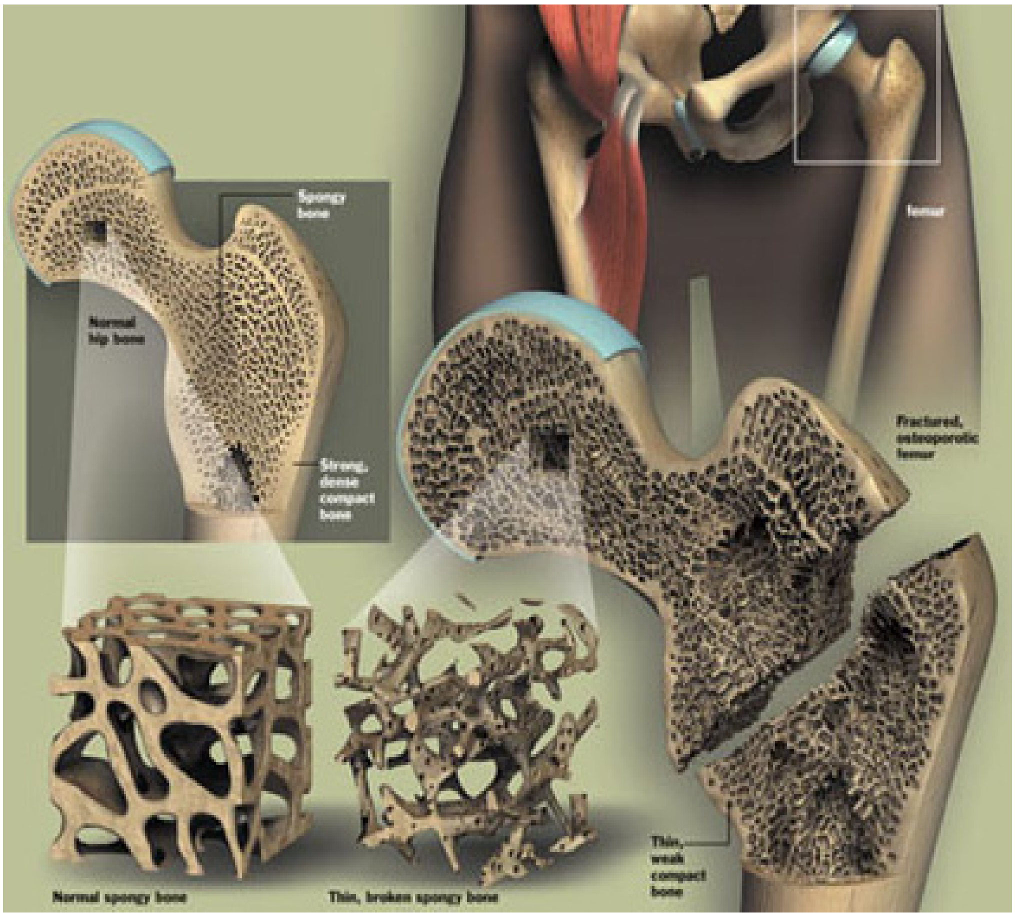
Spongy bone
Normal hip bone
Strong, dense compact bone
femur
Fractured, osteoporotic femur
Normal spongy bone
Thin, broken spongy bone
Thin, weak compact bone

1.1 Tissue engineering

The failure of organ function due to injury, disease or aging accounts for a significant number of clinical disorders with a large social and economic cost [1]. To overcome these limitations in organ transplantation and grafting, the field of tissue engineering emerged about two decades ago.

The tissue engineering definition has evolved over the last few years. Tissue engineering was initially defined, in 1988, by attendees of the first National Science Foundation sponsored meeting as the ‘‘application of the principles and methods of engineering and life sciences toward fundamental understanding of structure-function relationship in normal and pathological mammalian tissues and the development of biological substitutes for the repair or regeneration of tissue or organ function’’ [2]. Thereafter, Langer and Vacanti [3] defined tissue engineering as a multidisciplinary field that integrates principles of engineering and life sciences to develop biological substitutes that restore, maintain or improve tissue function. Such engineering field involves multidisciplinary knowledge that merges principles and innovations from engineering, biology, life sciences, biotechnology and, in recent years, micro- and nano-science and technology [4-6].

In order to achieve tissue regeneration, typically, three approaches have been investigated singularly or in combination: biocompatible scaffolds, cell-based therapies and tissue-inducing factors (figure 1.1). Thus, one of the basic strategies of the tissue engineering is the construction of a biocompatible scaffold, which can be combined with cells and bioreactor technologies in the design and fabrication of neo-tissues/organs [7-9].

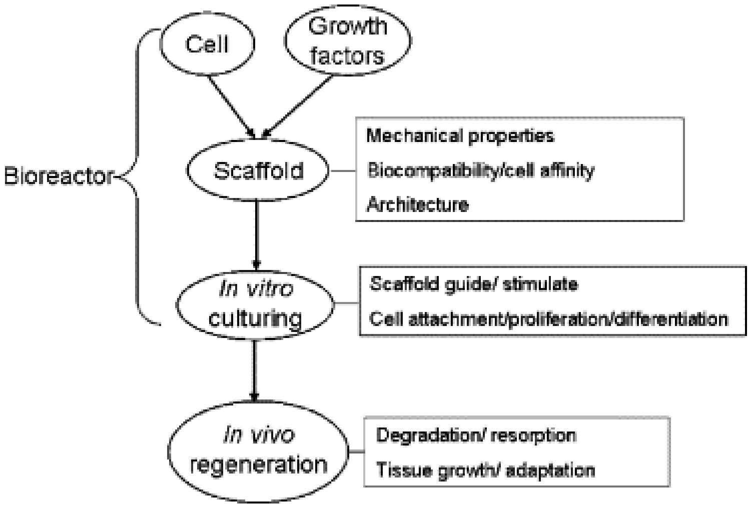
Cell
Growth factors
Bioreactor
Scaffold
Mechanical properties
Biocompatibility/cell affinity
Architecture
In vitro culturing
Scaffold guide/ stimulate
Cell attachment/proliferation/differentiation
In vivo regeneration
Degradation/ resorption
Tissue growth/ adaptation

Figure 1.1 – General process of tissue engineering. It involves seed cells on scaffold, culturing *in vitro* and implant into the patient [10].

One of the most sensitive steps with respect to the tissue engineering process consists on the choice of biomaterials with the desired features to be used as scaffolds.

1.1.1 Biomaterials for tissue engineering applications

In the last decades, a wide variety of biomaterials with different properties have been studied and developed for biomedical applications, in particular for tissue engineering. So, the first concern regarding the tissue engineering process is the choice of suitable material.

The basic requirements for biomaterials to be used as scaffolds are their biocompatibility and appropriate surface properties to favor cellular attachment, proliferation and differentiation [11-12]. In addition to their biocompatibility, the scaffolds from those materials should possess appropriate mechanical properties to provide the correct stress environment for the tissues [13-14], and exhibit appropriate surface structure and chemistry for cell adhesion [11, 15].

In general, materials can be divided into the following categories: metals, polymers (natural and synthetic), ceramics, and composites (combination of the previous mentioned materials).Over the last century, biocompatible materials such as metals, ceramics and polymers have been extensively used for surgical implantation [16-17]. Metals and ceramics have contributed to major advances in the medical field, particularly in orthopedic tissue replacement. However, metals and ceramics are not biodegradable (necessary for some applications) and their processability is limited. For this reason, polymer materials have received increasing attention and have been widely used in tissue engineering due to the easy control over processability and biodegradability. Polymeric scaffolds can be either synthetic or natural. Nevertheless, synthetic polymer offer, at the present moment, some advantages such as the possibility of being tailored within a wide range of physical and chemical properties, being fabricated into various shapes with desired morphologic features and large predictability.

In this way, a variety of synthetic polymers such as poly(lactic acid) (PLA) [18-19], poly(glycolic acid) (PGA) [20-21], poly(lactic-co-glycolic acid) (PLGA) [22-23], poly(ethylene glycol) (PEG) [24-25] and polycaprolactone (PCL) [26] have been widely used to produce materials/scaffolds for tissue engineering [27-28].

Although already exist an extensive list of polymer that have been studied regarding tissue engineering applications, most of the scaffolds have been used in a passive way, just as support for the cells and tissues. Nevertheless, it was verified that for some specific applications active behavior of the material can be taken to advantage, emerging, in this way, the need for development of smart materials for tissue engineering applications [13].

1.1.2 Design and development of membranes and scaffolds

The design of materials and scaffolds able to guide the process of tissue regeneration represents one of the most challenging features in tissue engineering. The biopolymer characteristics are determined by the fabrication technique, which must be developed such that it does not adversely affect the biocompatibility of the material [29].

Material and scaffold characteristics such as interconnectivity, pore size/curvature, microporosity, macroporosity and surface roughness influence cellular response and for this reason it is important to be able to control the process fabrication. Other highly desirable features concerning scaffold fabrication include near-net-shape fabrication and scalability for cost-effective production. It is also important to allow cell-seeded scaffolds to be subjected to a strain environment, in order to better understand how cells respond to mechanical stimuli.

The fabrication technique for the tissue engineered scaffold is directly related to the bulk and surface properties of the polymer and the proposed function of the scaffold. Different techniques have been developed with the objective to improve scaffold design by controlling the regular pore size, pore interconnectivity, porosity and pore characteristics suitable for rapid nutrient diffusion and cell attachment.

The most important property of polymer materials is that they can be tailored mechanically, chemically and biochemically to suit a specific application. The techniques and methods developed to process biomaterials, include, for example, include solvent-casting, gas foaming, fiber mesh and fiber bonding, phase separation, melt molding and electrospinning [30]. Traditional methods, through material processing and casting, have largely been unsuccessful for the control of internal architecture to a high degree of accuracy or homogeneity. It has been demonstrated that the control of the scaffold design is a crucial parameter for ensure vascularization and bone deposition [31].

In the last decade, electrospinning technique has attracted large interest as it allows the fabrication of fibrous non-woven micro- and nano- fibers for tissue engineering applications, mainly due to the structural similarity to the tissue extracellular matrix (ECM) [13].

1.1.2.1 Electrospinning

One attractive characteristic of electrospinning is its simplicity, possibility of large scale productions, as well as the fast processing and inexpensive nature of the setup [32]. The setup essentially consists on a capillary tube, a needle, attached to a syringe filled with the polymer solution, a grounded collector and a high voltage power supply connected to the capillary and the collector (Figure 1.2) [33].

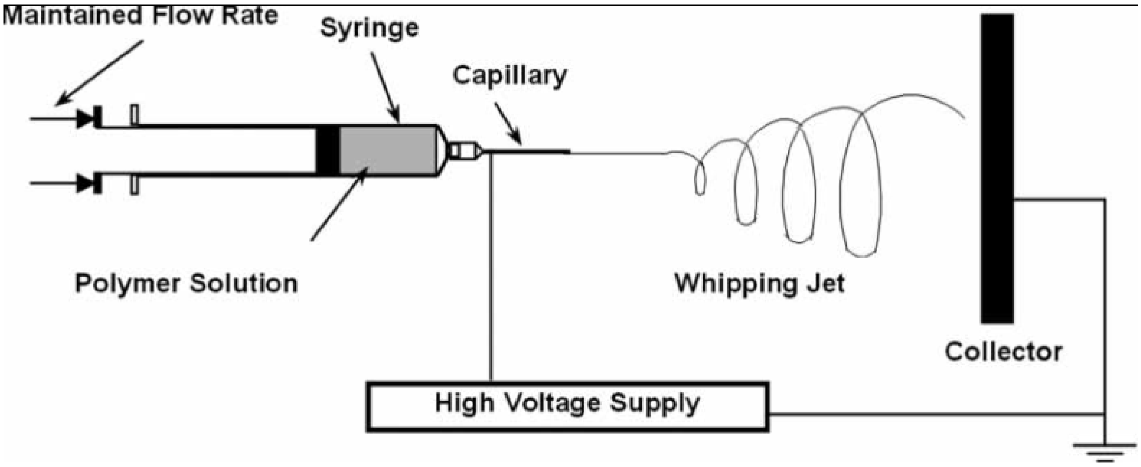

Figure 1.2 – Basic experimental electrospinning setup [34].

To obtain polymer based electrospun fibers, a polymeric solution is introduced in the syringe. The application of an electric field using the high-voltage source causes an electrostatic force that opposes the surface tension. Eventually, the charge repulsion overcomes the surface tension, causing the initiation of a jet. As this jet moves, the solvent evaporates and an appropriate collector can be used to capture the polymeric fiber. Stability and directionality of the jet is dependent on the electrostatic fields formed between the collector and the needle [33, 35-36]. The fiber morphology can be observed by scanning electron microscopy (SEM) (figure 1.3).

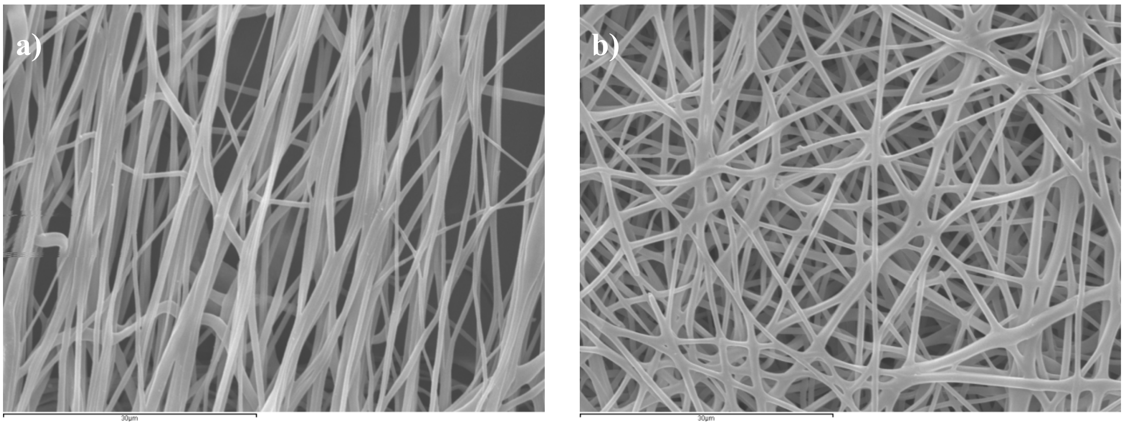

Figure 1.3 – SEM images of PLA nanofibers produced by electrospinning: a) aligned and b) non-aligned fibers (magnification of 2000X).

Many parameters influence the morphology of the resulting electrospun fibers, from beaded fibers to fibers with pores on its surface. These parameters can be classified in the type of polymer solution, processing conditions which include applied voltage, flow rate and effect of the collector, and ambient conditions [37]. Thereby, this technique has the ability to produced fibers with diameter from micrometers to a few nanometers, different orientation, high aspect ratio, high surface area, and having control over pore geometry [13, 38]. These characteristics are favorable for in vitro and in vivo cellular growth since they directly influence cell adhesion, cell expression, and transportation of oxygen and nutrients to the cells.

Many different polymeric nanofibers have already been successfully processed by electrospinning [39] and a large number are used in biomedical applications in membranes and scaffolds preparation for tissue engineering [40-43].

Has mentioned before, the use of active membranes and scaffolds is one of the most promising challenges in the tissue engineering process, thereby electroactive materials, the can provide electrical or mechanical stimuli to the cells, are a promising type of materials to be applied in this field.

1.2 Electroactive materials

Electroactive polymers (EAP) are polymers that respond to electrical stimulation with a significant shape or size change. For many years EAP received relatively low attention due to their poor actuation capability and the small number of available materials. However, in the last years, EAP materials received increased attention from industry and academia from different disciplines due to their wide variety of applications such as biosensors, artificial muscles, actuators, environmentally sensitive membranes, visual displays, components in high energy batteries and nano- and bio-related technologies [44-45]. So, the contemporary interest in EAP is that those “smart materials” can respond to a variety of external stimuli [46]. There are a significant number of different types of electroactive polymers that exhibit a variety of coupling mechanisms [47]. In this work, only piezoelectric materials, with the ability to convert a mechanical stimuli into a electrical one and vice-versa, will be discussed.

It has been shown that electrically charged surfaces influence cell behavior, such as cell adhesion and morphology [48], growth of different cell types [49], enhancement of cardiac [50-51] and nerve regeneration [50, 52]. Thus, a material that changes its surface charge as a response to mechanical stimuli present with the body can be a promising approach for many tissue engineering applications (e. g., bone, cartilage and nerve regeneration).

Various types of EAP materials have been investigated. Generally, they can be divided into two groups, ionic and electronic EAPs, according to their principle of activation (Table 1.1) [53].

Table 1.1 – Classification of electroactive polymers [53].

Electroactive polymers	
Ionic EAP	**Electronic EAP**
✓ Ionic polymer gels	✓ **Piezoelectric polymers**
✓ Ionometric polymer-metal composites	✓ Electroactive graft elastomers
✓ **Conductive polymers**	✓ Electrostrictive paper
✓ Carbon nanotubes	✓ Electrovisco-elastic elastomers
✓ Electrorheological fluids	✓ Liquid -crystal elastomers

In ionic EAPs, the activation forces are generated by diffusion of mobile ions, whereas electric EAPs are generated by dielectrics driven by electric field. The electronic polymers respond faster than ionic ones [54].

1.2.1 Conducting polymers

Conducting polymers have been studied for a wide range of potential applications in biotechnology, including tissue engineering (neural and cardiac applications) [55]. In those areas, the main used conductive polymers are polyaniline (PANI) [56], polypyrrole (PPy) [57], polythiophenes (PT) [58], poly(3,4-ethylenedioxythiophene) (PEDOT) [59].

A handful of studies have described experimental work assessing the biocompatibility of conducting polymers. PPy has been one of most studied electrically conducting polymers due to its good environmental stability, high conductivity, and easy preparation either by chemical or by electrochemical polymerization [60]. However, the poor mechanical properties and processability of PPy have restricted its applications [61]. For this reason, PANI appears to be a good alternative. Along the years, PANI has demonstrated to be the most important conducting polymer due to its good environmental stability, low cost and better processability [62].

Although some authors have highlighted the potential use of conducting polymers in regulating cell responses, their limited processability due to weak mechanical properties is an obstacle for fabrication of electrically active fibers for cell culture [51].

1.2.2 Piezoelectric polymers

In addition to conductive polymeric materials, piezoelectric polymers have been investigated and showed be an interesting and promising approach for tissue engineering applications. These polymers are being investigated for tissue engineering applications due to their ability to subject cells to an electrical stimulation.

Piezoelectric materials produce a transient electrical response when they are mechanically deformed. As a result, an electrical stimulus may be possible without direct connection to a voltage source [63]. Thus, the use of intrinsically charged piezoelectric polymers as tissue culture substrates can provide means of exposing cells directly to local time-varying electrical stimuli.

Some studies involving piezoelectric polymers have been reported regarding cell biocompatibility. One of the first studies was realized by Fine *et al.* [64]. Extruded tubular nerve guidance channels from a vinylidenefluoride-trifluoroethylene copolymer were used to repair a 10 mm gap in transected sciatic nerves of adult rats and it was verified that nerves regenerated in positively poled channels presented a significantly greater number of myelinated axons than those regenerated in unpoled channels. Hereafter, Valentini *et al.* [65] cultured neurons (mouse neuroblastoma (Nb2a) cells) directly on electrically charged poly(vinylidene fluoride) (PVDF) polymer growth substrates to determine if local electrical charges enhance nerve fiber outgrowth *in vitro*. It was also verified that the piezoelectric substrates exhibited significantly larger levels of process outgrowth and neurite lengths at all time periods. Therefore, the enhanced neurite outgrowth can been attributed to the surface charges presence [66]. This kind of polymers have been especially studied for neural tissue engineering applications where the piezoelectric response influence of different polymers was investigated: PVDF [65], poly[(vinylidenefluoride-co-trifluoroethylene] (PVDF-TrFE) [48, 67-69], PLGA [70] and poly(L-lactic acid) (PLLA) [71-72]. Furthermore, the piezoelectric polymers potential was also investigated for other fields of tissue engineering application such as wound healing [73]; bone [74-75] and cartilage [76] regeneration.

Although some initial studies on piezoelectric polymers are being performed for cell culture and tissue engineering applications, there is a need to fully understand their influence in different cell growth, proliferation and differentiation both under static and dynamic conditions. Further, it also has to be undertaken the tailoring of the electroactive materials morphology and electroactive response in order to be adequate to the different applications. PLLA, despite being one of the most investigated polymers, the influence of its piezoelectricity remains poorly explored for bio-applications. PVDF, on the other hand, is just beginning to the seen as an interesting biocompatible polymer and promising choose for tissue engineering applications.

1.3 Objectives

The main objective of this thesis is to develop piezoelectric biomaterials with different morphologies and properties for tissue engineering applications and to evaluate their biological response.

The main focus areas of the present work are:

- The production and characterization of piezoelectric materials: PLLA and PVDF.
- Study of the influence of the processing conditions on the micro and nano-structure, phase content, crystallinity and electroactive response of the materials.
- The fabrication of membranes of the aforementioned materials for cell culture and bioactivity studies.
- Study of the influence of these materials in cell growth, proliferation and differentiation under static conditions.
- Development of a bioreactor to apply mechanical stimulation and study cell growth and proliferation on the piezoelectric polymers under dynamical conditions.

1.4 Structure and methodology

The present thesis is divided in ten chapters intended to provide a comprehensive report of the progress achieved during this investigation. The chapters are presented in such a way that show the sequential progress obtained in a variety of works reported. Seven of those chapters are based on published or submitted scientific papers. Two different piezoelectric polymers were studied: PLLA and PVDF. Therefore the research on each of those polymers is presented in a sequential way.

The chapter 1 shows the main objectives, structure and methodology of this work and also refers to the literature review, where is given a general overview on the current knowledge about piezoelectric biomaterials for tissue engineering applications.

The chapter 2 consists on the production of PLLA microfibers by electrospinning, varying the applied potential, solution flow rate and collector conditions. PLLA fibers with smoothly oriented and random morphologies obtained were characterized by SEM, differential scanning calorimetry (DSC) and Fourier transform infrared (FTIR).

The PLLA fibers diameter was further reduced by the introduction of poly(ethylene oxide) (PEO) polymer. This effect was presented in chapter 3. Also, the influence of the PEO in the electrospinning process is discussed and the results are correlated to the evolution of the PLLA fiber diameter. The PLLA degradation in phosphate buffer solution (PBS) up to 20 weeks was also studied.

In the chapter 4, the local piezoelectric properties of the PLLA individual electrospun fibers by piezoresponse force microscopy (PFM) are presented.

The chapter 5 presents the bioactivity of the produced PLLA fibers. PLLA electrospun mats have been produced with random and aligned fiber orientation and different degrees of crystallinity. The influence of these two factors was evaluated on the samples hydrophobicity, adhesion, proliferation and differentiation of human chondrocytes cultured in these substrates.

In the chapter 6 it is reported the production of PVDF. PVDF electrospun membranes were obtained by electrospinning and the influence of the processing parameters on the fiber morphology and fiber orientation and on the crystallinity and crystal phase produced were studied. The local piezoelectric properties of individual electrospun fibers were studied by PFM.

On chapter 7, the influence of crystalline phase and the surface electrical charge of electroactive PVDF films on the hydrophilicity, fibronectin absorption and biological response in monolayer cell culture were evaluated with MC3T3-E1 osteoblast.

The chapter 8 focuses on the influence of the polarization of electroactive PVDF films on the biological response of osteoblast cells cultivated under static and dynamic conditions.

Finally, chapter 9 presents the overall conclusions and suggestions for future work.

1.5 References

1. Zhang, N. and D.H. Kohn, *Using Polymeric Materials to Control Stem Cell Behavior for Tissue Regeneration.* Birth Defects Research Part C-Embryo Today-Reviews, 2012. **96**(1): p. 63-81.
2. Chapekar, M.S., *Tissue engineering: Challenges and opportunities.* Journal of Biomedical Materials Research, 2000. **53**(6): p. 617-620.
3. Langer, R. and J.P. Vacanti, *Tissue engineering.* Science, 1993. **260**(5110): p. 920-926.
4. Gloria, A., R. De Santis, and L. Ambrosio, *Polymer-based composite scaffolds for tissue engineering.* Journal of Applied Biomaterials & Biomechanics, 2010. **8**(2): p. 57-67.
5. Stock, U.A. and J.P. Vacanti, *Tissue engineering: Current state and prospects.* Annual Review of Medicine, 2001. **52**: p. 443-451.
6. Ratner, B.D., *Biomaterials science : an introduction to materials in medicine*. 2004, Amsterdam; Boston: Elsevier Academic Press.
7. Barnes, C.P., et al., *Nanofiber technology: Designing the next generation of tissue engineering scaffolds.* Advanced Drug Delivery Reviews, 2007. **59**(14): p. 1413-1433.
8. Blitterswijk, C.A.v. *Tissue engineering*. 2007; Available from: http://www.engineeringvillage.com/controller/servlet/OpenURL?genre=book&isbn=9780123708694.
9. Meyer, U., *Fundamentals of tissue engineering and regenerative medicine*. 2009, Berlin: Springer.
10. Liu, C., Z. Xia, and J.T. Czernuszka, *Design and Development of Three-Dimensional Scaffolds for Tissue Engineering.* Chemical Engineering Research and Design, 2007. **85**(7): p. 1051-1064.
11. Yang, S.F., et al., *The design of scaffolds for use in tissue engineering. Part 1. Traditional factors.* Tissue Engineering, 2001. **7**(6): p. 679-689.
12. Slaughter, B.V., et al., *Hydrogels in Regenerative Medicine.* Advanced Materials, 2009. **21**(32-33): p. 3307-3329.
13. Ravichandran, R., et al., *Advances in Polymeric Systems for Tissue Engineering and Biomedical Applications.* Macromolecular Bioscience, 2012. **12**(3): p. 286-311.

14. Gentleman, E., et al., *Mechanical characterization of collagen fibers and scaffolds for tissue engineering.* Biomaterials, 2003. **24**(21): p. 3805-3813.
15. Roach, P., et al., *Modern biomaterials: a review-bulk properties and implications of surface modifications.* Journal of Materials Science-Materials in Medicine, 2007. **18**(7): p. 1263-1277.
16. Chen, G.P., T. Ushida, and T. Tateishi, *Scaffold design for tissue engineering.* Macromolecular Bioscience, 2002. **2**(2): p. 67-77.
17. Davis, J.R. and A.S.M. International, *Handbook of materials for medical devices*. 2003, Materials Park, OH: ASM International.
18. Khang, G., et al., *Preparation and characterization of small intestine submucosa powder impregnated poly(L-lactide) scaffolds: The application for tissue engineered bone and cartilage.* Macromolecular Research, 2002. **10**(3): p. 158-167.
19. Yuan, J., J. Shen, and I.K. Kang, *Fabrication of protein-doped PLA composite nanofibrous scaffolds for tissue engineering.* Polymer International, 2008. **57**(10): p. 1188-1193.
20. Boland, E.D., et al., *Utilizing acid pretreatment and electrospinning to improve biocompatibility of poly(glycolic acid) for tissue engineering.* Journal of Biomedical Materials Research Part B-Applied Biomaterials, 2004. **71B**(1): p. 144-152.
21. Boland, E.D., et al., *Tailoring tissue engineering scaffolds using electrostatic processing techniques: A study of poly(glycolic acid) electrospinning.* Journal of Macromolecular Science-Pure and Applied Chemistry, 2001. **38**(12): p. 1231-1243.
22. Kang, S.W., W.G. La, and B.S. Kim, *Open Macroporous Poly(lactic-co-glycolic Acid) Microspheres as an Injectable Scaffold for Cartilage Tissue Engineering.* Journal of Biomaterials Science-Polymer Edition, 2009. **20**(3): p. 399-409.
23. Shao, H.J., et al., *Designing a Three-dimensional Expanded Polytetrafluoroethylene-Poly(lactic-co-glycolic acid) Scaffold for Tissue Engineering.* Artificial Organs, 2009. **33**(4): p. 309-317.
24. Beamish, J.A., et al., *The effects of monoacrylated poly(ethylene glycol) on the properties of poly(ethylene glycol) diacrylate hydrogels used for tissue*

engineering. Journal of Biomedical Materials Research Part A, 2010. **92A**(2): p. 441-450.

25. Zhu, J.M., *Bioactive modification of poly(ethylene glycol) hydrogels for tissue engineering.* Biomaterials, 2010. **31**(17): p. 4639-4656.
26. Schappacher, M., et al., *Comparative in vitro Cytotoxicity Toward Human Osteoprogenitor Cells of Polycaprolactones Synthesized from Various Metallic Initiators.* Macromolecular Bioscience, 2010. **10**(1): p. 60-67.
27. Dublin/Galway Symposium on Biomechanical, E., et al. *Topics in bio-mechanical engineering : proceedings of the 1st symposium on biomechanical engineering held between the Trinity Centre for Bioengineering and the National Centre for Biomedical Engineering Science under the Programme for Research in Third Level Institutions*. Dublin; Galway: TCBE ; NCBES.
28. Liu, X.H. and P.X. Ma, *Polymeric scaffolds for bone tissue engineering.* Annals of Biomedical Engineering, 2004. **32**(3): p. 477-486.
29. Lanza, R.P., R.S. Langer, and J. Vacanti. *Principles of tissue engineering.* 2000; Available from: http://site.ebrary.com/id/10188250.
30. Eberli, D. and InTech. *Tissue engineering.* 2010; Available from: http://www.intechopen.com/books/show/title/tissue-engineering.
31. Chu, T.M.G., et al., *Mechanical and in vivo performance of hydroxyapatite implants with controlled architectures.* Biomaterials, 2002. **23**(5): p. 1283-1293.
32. Agarwal, S., J.H. Wendorff, and A. Greiner, *Use of electrospinning technique for biomedical applications.* Polymer, 2008. **49**(26): p. 5603-5621.
33. Ramakrishna, S., et al., *An Introduction to Electrospinning and Nanofibers*. 2005: World Scientific Publishing Company.
34. Moghe, A.K. and B.S. Gupta, *Co-axial electrospinning for nanofiber structures: Preparation and applications.* Polymer Reviews, 2008. **48**(2): p. 353-377.
35. Haynes, A.S. and P.I. Gouma, *Electrospun conducting polymer-based sensors for advanced pathogen detection.* Ieee Sensors Journal, 2008. **8**(5-6): p. 701-705.
36. Pham, Q.P., U. Sharma, and A.G. Mikos, *Electrospinning of polymeric nanofibers for tissue engineering applications: A review.* Tissue Engineering, 2006. **12**(5): p. 1197-1211.

37. Subbiah, T., et al., *Electrospinning of nanofibers.* Journal of Applied Polymer Science, 2005. **96**(2): p. 557-569.

38. Doshi, J. and D.H. Reneker, *Electrospinning process and applications of electrospun fibers.* Journal of Electrostatics, 1995. **35**(2-3): p. 151-160.

39. Huang, Z.M., et al., *A review on polymer nanofibers by electrospinning and their applications in nanocomposites.* Composites Science and Technology, 2003. **63**(15): p. 2223-2253.

40. Yang, F., et al., *Electrospinning of nano/micro scale poly(L-lactic acid) aligned fibers and their potential in neural tissue engineering.* Biomaterials, 2005. **26**(15): p. 2603-2610.

41. Ma, Z.W., et al., *Potential of nanofiber matrix as tissue-engineering scaffolds.* Tissue Engineering, 2005. **11**(1-2): p. 101-109.

42. Jeong, S.I., et al., *Electrospun gelatin/poly(L-lactide-co-epsilon-caprolactone) nanofibers for mechanically functional tissue-engineering scaffolds.* Journal of Biomaterials Science-Polymer Edition, 2008. **19**(3): p. 339-357.

43. Yoshimoto, H., et al., *A biodegradable nanofiber scaffold by electrospinning and its potential for bone tissue engineering.* Biomaterials, 2003. **24**(12): p. 2077-2082.

44. Finkenstadt, V. and J.L. Willett, *Preparation and Characterization of Electroactive Biopolymers.* Macromolecular Symposia, 2005. **227**(1): p. 367-372.

45. Yoseph, B.-C., et al., *Electroactive polymer materials.* Smart Materials and Structures, 2007. **16**(2).

46. Shankar, R., T.K. Ghosh, and R.J. Spontak, *Mechanical and actuation behavior of electroactive nanostructured polymers.* Sensors and Actuators a-Physical, 2009. **151**(1): p. 46-52.

47. Leo, D.J., *Electroactive Polymer Materials*, in *Engineering Analysis of Smart Material Systems*. 2008, John Wiley & Sons, Inc. p. 346-384.

48. Weber, N., et al., *Characterization and in vitro cytocompatibility of piezoelectric electrospun scaffolds.* Acta Biomaterialia, 2010. **6**(9): p. 3550-3556.

49. Huag, H.-S., et al., *Formation of microporous poly(hydroxybutyric acid) membranes for culture of osteoblast and fibroblast.* Polymers for Advanced Technologies, 2009. **20**(12): p. 1082-1090.

50. Li, M.Y., et al., *Electroactive and nanostructured polymers as scaffold materials for neuronal and cardiac tissue engineering.* Chinese Journal of Polymer Science, 2007. **25**(4): p. 331-339.

51. Jun, I., S. Jeong, and H. Shin, *The stimulation of myoblast differentiation by electrically conductive sub-micron fibers.* Biomaterials, 2009. **30**(11): p. 2038-2047.

52. Kotwal, A. and C.E. Schmidt, *Electrical stimulation alters protein adsorption and nerve cell interactions with electrically conducting biomaterials.* Biomaterials, 2001. **22**(10): p. 1055-1064.

53. Bar-Cohen, Y., *Biomimetics using electroactive polymers (EAP) as artificial muscles - A review.* Journal of Advanced Materials, 2006. **38**(4): p. 3-9.

54. Shankar, R., T.K. Ghosh, and R.J. Spontak, *Dielectric elastomers as next-generation polymeric actuators.* Soft Matter, 2007. **3**(9): p. 1116-1129.

55. Ravichandran, R., et al., *Applications of conducting polymers and their issues in biomedical engineering.* Journal of the Royal Society Interface, 2010. **7**: p. S559-S579.

56. Li, M.Y., et al., *Electrospinning polyaniline-contained gelatin nanofibers for tissue engineering applications.* Biomaterials, 2006. **27**(13): p. 2705-2715.

57. Kai, D., et al., *Polypyrrole-contained electrospun conductive nanofibrous membranes for cardiac tissue engineering.* Journal of Biomedical Materials Research Part A, 2011. **99A**(3): p. 376-385.

58. Breukers, R.D., et al., *Creating conductive structures for cell growth: Growth and alignment of myogenic cell types on polythiophenes.* Journal of Biomedical Materials Research Part A, 2010. **95A**(1): p. 256-268.

59. Hsiao, Y.S., et al., *Manipulating location, polarity, and outgrowth length of neuron-like pheochromocytoma (PC-12) cells on patterned organic electrode arrays.* Lab on a Chip, 2011. **11**(21): p. 3674-3680.

60. Zelikin, A.N., et al., *Erodible Conducting Polymers for Potential Biomedical Applications.* Angewandte Chemie International Edition, 2002. **41**(1): p. 141-144.

61. Lee, D.H., J.A. Chang, and J.K. Kim, *Block copolymer as a template for electrically conductive nanocomposites.* Journal of Materials Chemistry, 2006. **16**(47): p. 4575-4580.

62. Liu, S., et al., *Investigation on cell biocompatible behaviors of polyaniline film fabricated via electroless surface polymerization.* Applied Surface Science, 2010. **256**(11): p. 3427-3431.

63. Nelson, W.G., *Piezoelectric materials : structure, properties, and applications*. 2010, New York: Nova Science Publishers.

64. Fine, E.G., et al., *Improved nerve regeneration through piezoelectric vinylidenefluoride-trifluoroethylene copolymer guidance channels.* Biomaterials, 1991. **12**(8): p. 775-780.

65. Valentini, R.F., et al., *Electrically charged polymeric substrates enhance nerve fibre outgrowth In vitro.* Biomaterials, 1992. **13**(3): p. 183-190.

66. Schmidt, C.E., et al., *Stimulation of neurite outgrowth using an electrically conducting polymer.* Proceedings of the National Academy of Sciences of the United States of America, 1997. **94**(17): p. 8948-8953.

67. Lee, Y.S., et al., *An Electroactive Conduit for Spinal Cord Injury Repair*. 2009 35th Annual Northeast Bioengineering Conference. 2009, New York: Ieee. 82-83.

68. Lee, Y.S., G. Collins, and T.L. Arinzeh. *Neural differentiation of human neural stem/progenitor cells on piezoelectric scaffolds*. in *Bioengineering Conference, Proceedings of the 2010 IEEE 36th Annual Northeast*. 2010.

69. Lee, Y.S., G. Collins, and T.L. Arinzeh, *Neurite extension of primary neurons on electrospun piezoelectric scaffolds.* Acta Biomaterialia, 2011. **7**(11): p. 3877-3886.

70. Bryan, D.J., et al., *Enhanced peripheral nerve regeneration through a poled bioresorbable poly(lactic-co-glycolic acid) guidance channel.* Journal of neural engineering, 2004. **1**(2): p. 91-8.

71. Huang, L., et al., *Synthesis of biodegradable and electroactive multiblock polylactide and aniline pentamer copolymer for tissue engineering applications.* Biomacromolecules, 2008. **9**(3): p. 850-858.

72. Morelli, S., et al., *Influence of micro-patterned PLLA membranes on outgrowth and orientation of hippocampal neurites.* Biomaterials, 2010. **31**(27): p. 7000-7011.

73. Guo, H.F., et al., *Piezoelectric PU/PVDF electrospun scaffolds for wound healing applications.* Colloids and Surfaces B-Biointerfaces, 2012. **96**: p. 29-36.

74. Rodrigues, M.T., et al., *beta-PVDF Membranes Induce Cellular Proliferation and Differentiation in Static and Dynamic Conditions*, in *Advanced Materials Forum Iv*, A.T. Marques, et al., Editors. 2008, Trans Tech Publications Ltd: Stafa-Zurich. p. 72-76.
75. Ribeiro, C., et al., *Fibronectin adsorption and cell response on electroactive poly(vinylidene fluoride) films.* Biomedical Materials, 2012. **7**(3): p. 035004.
76. Areias, A.C., et al., *Influence of crystallinity and fiber orientation on hydrophobicity and biological response of poly(L-lactide) electrospun mats.* Soft Matter, 2012. **8**(21): p. 5818-5825.

2. Tailoring the morphology and crystallinity of poly(L-lactide acid) electrospun membranes

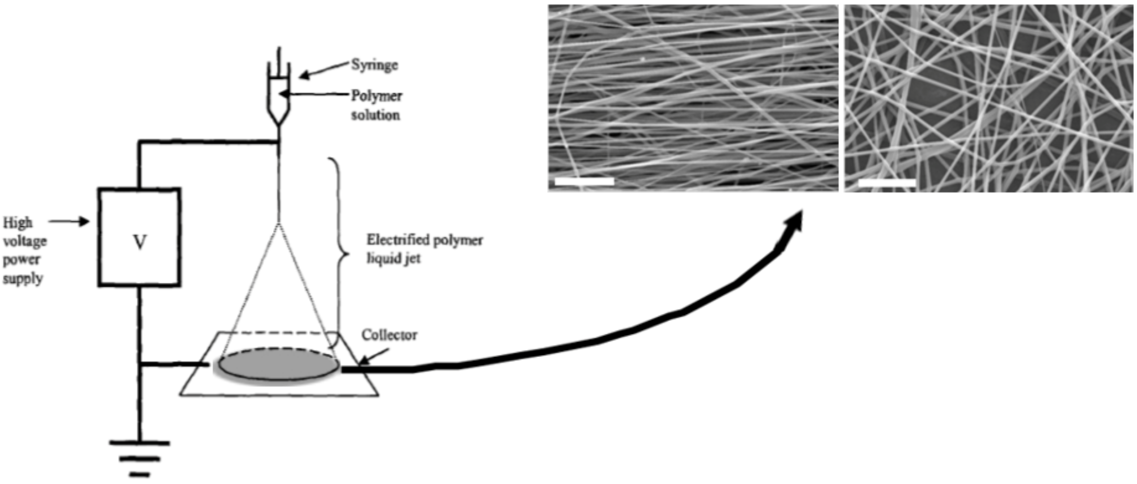
Syringe
Polymer solution
High voltage power supply
V
Electrified polymer liquid jet
Collector

This chapter is based on the following publication: C. Ribeiro, V. Sencadas, C. M. Costa, J. L. Gómez Ribelles and S. Lanceros-Méndez. *Tailoring the morphology and crystallinity of poly(L-lactide acid) electrospun membranes.* . 2011. 12: 015001.

2.1 Introduction

Nanofibers can be produced by a variety of methods such as drawing, template synthesis, self-assembly, wet spinning, electrospinning and phase separation [1]. However, most of these techniques cannot be upscaled, are specific to certain polymers or cannot control the diameter and orientation of the fibers. Electrospinning has proven to be an excellent method for the synthesis of thin fibers for a wide range of polymeric materials. The electrospinning process was described by Formhals in the 1930s, and was developed with the aim of commercializing textiles yarns [1]. This technique is relatively versatile, simple, fast and efficient. Electrospun membranes have potential biomedical applications such as scaffolds for tissue engineering, sutures, implants and controlled drug delivery systems [2-4].

Poly(lactic acid) is one of the most commonly used biomaterials and exhibits a low density, low processing power, elastomeric behavior, corrosion resistance and versatile fabrication [5]. The use of PLA in the medical field has increased owing to its biocompatibility, bioresorption, degradation, low toxicity and high mechanical performance.

PLA is a linear polyester that exists in the form of two stereoisomers: poly(L-lactic acid) and poly(D-lactic acid) (PDLA) and their racemic mixture is poly(D,L-lactic acid) (PDLLA) [6]. PLLA is mainly used in biomedical applications. PLLA and PDLA are semi-crystalline and PDLLA is an amorphous polymer [6-8]. The properties of PLA, such as mechanical strength, crystallinity and melting temperature, are determined by the polymer structure (which in turn is affected by the L and D ratio) and molecular weight [9].

The most common stereoisomer, PLLA, crystallizes, depending on the conditions, in the α-, β- or γ- form. The α- form is the most common and stable polymorph. The α-form is characterized by a 10_3 helical chain conformation where two chains belong to an orthorhombic unit cell. The β-form is typically produced by stretching the α-form at high drawing ratios and high temperatures. The γ-form is produced by epitaxial crystallization [6, 10-11].

Several processing parameters affect the morphology and properties of electrospun fibers. The most important ones are those corresponding to the initial polymer solution, namely the solvent (its dielectric constant, volatility, boiling point, etc), the solution concentration (which determines the viscosity) and the molecular weight of the polymer (which must take into account polymer entanglement) [3]. Other important parameters controlling the jet formation and solvent evaporation are the flow rate through the needle, the needle diameter, the distance from the tip to the collector, temperature, applied voltage, and the collection procedure (static or dynamic, i.e. the use of a rotating drum collector). The rotating speed of the drum collector determines the fiber diameter and orientation [12].

Several groups have reported the effect of electrospinning processing parameters on the morphology of PLA fibers [13-16]. Tsuji *et al.* [13] found that the fiber diameter decreases with increasing applied voltage. Tomaszewski *et al.* [14] studied the effect of PLLA molecular weight and the viscosity of the spinning solution on the fiber dimensions. Gu and Ren [15] investigated the effect of applied voltage and polymer concentration on fiber diameter and found that the diameter increases with increasing polymer concentration and decreases with increasing applied voltage. Zeng *et al.* reported the effect of solution viscosity and electrical conductivity on the diameter and morphology of fibers. A decrease in the fiber diameter and the formation of beaded fibers were observed for low PLA concentrations in the spinning solution. However, an increase in the electrical conductivity of the solution reduced bead formation [16]. Despite these studies, the control of electrospinning parameters to obtain fibers with the desired morphology, crystallinity and molecular structure has yet to be achieved.

In this work, we studied the effect of the applied voltage, solution flow rate and collecting procedure on the fiber characteristics and orientation. Furthermore, we analyzed the development of microfiber crystallinity upon the annealing of PLLA electrospun samples using DSC and FTIR.

2.2 Experimental

Materials: Purasorb PL18 PLLA, with an average molecular weight of 217.000-225.000 g.mol^{-1}, was purchased from Purac and dissolved in a 3/7 vol/vol mixture of

N,N-dimethylformamide (DMF, *Merck*) and dichloromethane (MC, *Sigma-Aldrich*) to achieve a polymer concentration of 10 wt.% of the solution. The process was conducted at room temperature using a magnetic stirrer until complete polymer dissolution.

Electrospinning: The polymer solution was placed in a commercial plastic syringe (10 mL) fitted with a steel needle with 500 μm inner diameter. Electrospinning was conducted by applying a voltage between 12 and 25 kV with a PS/FC30P04 power supply (*Glassman*). A syringe pump (*Syringepump)* fed the polymer solution into the needle tip at a rate between 1 and 8 mL.h^{-1}. The electrospun fibers were collected on a grounded collecting plate (random fibers) placed 15 cm away from the needle. Oriented fibers were produced using a grounded collecting drum of 20.3 cm.

Characterization: Electrospun fibers were coated with a thin gold layer using a sputter coater (*Polaron,* SC502) and observed with SEM (JSM-6300, *JEOL*) at an accelerating voltage of 20 kV. The mean fiber diameter and its distribution was calculated using SEM image of a 40 fibers taken at 1000X magnification and Image J software [17].

FTIR measurements were performed at room temperature with a Perkin-Elmer Spectrum 100 apparatus in the attenuated total reflectance mode from 4000 to 650 cm^{-1}. FTIR spectra were collected by performing 32 scans with a resolution of 4 cm^{-1}.

The stability of the electrospun fiber mats was analyzed by DSC with a Perkin Elmer Diamond setup. The samples were cut into ~2×2 mm^{-2}, 6 mg pieces, from the middle region of the electrospun membranes, placed in 40 μl aluminum pans and heated between 30 and 200 ºC at a heating rate of 10 ºC.min^{-1}. All experiments were performed under a nitrogen gas flow. The glass transition temperature (T_g), cold-crystallization temperature (T_{CC}), melting temperature (T_m), cold-crystallization enthalpy (ΔH_{CC}), melting enthalpy (ΔH_m) and degree of crystallinity (ΔX_C) of all electrospun fiber mats were evaluated.

2.3 Results and discussion

2.3.1 Processing parameters

Among the parameters affecting the fiber morphology and properties of electrospun PLLA membranes, this work focuses on the effects of applied voltage, flow rate and collector conditions (stating or rotating). The effect of applied high voltage was investigated while keeping the needle diameter constant at 0.5 mm, the flow rate at 4 mL.h^{-1} and the travelling distance at 15 cm. The SEM pictures in figure 2.1 show the effect of the applied voltage on the diameter of the electrospun fibers, as well as the mean value ± standard deviation of the diameter.

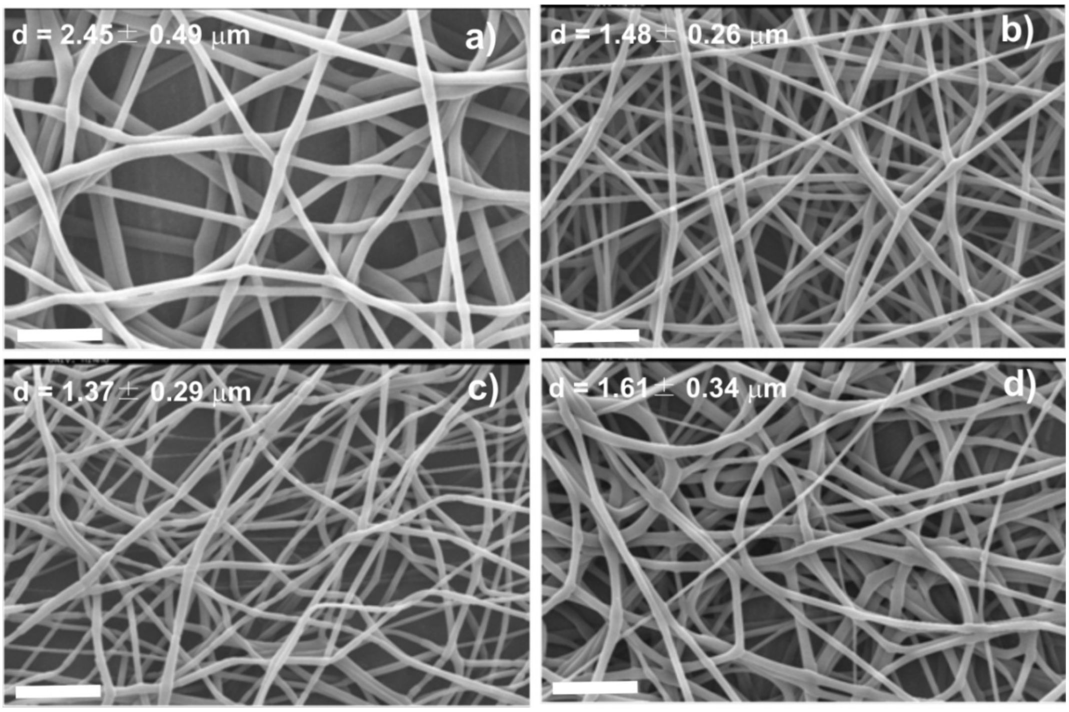

Figure 2.1 – SEM images of PLLA mats electrospun at a traveling distance of 15 cm, a needle diameter of 0.50 mm, a flow rate of 4 mL.h^{-1} and an applied voltage of a) 12 kV, b) 15 kV, c) 20 kV and d) 25 kV. The scale bar corresponds to 20 µm.

The diameter of the PLLA fibers ranges from 1.37 to 2.45 µm. It decreases when the voltage is raised from 12 to 20 kV (figures 2.1 a) - c)) and increases at higher voltages (figure 2.1 d)). The increase in fiber diameter with increasing voltage between 20 and 25 kV might be related to changes in the mass flow and jet dynamics [1, 15]. The mean fiber diameters are smaller for the PLLA mats than for PLLA fibers prepared by conventional solution-spinning (60 - 108 µm [18]) and melt-spinning methods (20 - 500 µm [19]). A porous structure with a maximum pore size of ~ 60 µm is created in the PLLA electrospun mats.

Figure 2.2 shows SEM images of the samples obtained at 20 kV with a needle diameter of 0.50 mm. The travelling distance was 15 cm and the solution feed rate was varied between 1 and 8 mL.h^{-1}. The images reveal that the average fiber diameter increases with increasing polymer feed rate from 1.03 µm at 1 mL.h^{-1} to 1.91 µm at 8 mL.h^{-1}. The fibers have a smooth surface but contain numerous pores with a size larger than 30 µm.

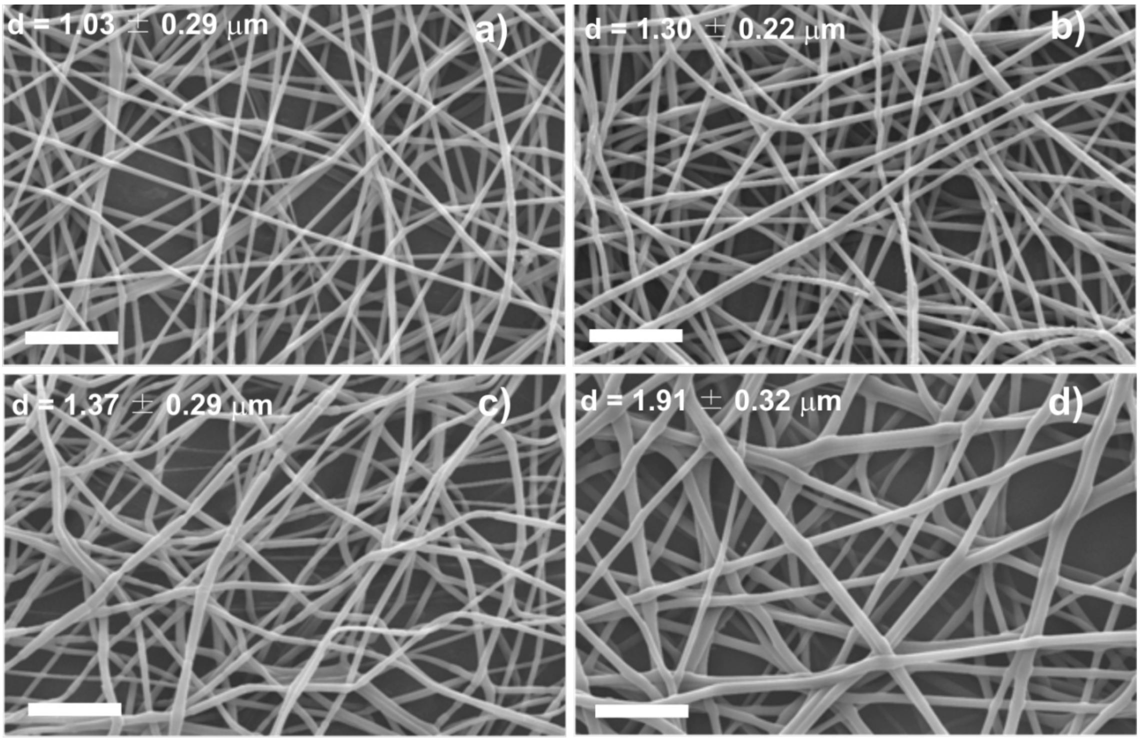

Figure 2.2 – SEM image of PLLA electrospun mats obtained at a traveling distance of 15 cm, needle diameter of 0.50 mm, applied voltage of 20 kV and a flow rate of a) 1 mL.h^{-1}, b) 2 mL.h^{-1}, c) 4 mL.h^{-1} and d) 8 mL.h^{-1}. The scale bar corresponds to 20 µm.

The shape of the droplet on the hole of the electrode (steel needle tip) at the initial stage of the electrospinning process was affect by several processing parameters such as electrospinning voltage. Consequently, the resulting fiber morphology could be changed from a typical cylindrical shape to a bead or string-of-pearls structure. The electric field initiated the jet. Once the electric field is applied to the droplet of polymer solution at the tip of the spinneret, the liquid surface is charged owing to the motion of the ions through the liquid. At a high field, the electric force overcomes the surface tension and a quasi-stable, straight and electrically charged jet is ejected [3, 20]. The balance between the surface tension and the electric force determine the initial cone shape of the polymer solution at the needle tip.

2.3.2 Fibrils orientation using a rotating collector

Electrospun mats can be oriented using a rotating collector. The effect of the rotation speed on fiber diameter and orientation is presented in figure 2.3, where the voltage was maintained at 20 kV, the flow rate of 4 mL.h^{-1}, the needle diameter at 0.50 mm and the travelling distance at 15 cm. Figure 2.3 shows the PLLA fiber mats obtained by electrospinning using a 20.3 cm drum collector, as well as the mean ± standard deviation of the fiber distribution.

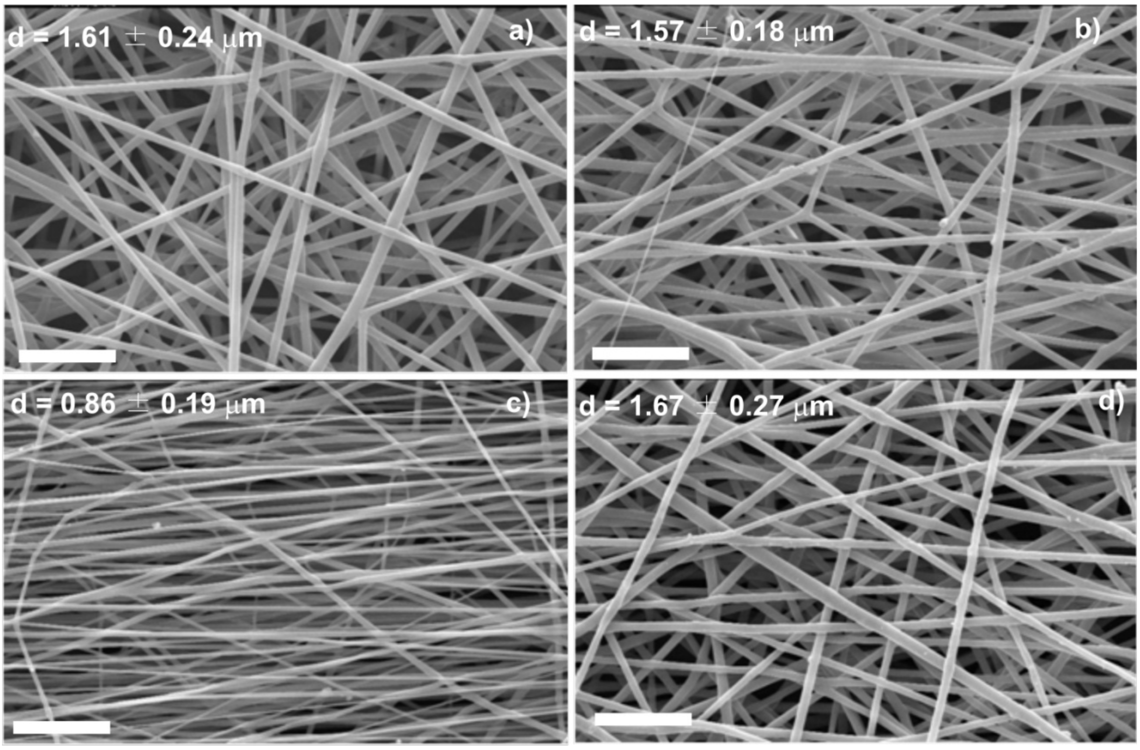

Figure 2.3 – SEM images of PLLA nanofibers electrospun obtained at a traveling distance of 15 cm, a needle diameter of 0.50 mm, an applied voltage of 20 kV, a flow rate of 4 mL.h^{-1} and a rotation speed of a) 500 rpm, b) 750 rpm, c) 1000 rpm, and d) 1500 rpm. The scale bar corresponds to 20 μm.

The mean fiber diameter was larger at the lowest rotating speeds (500 and 750 rpm) and the fiber orientation was partly random at these speeds. At higher rotation speeds (1000 rpm), the fibers had a minimum diameter of the 0.86 μm and were aligned in one preferential direction; their pores were smaller and the structure more compact with other samples. The fiber orientation had poorer alignment at 2000 rpm. The physical mechanisms of electrospinning are still not well understood and some intuitive conjectures are given as follows. When the linear speed of the rotating drum surface, which serves as a fiber collector, matches that of evaporated jet depositions, the fibers are collected at the surface of the cylinder tightly in a circumferential manner, resulting in good alignment. Such a speed can be called the alignment speed, and it is about 1000 rpm for PLLA. Randomly oriented fibers are collected at lower surface speeds, at which the rapid caotic motion of the jet determines the deposition (figure 2.3 a) and b), 500 and 750 rpm, respectively) [21]. On the other hand, there is a limiting rotation speed above which continuous fibers cannot be collected (figure 2.3 d), 1500 rpm). The optimum rotation speed depends on the material used and the polymer concentration [2, 12, 22-23].

2.3.3 Isothermal crystallization of electrospun mats

The thermal properties of electrospun PLLA were studied for an unoriented mat obtained at an applied voltage of 20 kV, a traveling distance of 15 cm, a needle diameter of 0.50 mm and a flow rate of 2 $mL.h^{-1}$. However, the results and discussion can also be applied to the samples obtained under other electrospinning conditions.

The deformation of the jet with rapid solidification during electrospinning often results in a metastable phase [24]. In the case of PLLA, as it is a slowly crystallizing polymer and because its glass transition temperature is above room temperature, the dry samples collected at room temperature maintain a stable crystalline fraction.

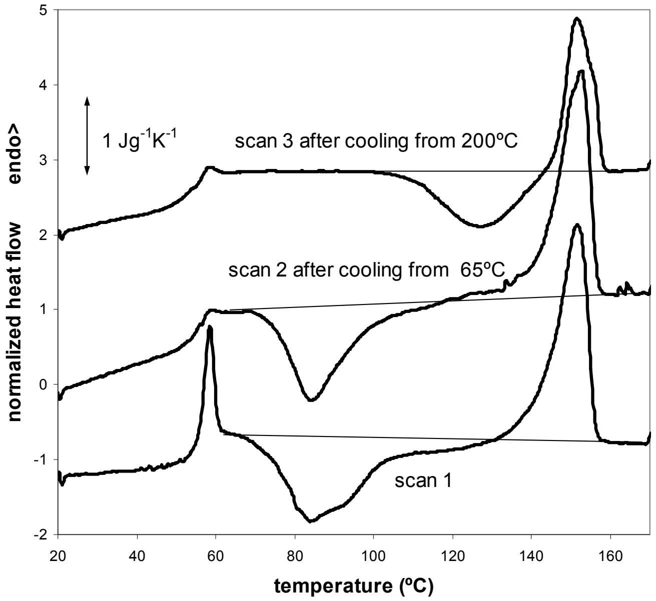

Figure 2.4 – DSC normalized thermograms of a PLLA sample electrospun at a traveling distance of 15 cm, a needle diameter of 0.50 mm, an applied voltage of 20 kV and a flow rate of 2 mL.h^{-1}. Scan 1 is the first heating scan, scan 2 was recorded after heating the sample to 65 ºC followed by cooling at 40 ºC.min^{-1} to 20 ºC, and scan 3 was performed after cooling the sample at 10 ºC.min^{-1} from 200 ºC to 20 ºC.

PLLA fibers electrospun from solution usually exhibit a cold-crystallization peak in DSC heating scans [25-26]. Figure 2.4 shows three DSC heating scans performed on electrospun PLLA samples. Scan 1 shows a normalized thermogram (heat flow divided by sample mass and heating rate) recorded upon heating an untreated electrospun mat at a rate of 10 ºC.min^{-1}. A strong endothermic peak is observed at 59 ºC and corresponds to the glass transition in PLLA. This peak can be ascribed to the recovery of the enthalpy of the sample, which was stored at room temperature (approximately 30 ºC), i.e. below T_g, and therefore subjected to physical ageing. The second scan was recorded after heating the sample to 65 ºC (slightly above the glass transition temperature) and rapidly cooling it to 20 ºC. The glass transition peak is hardly apparent in this case since physical ageing is erased by the first scan. Cold crystallization started immediately above the glass transition temperature in scans 1 and 2 and corresponds to the broad exotherm in the range of 65–120 ºC with a minimum at 85 ºC. Melting takes place between 120 and 160 ºC. The crystallinity degree of the electrospun mats was calculated using the following equation:

$$\Delta X_c = \frac{\Delta H}{\Delta H_m^0} * 100 \qquad \text{(Eq. 2.1)}$$

Here ΔH is the area under the thermogram between 65 and 160 ºC (the baseline for integration is shown in figure 2.4) and ΔH_m^0 is the enthalpy of melting for a fully crystallized PLLA sample (93.1 J.g^{-1} [27]). The calculation reveals that electrospun fibers are nearly amorphous because the area between the thermogram and the integration baseline is zero within the accuracy of the integration. From the area of melting peak between 120 and 160 ºC, the maximum degree of crystallinity produced in the sample during the heating scan after cool crystallization was estimated as 30%. The third heating scan, scan 3, was recorded after cooling the sample from 200 to 20 ºC at a rate of 10 ºC.min^{-1}. As for the first scan, the total enthalpy of the exothermic and endothermic peak is zero within the measurement accuracy, indicating that PLLA did not crystallize from the melt at the cooling rate of 10 ºC.min^{-1}, in agreement with previous experiments [29]. Interestingly, cold crystallization in scan 3 is shifted by more than 40 ºC towards higher temperatures with respect to scans 1 and 2, and the minimum of the exothermic peak is located at approximately 130 ºC. The maximum crystalline fraction produced by cold crystallization during the heating scan is 17%, as evaluated by the area under the melting peak.

The differences between the thermograms corresponding to scans 1 and 3 suggest the existence of different conformations of the polymer chains at the beginning of the scans. The temperature range of cold crystallization in scan 1, immediately above the glass transition temperature, indicates that numerous crystal nuclei were already present in the glass [28-29]. The presence of these nuclei can be related to nonequilibrium chain conformations imposed by the electrospinning process that were frozen upon the evaporation of the solvent. The similarity between scans 1 and 2 in terms of the cold-crystallization peak shows that nucleation is not due to physical ageing, which can create crystal nuclei [29, 31]. During scan 1, PLLA crystallizes, melts and finally stabilizes at 200 ºC with equilibrium chain conformations which are then preserved upon fast cooling to the glassy state. The cold crystallization of the PLLA initially in this conformation is clearly slower than in the electrospun mat.

No significant difference was found in the value of $\Delta C_p = 0.39$ J.g^{-1}.K^{-1} between scans 2 and 3. In both cases, the sample was nearly amorphous when the glass transition occurred.

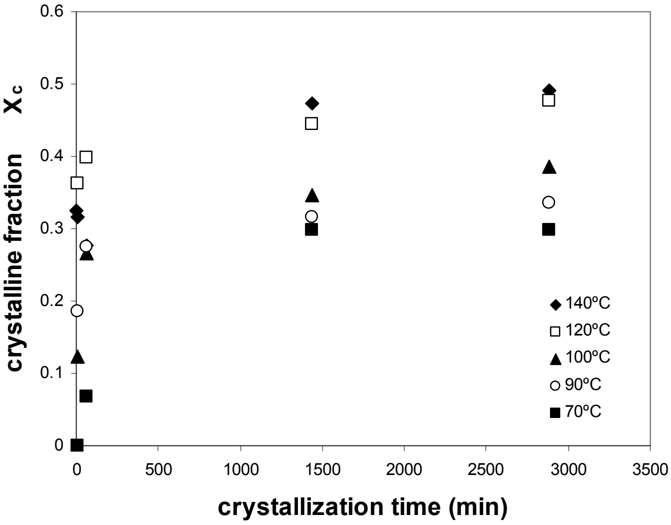

Figure 2.5 – Crystalline fraction of electrospun samples annealed at different temperatures.

The development of crystallinity in the electrospun mats was further studied by annealing them between the glass transition temperature and 140 ºC for up to 48 h. The samples were heated to the crystallization temperature in an oven, quenched to room temperature and then transferred to the DSC setup and subjected to a heating scan at 10 ºC.min^{-1} from room temperature to 200 ºC. Figure 2.5 shows the crystalline fraction of the sample measured by DSC. Samples subjected to annealing at temperatures above 90 ºC or for longer than 1 h did not exhibit a significant cold-crystallization exotherm during the DSC heating scan. The crystalline fraction rapidly increases in the first few minutes of annealing, as expected from the heating scan. For instance, after only 2 min of annealing at 140 ºC, crystallinity reaches 31%, whereas the maximum value for this temperature is 49%. This result indicates that numerous nucleation centers are present in the electrospun mat that grows simultaneously upon heating. This behavior is further confirmed by the fact that PLLA films, obtained by casting from the solution used for electrospinning and subjected to brief annealing at a low temperature, develop much lower crystallinity than the electrospun mats. For instance, annealing at 90 ºC for 1 h yields an electrospun mat with 27% crystallinity, whereas the crystalline fraction of the films subjected to the same treatment is only 9%. The total crystalline fraction after prolonged annealing at a high temperature does not significantly differ for electrospun mats and PLLA films, whereas the distribution of crystal sizes is different since the melting peaks are broader and shifted towards low temperatures for the electrospun mat with respect to the film, as can be observed in figure 2.6.

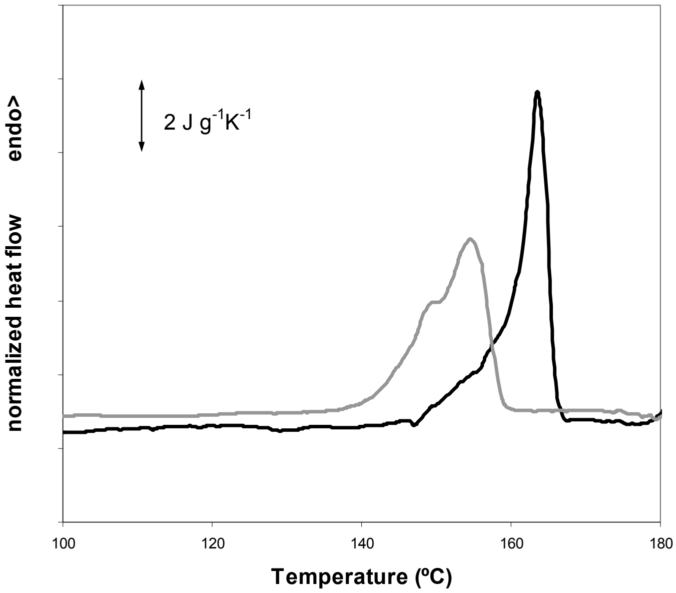

Figure 2.6 – Melting peaks of a PLLA film (black line) and an electrospun mat annealed at 140 ºC for 48 h.

The effect of the high crystalline fractions obtained by isothermal treatment on the properties of the electrospun fibers should be significant. Although characterization of the mechanical properties of the electrospun mats is beyond the scope of this work, SEM images taken before and after annealing (figure 2.7) show that highly crystalline fibers become fragile and break spontaneously during isothermal crystallization. This can be attributed to the fiber contraction induced by crystallization and the release of internal residual stresses generated during processing. Figure 2.7 a) shows an image of an untreated electrospun mat, in which PLLA is amorphous. No apparent change can be observed in figure 2.7 b), which corresponds to a sample annealed at 70 ºC for 48 h with X_c = 30%. On the other hand, in the sample crystallized at 140 ºC (figures 2.7 c) and 2.7 d)) some fibers are broken and others have a rough surface.

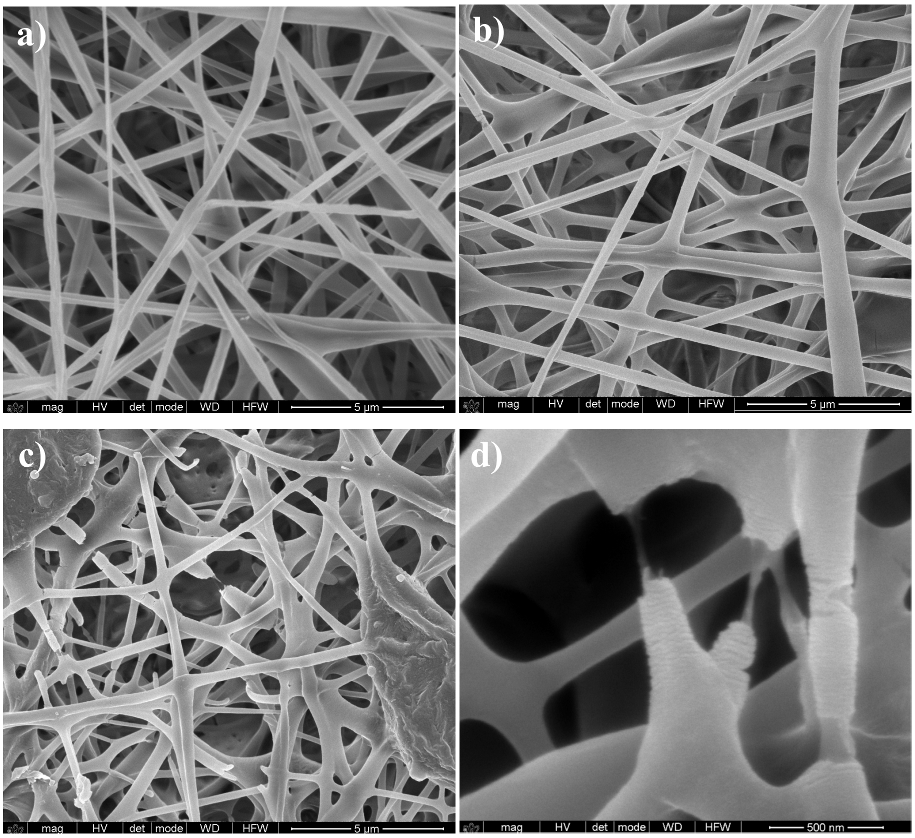
a)
b)
c)
d)
mag | HV | det | mode | WD | HFW | 5 µm
mag | HV | det | mode | WD | HFW | 5 µm
mag | HV | det | mode | WD | HFW | 5 µm
mag | HV | det | mode | WD | HFW | 500 nm

Figure 2.7 – SEM image of PLLA mats electrospun at a traveling distance of 15 cm, a needle diameter of 0.50 mm, an applied voltage of 20 kV and a flow rate of 2 mL.h^{-1}: a) as-produced, b) crystallized at 70 ºC for 48 h, c) and d) crystallized at 140 ºC for 48 h. The scale bar corresponds to 5 μm in a)-c) and to 0.5 μm in d).

2.3.4 Phase content

Previous studies have identified specific infrared absorption bands that are characteristic of the vibrations of certain molecular groups of PLA in a given crystalline phase (table 2.1). Thus, the evolution of the infrared spectra can be used to monitor the development of crystallinity in this polymer. Whereas some vibration frequencies have fixed frequencies, others shift significantly between the amorphous and crystalline α and α’ forms.

In this work we followed the evolution of the FTIR transmission spectra after annealing between 40 and 140 ºC for up to 48 h, that is the same thermal treatment as that in the DSC experiments. Figure 2.8 (and, in more detail, figure 2.9) shows the spectra after 48 h annealing at different temperatures. As can be seen in figure 2.5, the crystalline fraction continuously increases with increasing annealing temperature.

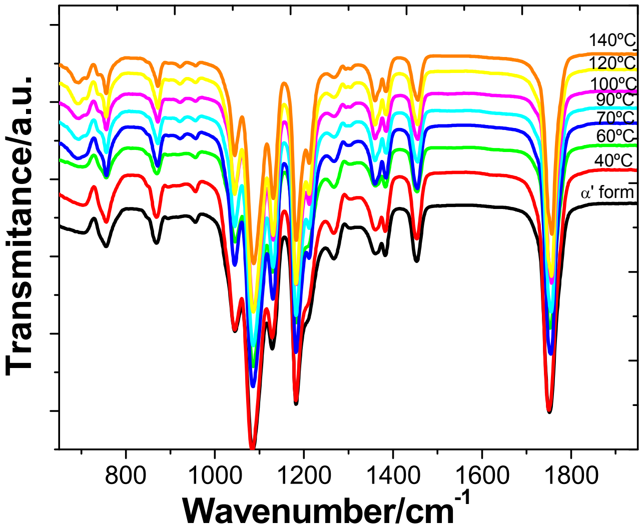

Figure 2.8 – FTIR transmission spectra of PLLA electrospun scaffolds before and after annealing at the indicated temperatures for 48 h.

The FTIR spectrum of the as-produced samples does not depend significantly on the electrospinning conditions. The effect of the applied voltage, flow rate and microfiber orientation was systematically studied, and in all samples the infrared spectrum corresponds to that of amorphous PLLA, in good agreement with the DSC results. In particular, it is worth noting the absence of the absorption band at 921 cm^{-1}. PLLA crystallizes into the α-form with the distorted 10_3 helix conformation from solution or melt. Kang *et al.* reported that the 921 cm^{-1} absorption band is characteristic of the α-crystals [30], associated with the transition moment perpendicular to the chain axis, to the CH_3 rocking mode combined with a minor contribution from the C–COO and O–CH stretching modes of the α-crystals [31]. The characteristic band of the PLLA β crystal at 908 cm^{-1} is absent in our spectra [32-33], suggesting that β PLLA does not form after electrospinning or after subsequent annealing (figure 2.9 a)).

Table 2.1 – Literature review of the relevant infrared bands associated with different phases of PLLA.

IR frequency (cm$^{-1)}$	Phase form	Assignment	Ref. No.
860	Amorphous		[30]
871	α		[11,30]
908	β		[37]
921	α	Coupling of the C-C backbone stretching with the CH_3 rocking mode	[11,30,37]
955	Amorphous		[11,30,37]
1044	Amorphous, α’ and α	ν(C-CH_3)	[38,39]
1053	α	ν(C-CH_3)	[6,38]
1092	α’ and α	ν_s(C-O-C)	[38]
1107	α’ and α		[38]
1134	Amorphous, α’ and α	r_s(CH_3)	[38,39]
1183	Amorphous, α’ and α	ν_{as}(C-O-C)+r_{as}(CH_3)	[38,39]
1213	α’ and α	ν_{as}(C-O-C)+r_{as}(CH_3)	[38]
1222	α	ν_{as}(C-O-C)+r_{as}(CH_3)	[6,38]
1268	Amorphous + semicrystalline	ν(CH)+ ν(COC)	[39]
1302	Amorphous	C-H stretching	[11]
1360	Semicrystalline	δ(CH), CH wagging (bending)	[39]
1363	Amorphous	δ(CH), CH wagging (bending)	[39]
1368	Semicrystalline	δ(CH), CH wagging (bending)	[39]
1382	α	δ_s(CH_3)	[6,37]
1386	α’ e α	δ_s(CH_3)	[37]
1387	Amorphous	δ_s(CH_3)	[37]
1444	α	δ_{as}(CH_3)	[30,37]
1454	Amorphous	δ_{as}(CH_3)	[30,37]
1457	α’ and α	δ_{as}(CH_3)	[30,37]
1749	α	ν(C=O)	[6,37,38]
1757	Amorphous	ν(C=O)	[37]
1759	α	ν(C=O)	[37]
1761	α’	ν(C=O)	[37]
2945	Amorphous	ν_s(CH_3)	[37]
2946	α’ and α	ν_s(CH_3)	[37]
2964	α	ν_s(CH_3)	[6,37]
2995	Amorphous	ν_s(CH_3)	[37]
2997	α’ and α	ν_{as}(CH_3)	[37]
3006	α	ν_{as}(CH_3)	[6,37]

As shown in figure 2.9 a), the increase in the crystallization degree is accompanied by a change in the shape of the absorption band between 840 and 880 cm^{-1}. The 860 and 871 cm^{-1} bands, respectively, ascribed to the skeletal stretching and CH_3 rocking of amorphous and crystalline (α) phases, overlap in this range [34]. With increasing annealing temperature, and thus increasing degree of crystallinity, the peak shifts to higher frequencies and significantly narrows as expected for crystal formation. Similar changes occur in the region of the ν_{as}(C-O-C) + $r_{as}(CH_3)$ modes in the amorphous phase and in the α' and α crystals (figure 2.9 b)), although the changes in the 955 cm^{-1} band, corresponding to the amorphous phase are less clear.

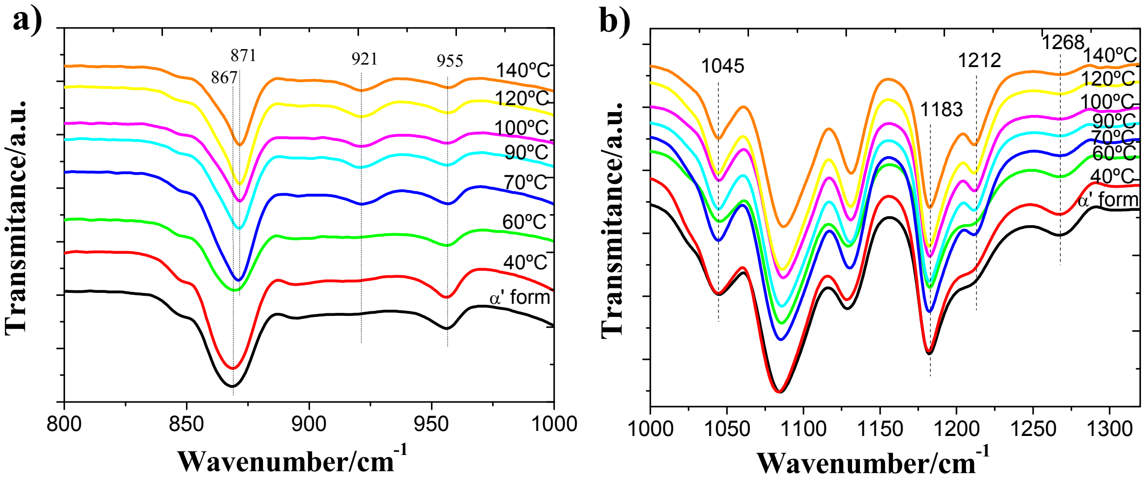

Figure 2.9 – FTIR transmission spectra of PLLA electrospun scaffolds before and after annealing at the indicated temperatures for 48 h.

The evolution of the infrared spectrum with annealing time follows similar trends. Figure 2.10 a) shows the appearance of the 921 cm^{-1} band and the shape change of the 840 and 880 cm^{-1} bands, which is consistent with the increasing degree of crystallinity. Figure 2.10 b) illustrates the changes in the region of the C=O stretching band (1800–1700 cm^{-1}), where the sift to higher frequency corresponds to the increasing crystallization. In summary, we can conclude that the crystallization of our samples is due to the presence of α-crystals in the mats.

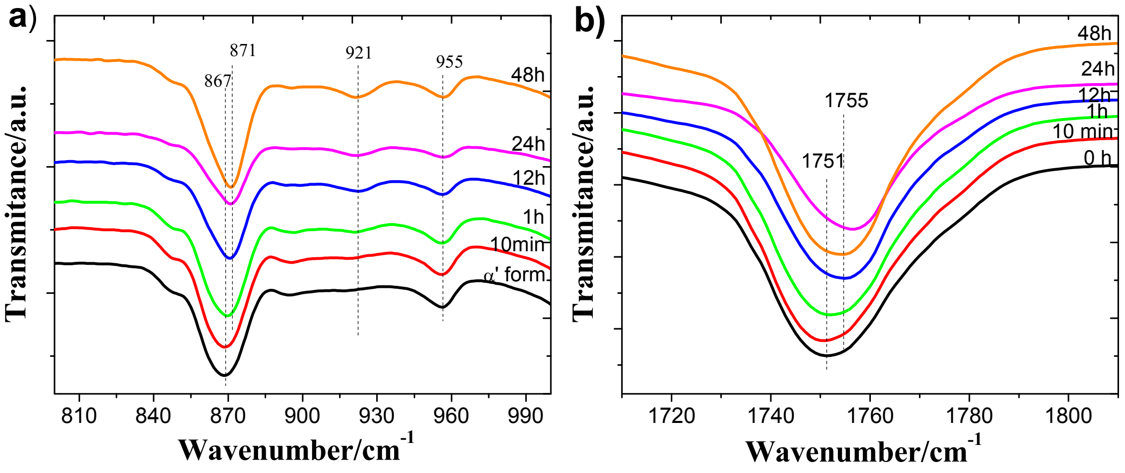

Figure 2.10 – FTIR transmission spectra of PLLA electrospun scaffolds before and after annealing at 70 ºC for the indicated times.

2.4 Conclusions

The fiber morphology of electrospun PLLA mats can be controlled by changing process parameters such as the applied voltage, feed rate and the collector system. Moreover, the degree of crystallinity of electrospun fibers can be easily tailored to between 50% and 0%, i.e. amorphous fibers. Samples with the highest crystallinity are fragile and spontaneously break during crystallization.

Random nanofibers were obtained on a plate collector, while oriented nanofibers were collected using a 20.3 cm diameter drum. The optimum fiber alignment was observed for a rotation speed of 1000 rpm, and for higher and lower drum rotation speeds, the rapid chaotic motion of the jet resulted in randomly oriented fibers. The deformation of the jet deformation with rapid solidification during electrospinning often results in a metastable phase. PLLA electrospun scaffolds are nearly amorphous but are highly nucleated. Crystals rapidly grow when the electrospun mat is heated to 70-140 ºC. Infrared transmission measurement suggests that the processing did not affect the PLLA samples at a molecular level and that the development of crystallinity in the samples after thermal annealing is due to the presence of the α-crystals in the electrospun mats.

2.5 References

1. Ramakrishna, S., et al., *An Introduction to Electrospinning and Nanofibers*. 2005: World Scientific Publishing Company.

2. Formhals, A., *Process and apparatus for preparing artificial threads*. 1934: United States.

3. Venugopal, J., Y.Z. Zhang, and S. Ramakrishna, *Fabrication of modified and functionalized polycaprolactone nanofibre scaffolds for vascular tissue engineering.* Nanotechnology, 2005. **16**(10): p. 2138-2142.

4. Kumbar, S.G., et al., *Reecent patents on electrospun biomedical nanostructures: an overview.* Recent patents on biomedical engineering, 2008. **1**(1): p. 68-78.

5. Garlotta, D., *A Literature Review of Poly(Lactic Acid).* Journal of Polymers and the Environment, 2001. **9**(2): p. 63-84.

6. Pan, P., et al., *Blending Effects on Polymorphic Crystallization of Poly(l-lactide).* Macromolecules, 2009. **42**(9): p. 3374-3380.

7. Tsuji, H. and Y. Ikada, *Blends of crystalline and amorphous poly(lactide). III. Hydrolysis of solution-cast blend films.* Journal of Applied Polymer Science, 1997. **63**(7): p. 855-863.

8. Moon, S.I., et al., *Synthesis and properties of high-molecular-weight poly(L-lactic acid) by melt/solid polycondensation under different reaction conditions.* High Performance Polymers, 2001. **13**(2): p. S189-S196.

9. Auras, R.A., et al., *Mechanical, physical, and barrier properties of poly(lactide) films.* Journal of Plastic Film & Sheeting, 2003. **19**(2): p. 123-135.

10. Pan, P., et al., *Polymorphous Crystallization and Multiple Melting Behavior of Poly(l-lactide): Molecular Weight Dependence.* Macromolecules, 2007. **40**(19): p. 6898-6905.

11. Vasanthan, N. and O. Ly, *Effect of microstructure on hydrolytic degradation studies of poly (l-lactic acid) by FTIR spectroscopy and differential scanning calorimetry.* Polymer Degradation and Stability, 2009. **94**(9): p. 1364-1372.

12. Pan, H., et al., *Continuous aligned polymer fibers produced by a modified electrospinning method.* Polymer, 2006. **47**(14): p. 4901-4904.

13. Tsuji, H., et al., *Electrospinning of Poly(lactic acid) Stereocomplex Nanofibers.* Biomacromolecules, 2006. **7**(12): p. 3316-3320.

14. Tomaszewski, W., et al., *Poly(L-lactide) Nano- and Microfibers by Electrospinning: Influence of Poly(L-lactide) Molecular Weight.* Macromolecular Symposia, 2008. **272**(1): p. 70-74.

15. Gu, S.-Y. and J. Ren, *Process Optimization and Empirical Modeling for Electrospun Poly(D,L-lactide) Fibers using Response Surface Methodology.* Macromolecular Materials and Engineering, 2005. **290**(11): p. 1097-1105.

16. http://rsbweb.nih.gov/ij/index.html, *Image J.* 2009

17. Jun, Z., et al., *Poly-L-lactide nanofibers by electrospinning - Influence of solution viscosity and electrical conductivity on fiber diameter and fiber morphology.* E-Polymers, 2003.

18. Takasaki, M., H. Ito, and T. Kikutani, *Development of Stereocomplex Crystal of Polylactide in High-Speed Melt Spinning and Subsequent Drawing and Annealing Processes.* Journal of Macromolecular Science, Part B, 2003. **42**(3-4): p. 403-420.

19. Zong, X., et al., *Structure and process relationship of electrospun bioabsorbable nanofiber membranes.* Polymer, 2002. **43**(16): p. 4403-4412.

20. Huang, Z.M., et al., *A review on polymer nanofibers by electrospinning and their applications in nanocomposites.* Composites Science and Technology, 2003. **63**(15): p. 2223-2253.

21. Katta, P., et al., *Continuous Electrospinning of Aligned Polymer Nanofibers onto a Wire Drum Collector.* Nano Letters, 2004. **4**(11): p. 2215-2218.

22. Pawlowski, K.J., et al. *Electrospun electroactive polymers for aerospace applications*. 2003.

23. Zhou, H., T.B. Green, and Y.L. Joo, *The thermal effects on electrospinning of polylactic acid melts.* Polymer, 2006. **47**(21): p. 7497-7505.

24. Tsuji, H., et al., *Stereocomplex formation between enantiomeric poly(lactic acid). VIII. Complex fibers spun from mixed solution of poly(D-lactic acid) and poly(L-lactic acid).* Journal of Applied Polymer Science, 1994. **51**(2): p. 337-344.

25. Zeng, J., et al., *Enzymatic Degradation of Poly(L-lactide) and Poly(ε-caprolactone) Electrospun Fibers.* Macromolecular Bioscience, 2004. **4**(12): p. 1118-1125.

26. Inai, R., M. Kotaki, and S. Ramakrishna, *Deformation behavior of electrospun poly(L-lactide-co-ε-caprolactone) nonwoven membranes under uniaxial tensile loading.* Journal of Polymer Science Part B: Polymer Physics, 2005. **43**(22): p. 3205-3212.

27. Migliaresi, C., et al., *Dynamic mechanical and calorimetric analysis of compression-molded PLLA of different molecular weights: Effect of thermal treatments.* Journal of Applied Polymer Science, 1991. **43**(1): p. 83-95.

28. Hernández Sánchez, F., et al., *Influence of Low-Temperature Nucleation on the Crystallization Process of Poly(l-lactide).* Biomacromolecules, 2005. **6**(6): p. 3283-3290.

29. Salmerón Sánchez, M., et al., *Effect of the Cooling Rate on the Nucleation Kinetics of Poly(l-Lactic Acid) and Its Influence on Morphology.* Macromolecules, 2007. **40**(22): p. 7989-7997.

30. Zhang, J., et al., *Weak Intermolecular Interactions during the Melt Crystallization of Poly(l-lactide) Investigated by Two-Dimensional Infrared Correlation Spectroscopy.* The Journal of Physical Chemistry B, 2004. **108**(31): p. 11514-11520.

31. Kiflie, Z., S. Piccarolo, and E. Vassileva, *Influence of physical cross-links in amorphous PET on room temperature ageing.* Macromolecular Symposia, 2002. **185**(1): p. 35-51.

32. Kang, S., et al., *A Spectroscopic Analysis of Poly(lactic acid) Structure.* Macromolecules, 2001. **34**(13): p. 4542-4548.

33. Mijović, J. and J.-W. Sy, *Molecular Dynamics during Crystallization of Poly(l-lactic acid) As Studied by Broad-Band Dielectric Relaxation Spectroscopy.* Macromolecules, 2002. **35**(16): p. 6370-6376.

34. Urayama, H., S.-I. Moon, and Y. Kimura, *Microstructure and Thermal Properties of Polylactides with Different L- and D-Unit Sequences: Importance of the Helical Nature of the L-Sequenced Segments.* Macromolecular Materials and Engineering, 2003. **288**(2): p. 137-143.

35. Branciforti, M.C., et al., *Characterization of Nano-Structured Poly(D,L-lactic acid) Nonwoven Mats Obtained from Different Solutions by Electrospinning.* Journal of Macromolecular Science, Part B, 2009. **48**(6): p. 1222-1240.

36. Kister, G., G. Cassanas, and M. Vert, *Effects of morphology, conformation and configuration on the IR and Raman spectra of various poly(lactic acid)s.* Polymer, 1998. **39**(2): p. 267-273.

37. Zhang, J., et al., *Crystal Modifications and Thermal Behavior of Poly(l-lactic acid) Revealed by Infrared Spectroscopy.* Macromolecules, 2005. **38**(19): p. 8012-8021.

38. Pan, P., et al., *Polymorphic Transition in Disordered Poly(l-lactide) Crystals Induced by Annealing at Elevated Temperatures.* Macromolecules, 2008. **41**(12): p. 4296-4304.

39. Zhang, J., et al., *Structural Changes and Crystallization Dynamics of Poly(l-lactide) during the Cold-Crystallization Process Investigated by Infrared and Two-Dimensional Infrared Correlation Spectroscopy.* Macromolecules, 2004. **37**(17): p. 6433-6439.

3. Fabrication of poly(lactic acid)-poly(ethylene oxide) electrospun membranes with controlled micro to nanofiber sizes

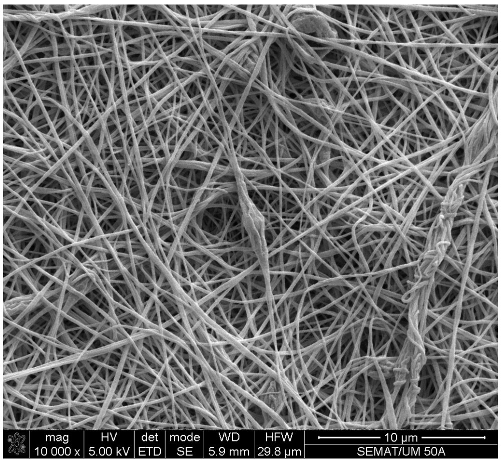
mag
10 000 x
HV
5.00 kV
det
ETD
mode
SE
WD
5.9 mm
HFW
29.8 µm
10 µm
SEMAT/UM 50A

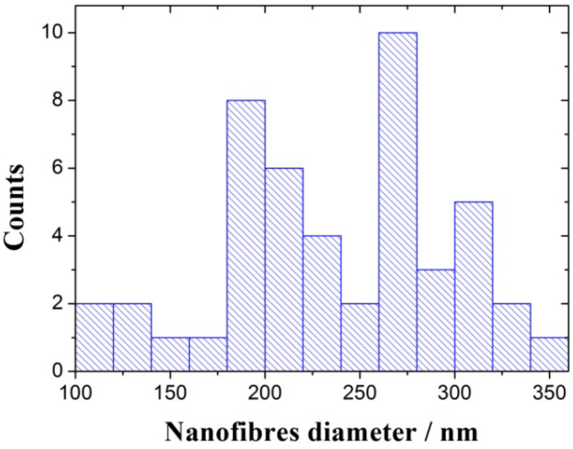

This chapter is based on the following publication: C. Ribeiro, V. Sencadas, C. Caparros, J. L. Gómez Ribelles and S. Lanceros-Méndez. *Fabrication of poly(lactic acid)-poly(ethylene oxide) electrospun membranes with controlled micro to nanofiber sizes*. Journal of Nanoscience and Nanotechnology. 2012. 12: 6746-6753.

3.1 Introduction

When the average diameter of polymer fibers are shrunk from micrometers to nanometers, there appear several interesting characteristics such as larger surface area to volume ratio, flexibility in surface functionalities and superior mechanical properties, when compared to any other known form of the material [1-2].

It has been found that morphological characteristics such as fiber diameter and the uniformity of the electrospun polymer fibers are dependent on parameters such as processing conditions, solution properties and environmental conditions [2].

Electrospinning has proven to be an excellent method for the synthesis of submicron- or nano-fibers from polymer solutions for a wide range of polymeric materials. The electrospinning process was described by Formhals at the beginning of the 1930s, towards the commercialization of textiles yarns [3]. This technique is relatively versatile, simple, fast and efficient. Electrospinning membranes have attracted interest to be used in biomedical applications, such as scaffolds for tissue engineering, sutures, implants and controlled drug delivery systems, but also in other applications including filtration, sensors, batteries, cell phones and for chemical warfare protection, among others. [4-6]. In all these applications fiber diameter and membrane porosity are among the key factors defining membrane performance.

Several processing parameters can influence the morphology and properties of the electrospun fibers. The most important ones are those corresponding to the initial polymer solution, the solution concentration and the molecular weight of the polymer [5]. Moreover, the parameters that control the jet formation and solvent evaporation are the flow rate through the needle, the needle diameter, distance from the tip to the collector, temperature, applied voltage, and the collection procedure, static or dynamic, using a rotating drum collector [7].

PLLA is a biodegradable polyester that has been used as a biomaterial for temporary therapeutic applications, controlled drug release, support for cell culture and tissue engineering. Its degradation by simple hydrolysis of the ester backbone in aqueous environments such as body fluids makes it a good candidate for the implementation of temporary applications.

There are several works showing the effect of the electrospinning processing parameters on the morphology of PLLA fibers [7-10]. Tsuji *et al.* found that the fiber diameter decreases with increasing applied voltage [8]. Tomaszewski *et al.* studied the effect of PLLA molecular weight and viscosity of spinning solutions in fiber thickness [9]. Gu and Ren investigated the influence of applied voltage and polymer concentration on fiber diameter, and found that fiber diameter tended to increase with increasing polymer concentration and decreases with increasing applied voltage [10]. The influence of solution viscosity and electrical conductivity on fiber diameter and morphology was also investigated [11]. It was found that by reducing the PLLA concentrations in the solution the fiber diameter decreases but, on the other hand, the formation of beaded fibers was observed. The formation of beads can be reduced nevertheless by increasing the electrical conductivity of the solution.

Despite these efforts, the precise knowledge for controlling the electrospinning parameters in order to obtain fibers with the desired morphology, crystallinity and molecular structure is still lacking, in particular in the case that nanosize fibers are to be obtained.

The processing of an inorganic nanocomponent or polymer into another kind of polymer or inorganic matrix by using electrospinning has been also studied by several authors [12]. By co-electrospinning of two components that can be dissolved in a common solvent, composite nanofibers can be obtained after the solvent evaporation. The basic idea is to synthesize composite nanofibers allowing to provide new properties to the composite materials or to control the fiber morphology [12]. Several studies prove that it is possible to control the morphology of the composite nanofibers by proper understanding the electrospinning process. As an example, Jing and coworkers prove to obtain core/shell nanofibers of poly(ethylene oxide)/poly(ethylene glycol)-poly(l-lactic acid) (PEO/PEG-PLA) by electrospinning [13]. It was observed that the polymer with higher viscosity moves into the center of the electrospun fibers and the component with lower viscosity is located outside. Additionally, as solvent evaporation is fast, the formation of core/shell fibers occurs in blend system with high molecular mobility. In this way, polymer blends with lower molecular weight tend to form core/shell fibers rather than a co-continuous structure, as a result of their higher molecular mobility [14].

Poly(ethylene oxide) is a semi-crystalline hydrophilic polymer with high potential for biomedical applications, due to its good biocompatibility and low toxicity.

Miscibility and phase separation of PLLA and PEO have been studied by several authors [15-18]. It was found that melting point reduction of both PLLA and PEO polymers occurs, in particular at PEO contents below 0.2 weight fraction. It was also suggested that the inclusion of the two polymer molecules occurs in the amorphous state [18]. Nakafaku studied the melting and crystallization behavior under pressure, assuming its semi-miscible behavior. However, it is claimed that the melting and crystallization behavior under different synthesization parameters is different depending on the molecular weight of the PLLA and PEO [19].

Although the influence of the parameters of the electrospinning process on fiber diameter has been well analyzed in PLLA, the information on the conditions required to obtain ultra-fine nanofibers is scarce yet. In this work, PLLA and PEO blends were prepared by electrospinning in order to achieve PLLA membranes with nanosize fibers. The influence of the PEO in the blend electrospinning process is discussed, and the results are correlated to the evolution of the PLLA fiber diameter. The selective removal of PEO by water gives origin to smaller fiber diameter and to increased porosity of the membranes in comparison to the PLLA membranes obtained under the same electrospinning conditions. This study shows therefore an easy route to obtain nanosized fiber PLLA porous membranes with large application potential in the biomedical field.

3.2 Experimental

Materials: PLLA with a average molecular weight of 217.000 – 225.000 g.mol^{-1}, Purasorb PL18 (*Purac*) and PEO with an average molecular weight of 100.000 g.mol^{-1} (*Polysciences*) were dissolved in a mixture of DMF (*Merck*) and MC (*Sigma-Aldrich*) (3/7 vol/vol) to achieve a polymer concentration of 10 wt.% of the total solution. The PLLA/PEO blends used in this work contained 75% and 50% by weight respectively of PLLA. The polymer blend was dissolved at room temperature in a magnetic stirrer until complete polymer dissolution.

Electrospinning: The polymer solution was placed in a commercial plastic syringe (10 mL) fitted with a steel needle with 500 μm of inner diameter. Electrospinning was conducted at 20 kV with a high voltage power supply (*Glassman,* model PS/FC30P04). A syringe pump (*Syringepump*) was used to feed the polymer solution into the needle tip at rate between 2 mL.h^{-1}. The electrospun fibers were collected in a ground collecting plate (random fibers), placed at 15 cm from the needle.

Characterization: Electrospun fiber samples after and before PEO removal in water were coated with a thin gold layer using a sputter coating (*Polaron,* model SC502 sputter coater) and their morphology was analyzed using a SEM (model JSM-6300, *JEOL*) with an accelerating voltage of 5 kV. The nanofibers average diameter and its distribution was calculated over approximately 50 fibers using de SEM image (5000X magnification) and the Image J software [20]. A scanning probe microscope (Model 5500, *Agilent*) was employed for the atomic force microscopy (AFM) analysis of the samples before and after PEO removal.

FTIR measurements were performed at room temperature in a Perkin-Elmer Spectrum 100 apparatus in attenuated total reflection (ATR) mode from 4000 to 650 cm^{-1}. FTIR spectra were collected with 32 scans and a resolution of 4 cm^{-1}.

The thermal behavior of the electrospun fiber mats was analyzed by DSC (measurements with a *Perkin Elmer Diamond* DSC apparatus). The samples were cut into small pieces from the middle region of the electrospun membranes, placed into 40 μl aluminum pans and heated between 30 and 200 ºC at a heating rate of 10 ºC.min^{-1}. All experiments were performed under a nitrogen purge. T_g, T_{CC}, T_m, ΔH_{CC}, ΔH_m and ΔX_C of all electrospun samples were obtained.

Thermogravimetric analysis (TGA) was carried out in a *Perkin-Elmer* Pyris-1 TGA apparatus from 30 to 700 ºC at 20 ºC.min^{-1} under a nitrogen atmosphere.

Due to the porous nature of the membrane, which is fully opened and interconnected, a suitable method to estimate the porosity of the samples is the pycnometer test. In this work, and due to nature of the polymers used (PEO is water soluble), the porosity of the samples were measured by an improved weight-method. The weight of the pycnometer, filled with ethanol, was weighted and labeled as W1; the sample, whose weight was Ws, was immersed in ethanol. After the pores of the membranes were saturated by ethanol, additional ethanol was added to complete the volume of the pycnometer. Then, the pycnometer was weighted and labeled as W2 and the sample filled with ethanol was taken out of the pycnometer. The residual weight of the ethanol and the pycnometer was labeled. The porosity of the scaffold was calculated according to

$$\varepsilon = \frac{W_2 - W_3 - W_s}{W_1 - W_3} \qquad \text{(Eq. 3.1)}$$

The porosity of each membrane was obtained as the average of the values determined in three samples.

Hydrolytic degradation: *In vitro* degradation of PLLA fibers with initial crystallinity of 0, 20, 30 and 45% and fiber size of 235 ± 58, 583 ± 225 and 1883 ± 363 was carried out in PBS. The samples were cut into squares of 15 x15 mm^2 (triplicate samples were used for statistical purposes), immersed in 15 mL of PBS (pH 7.4; 0.8 g NaCl; 0.2 g KCl; 1.44 g $Na_2HPO_4.2H_2O$ and 0.2 g KH_2PO_4 dissolved in 1 L of distilled water) and incubated in an air circulation oven (HERAEUS Vacuotherm) at 37 ºC over 20 weeks. The pH of the PBS solution was measured and renewed every 48 h. After various periods of degradation one of the membrane samples was removed from the PBS, washed with deionized water and dried in a vacuum oven (JP SELECTA (VacuoTherm)) at 30 ºC for 48 h. DSC, SEM and gel permeation chromatography (GPC) -(*Waters 1525 Binary HPLC* pump, 4 columns *Styragel® HR1THF 7,8X300mm Waters HPLC*) performed at 35 ºC with tetrahydrofuran as solvent, using a refractive index detector (*Waters 2414*)- was performed after 2, 14 , 28 and 140 days.

3.3 Results and discussion

3.3.1 Scanning electron microscopy

Electrospinning of PLLA generally results in fibers with diameters in the range between 0.6 – 6.0 µm, depending on the variation of the selected processing parameters [21]. Ultra-fine nanofibers with average diameter lower than 100 nm are obtained using a mixture of solvents like dichloromethane/pyridine [2].

A quite high number of parameters have influence in the electrospinning process and any study must fix some of them [1, 22]. In this work, solutions of PLLA and PEO in a blended solution of MC and DMF has been used. The high polarity of the DMF facilitates the fiber formation while the high volatility of the MC allows a quick evaporation from the fiber, maintaining the integrity of the fiber during the traveling from the tip of the needle to the target.

Once the PLLA-PEO membranes are obtained, PEO was removed by immersing the membranes in deionized water. After 24 h, the samples were dried at 40 ºC until they reach a constant mass. The PEO was in this way fully removed from the PLLA-PEO electrospun fiber mesh, which is accompanied by a mass reduction of 25 and 50% of the membrane, respectively. Figure 3.1 shows the SEM images of the obtained membrane for the PLLA-PEO samples with 50 and 75% of PLLA, before the PEO removal, and the respective fiber diameter distribution. It is observed that all fibrils present a very smooth surface and that the obtained membranes are very porous.

From figure 3.1, it is possible to observe that the amount of PEO in the sample strongly influences the fiber distribution in the electrospun mesh. For the sample with 75% of PLLA and 25% of PEO, the fiber average diameter was 447 ± 115 nm (figure 3.1 c)) and d)), but for the sample with 50% of PLLA and 50% of PEO a reduction of the fiber average diameter to 262 ± 70 nm (figure 3.1 a) and b)) was observed. The samples obtained under the same processing conditions for pure PLLA sample has an average fiber diameter of 1000 nm ± 300 nm, as can be observed in figure 3.2.

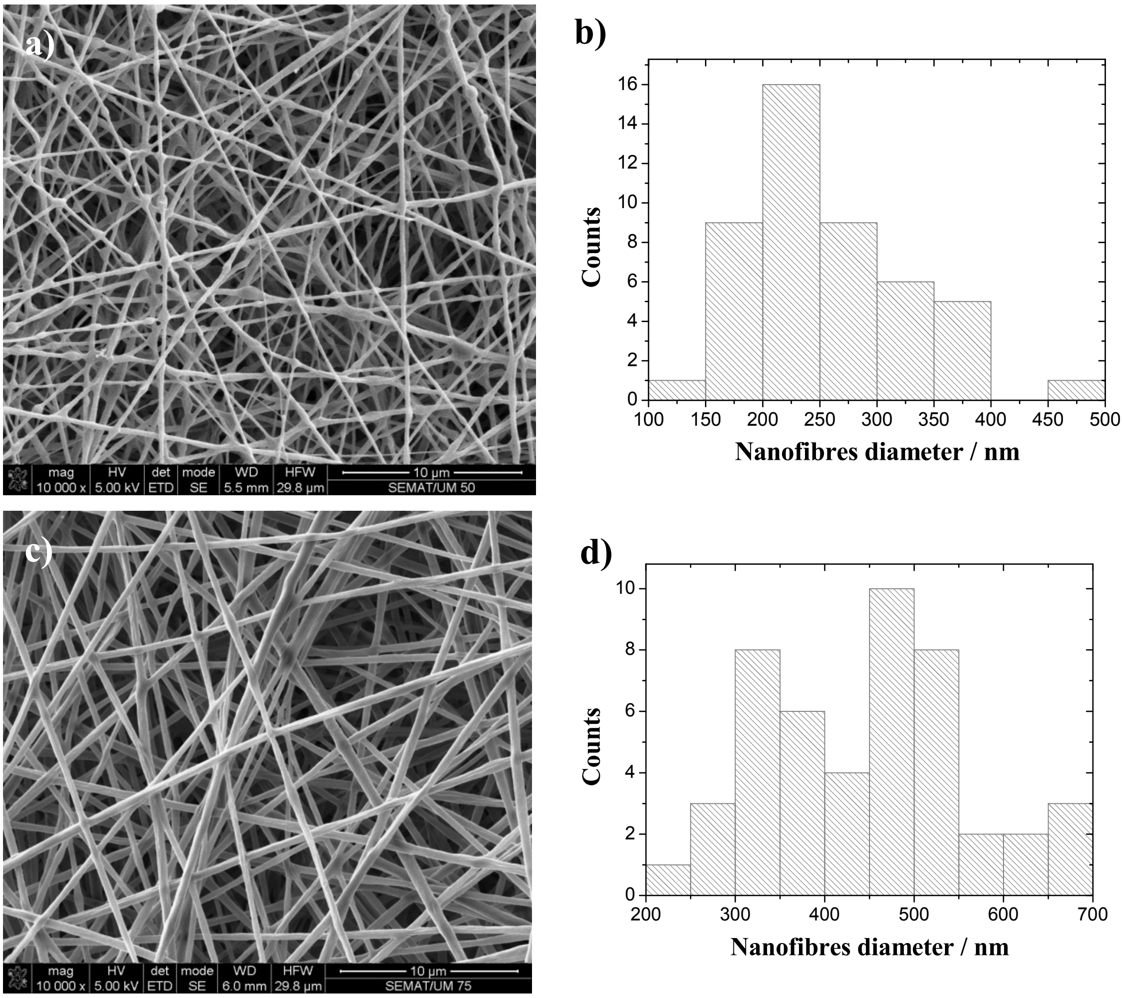

Figure 3.1 – Morphology of the PLLA-PEO membranes before PEO removal: **a)** SEM image of the sample with 50% of PLLA, **b)** Fiber distribution for the 50/50 PLLA-PEO membrane, **c)** SEM image of the sample with 75% of PLLA sample, **d)** Fiber distribution for the 75/25 PLLA-PEO scaffold.

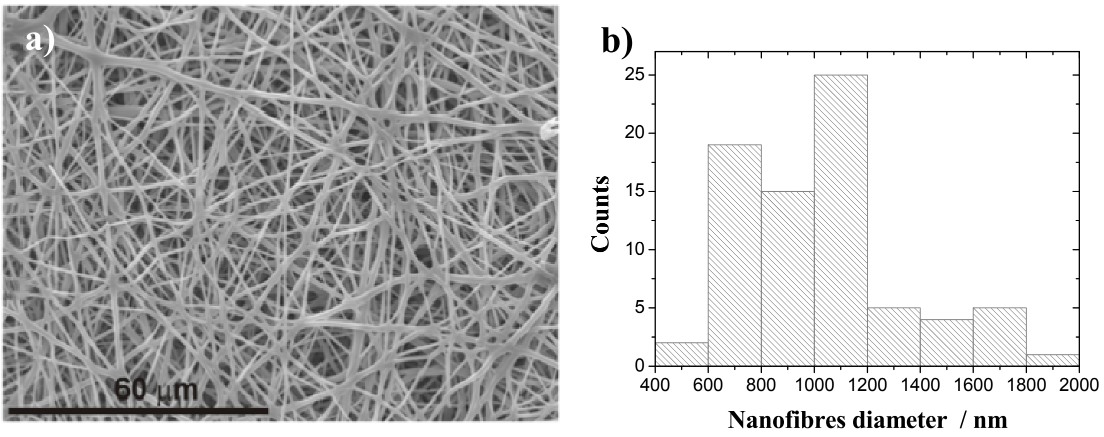

Figure 3.2 – PLLA membrane obtained for the pure polymer by electrospinning at 20 kV with a 0.5 mm inner diameter needle placed at 15 cm from the collector.

This decrease of the nanofiber diameter with increasing PEO leads to the conclusion that the critical electric field needed to start the Taylor cone and consequently the polymer jet for the PLLA and PEO are not the same, being smaller for the PEO polymer. Therefore, the influence of the applied voltage on both polymer chains is not the same.

The electric field is the drive motor to the jet initiation. In general, once the electric field is applied on the droplet of the polymer solution at the tip of the spinneret, the liquid surface becomes charged due to the motion of the ions through the liquid. When the electric field is high enough such that the electric force overcomes the forces associated to the surface tension, a quasi-stable, straight and electrically charged jet is ejected [1, 22]. The balance between the surface tension and the electric force is critical to determine the initial cone shape of the polymer solution at the needle tip. It was observed in our samples that the diameter of the nanofibers for the solution with PLLA polymer is larger than for the PLLA-PEO blend solution.

The mechanisms behind the electrospinning technique are not well understood in detail so far and some intuitive conjectures are given as follows to explain the observed facts. In the case of the PLLA-PEO electrospun nanofibers, the critical electric field at which the repulsive electrostatic forces overcome the surface tension are not the same for both polymers. The discharge polymer solution undergoes instability and elongation process, which allows the jet to become very long and thin and, in this stage, is the elongation of the PEO in the solution that stretches the PLLA present in the solution, giving origin to PLLA nanofibers with smaller diameter for the membranes with higher PEO content (figures 3.1 and 3.2).

Another explanation for the significant reduction on the fiber diameter is related to the viscosity of the solution that decreases in the presence of the PEO [15-16].

After removal of the PEO from the polymer mesh by immersing the scaffold in water, the fiber distribution, morphology and geometry was characterized by SEM, and the results are shown in figure 3.3.

It was observed that for the case of the PLLA-PEO electrospun polymer blend the average diameter of the nanofibers decrease in both cases after removal of the PEO, being more pronounced for the 75/25 PLLA-PEO polymer blend. The average diameter found for the samples with 75/25 of PLLA-PEO suffer a reduction from 447 ± 115 nm to 353 ± 80 nm, and for the 50/50 PLLA-PEO, that reduction was not so pronounced, and the average diameter of the nanofibers decreased from 262 ± 70 nm to 235 ± 58 nm (figure 3.3). The fact that the average fiber diameter decreases more for the fibers with lower PEO content shows that in this case lager amounts of PEO are located at the surface of the fibers than in their interior. Therefore, a complete random distribution of PLLA and PEO all along the fiber is not observed. Due to the semimiscible nature of the polymers [9], for larger PLLA contents, phase separation is more provable to occur and due to the lower relative density of the PEO in the solution it is drag to the fiber surface. This process cannot take place completely before solvent evaporation in the PLLA-PEO solution with 50% of each phase, where a more random polymer distribution all along the fibers are obtained, with larger amounts of PEO located at the interior of the fibers.

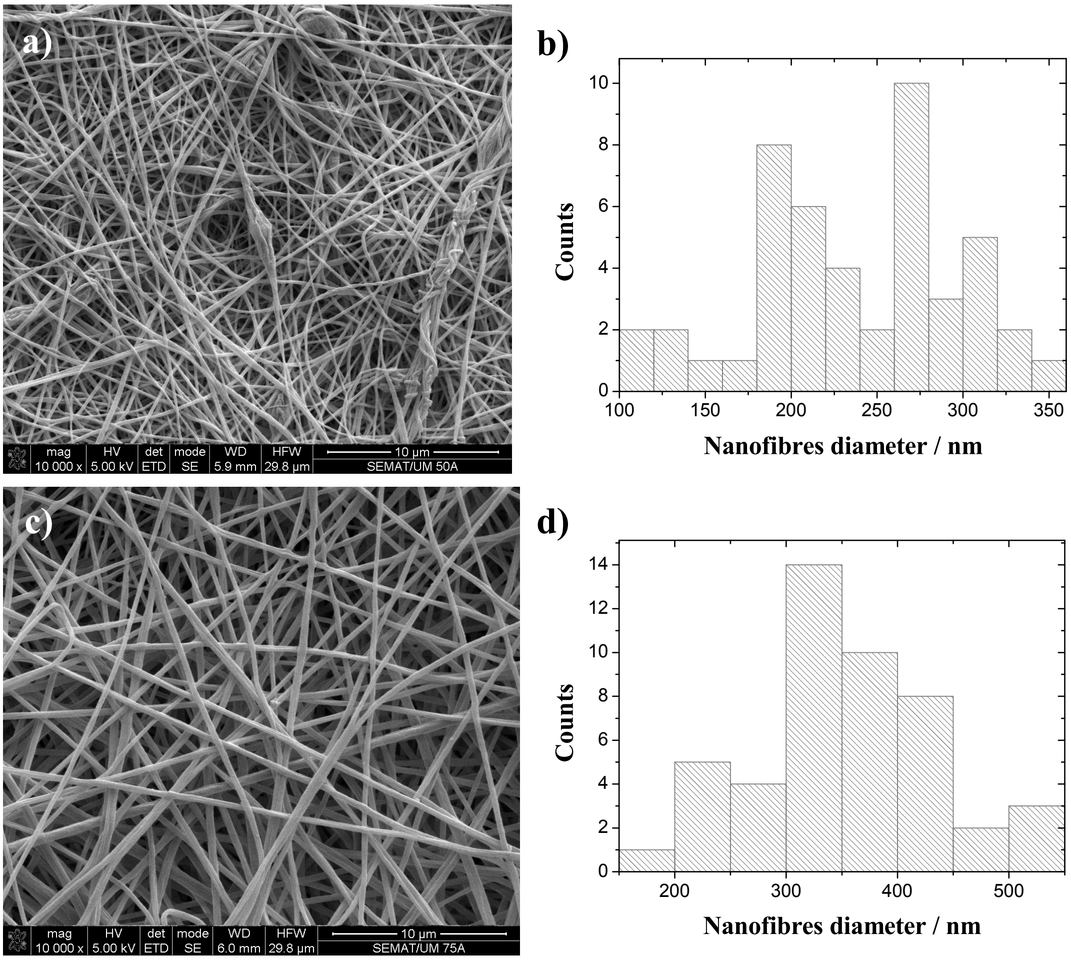

Figure 3.3 – Morphology of the PLLA-PEO scaffolds after PEO removal: **a)** SEM image of the sample with 50% of PLLA, **b)** Fiber distribution for the 50/50 PLLA-PEO membrane, **c)** SEM image of the membrane with 75% PLLA, **d)** Fiber distribution for the 75/25 PLLA-PEO membrane.

In order to understand the influence of the PEO on the PLLA electrospun fibrils, the topography of the samples was characterized by AFM (figure 3.4). It can be observed that the electrospun fibers of the PLLA-PEO blend are quite smooth (figure 3.4 a)), but on the other hand, after PEO removal, the presence of higher roughness and porosity indicates that when processed, PLLA and PEO crystallizes along the nanofiber in a random distribution, and after water dissolution of the PEO polymer from the membrane, the volume occupied by this one gives rise to small pores distributed along the fiber structure, resulting therefore in a higher roughness of the electrospun PLLA remaining fibers.

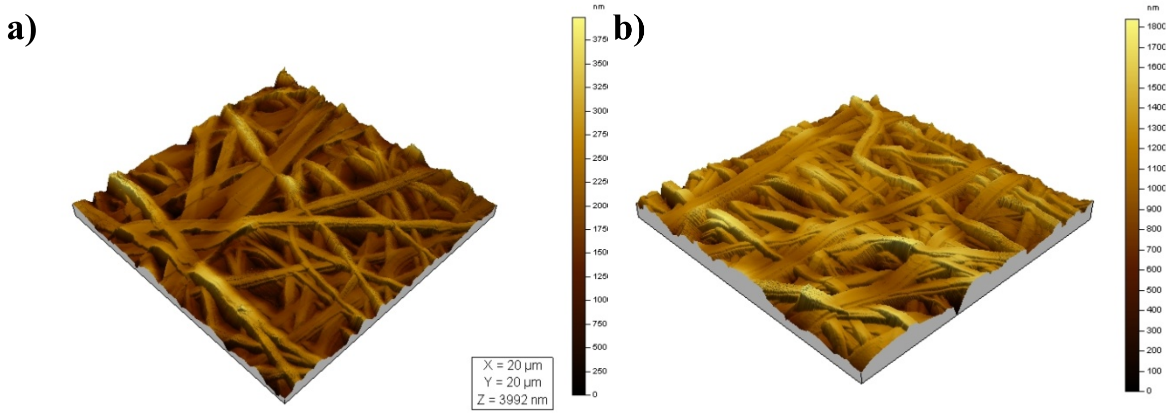
a)
nm
375
350
325
300
275
250
225
200
175
150
125
100
750
500
250
0
X = 20 µm
Y = 20 µm
Z = 3992 nm
b)
nm
1800
1700
1600
1500
1400
1300
1200
1100
1000
900
800
700
600
500
400
300
200
100
0

Figure 3.4 – AFM topographic surface images of the PLLA-PEO (50/50) sample: **a)** before PEO removal and **b)** after PEO removal in water for 24 h.

Finally, the porosity of the membranes was calculated according to equation 3.1 and the results are presented in table 3.1.

Table 3.1 – Porosity of the PLLA-PEO samples for different PEO contents before and after PEO removal.

PEO Amount (%)	Porosity before PEO Removal (%)	Porosity After PEO Removal (%)
0	66 ± 3	-
25	70 ± 3	75 ± 3
50	71 ± 3	79 ± 4

The electrospun mats of the PLLA with PEO have similar porosity than the one found for the pure PLLA polymer membrane. Just a slight increase of the porosity is observed for the PLLA-PEO membranes, when the PEO was removed. These facts support that, despite larger amounts of PEO are at the surface of the fibers for the PLLA-PEO 75/25 samples, as the fiber average diameter decreases more than in the 50/50 membranes, basically a random distribution of PEO and PLLA along the fibers is observed. Other ways, larger diminution of the fiber diameter and increase of the fiber porosity will occur by removing the relatively large quantity of PEO material from the membranes.

3.3.2 Thermal behavior

Figure 3.5 shows the thermo-gravimetric analysis for the pure PLLA, PEO and blends. For the pure materials, as expected, one single degradation process was observed. The degradation of PEO occurs at higher temperatures when compared to pure PLLA. In the case of the polymer blends, two main degradation processes were observed. The first one was due to the PLLA and the second one to the PEO thermal degradation processes, respectively (figure 3.5). It was also observed that the blends have less thermal stability than the pure PLLA and the T_{onset} of the blends occurs at lowest temperatures when compared to the pure polymers. It is also noticed that the increase of the PEO content in the polymer blend decreases the T_{onset} of the blend (figure 3.6).

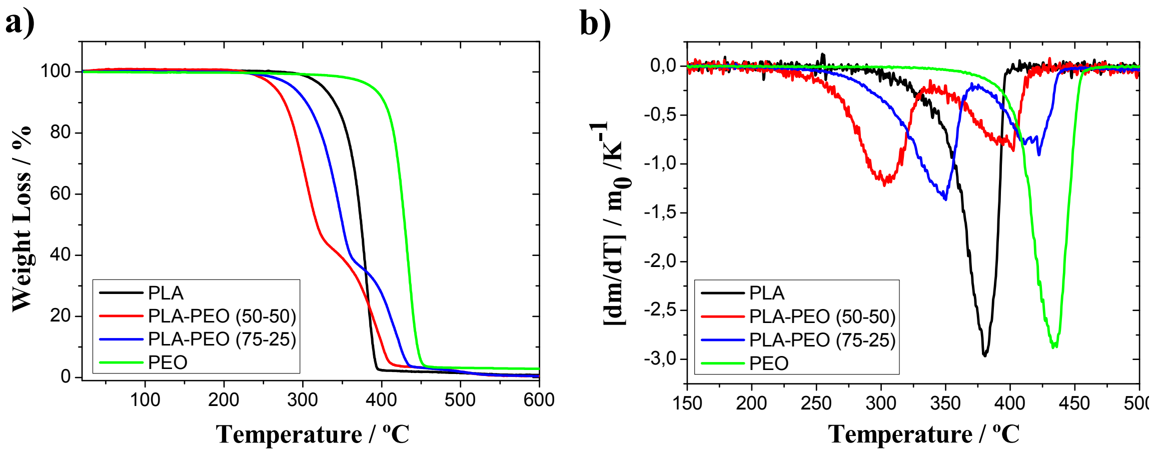

Figure 3.5 – a) TGA data for pure PLLA and PEO samples, as well as for the PLLA-PEO and **b)** DTG curves for the obtained scaffolds.

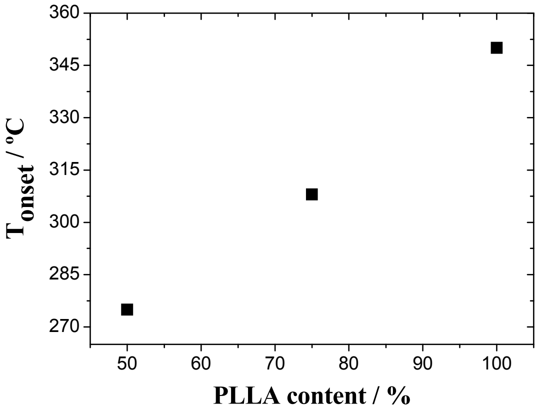

Figure 3.6 – Evolution of the T_{onset} for the PLLA-PEO blends.

The jet instability and deformation with fast solidification during the electrospinning process often results in a meta-stable phase [23]. Since PLLA is a slowly crystallizing polymer and its glass transition temperature is above room temperature, the samples collected at room temperature maintain a stable crystalline fraction. As mentioned in the literature [24-25], PLLA electrospun fibers from solution usually exhibits a cold-crystallization peak in DSC heating scans performed at 10 ºC min^{-1}. Figure 3.7 shows the first run of the DSC heating scans performed on electrospun PLLA, PEO as well as for the electrospun blends.

In figure 3.7, the endothermic peak of PEO appears at about 56 ºC. One method to evaluate the miscibility of the polymers in the blend is the measurement of the variation of T_g with the change of the weight fraction of the blend. The glass transition temperature in the miscible amorphous polymer blend changes continuously between the T_g temperatures of the polymer components. In the case of the immiscible pair of blends, two glass transition temperatures appear separately due to the mixed polymers, and they not change with the weight fraction [26]. In this polymer blend, the T_g of the PLLA appears in the same temperature range and the variations of the glass transition temperature of the PLLA with the weight faction is very difficult to detect, as it can be observed in figure 3.7 a).

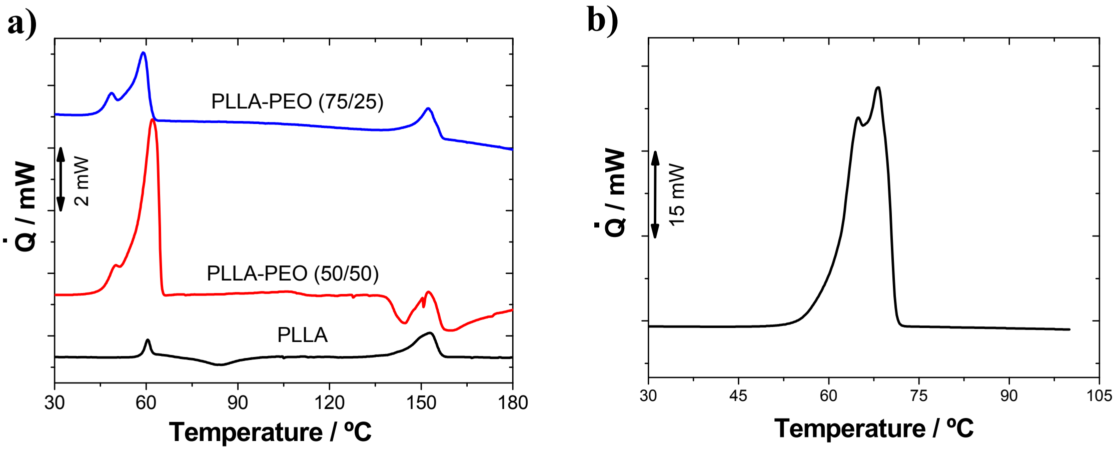

Figure 3.7 – DSC normalized thermograms of: **a)** electrospun PLLA and blend samples and **b)** first heating scan of the pure PEO mesh.

T_g of the PEO appears at about - 60 ºC and the changes in the T_g of the PEO should be detected. Nakafuku [18] showed that the T_g of the PEO increase slightly with the decreasing of the weight fraction of the PEO, but the increasing rate was very small, much smaller than the value that could be predicted using Fox equation. The authors concluded that PLLA and PEO molecules are semimiscible [18].

The melting peak of the PLLA and PEO appears in the blends but the re-crystallization peak of the PLLA only is clearly observed in the PLLA-PEO (50/50) blend during heating. The temperature corresponding to the peak of the melting of the PLLA in the blends is quite similar to the one observed to the pure PLLA.

In pure PLLA, a large overshot can be observed in the region of the glass transition, around 54 ºC. This endothermic peak can be ascribed to the recovering of enthalpy of the sample stored at room temperature, around 30 ºC below T_g and thus subjected to physical ageing. The effect is also observed in the blends by a small peak that appears at low temperature just before the melting temperature of the PEO and is more pronounced for the blend with 75% PLLA. The melting temperature of the PEO in the blends slightly increases with increasing amount of PEO present in the sample. Some authors attribute this effect to morphological effects (lamellar size effects) [18]. They point that the crystallization of the PEO is hindered by the PLLA molecule, because it is possible that the PEO crystallize between the lamellae of the crystallized PLLA.

3.3.3 Infrared spectra

Infrared measurements do not reveal any new vibrational modes or significant shifts of the peak frequencies with respect to the characteristic absorption bands of the pure components of the blends, what still supports the phase separation of the two polymers in the blend.

FTIR spectra show that the PLLA-PEO membranes are composed by almost amorphous PLLA nanofibers and by high crystalline PEO electrospun nanofibers, in good agreement with DSC results and the morphology variations of the fibers after PEO removal.

The absence of the absorption band at 921 cm^{-1} in pure PLLA reveals that the polymer crystallizes into α-crystals with the distorted 10_3 helix conformation from solution or melt. Kister *et al.* reported that an absorption band at 921 cm^{-1} is characteristic of the α-crystals [27]. Kang *et al.* assigned this vibrational band associated to the transition moment perpendicular to the chain axis to the CH_3 rocking mode combined with a minor contribution from the C–COO and O–CH stretching modes of the α-crystals [28]. In our membranes there is a lack of the characteristic band of the PLLA β crystal at 908 cm^{-1} [29-30], which reveals the nonexistence of this kind of crystalline structure neither in the samples as obtained by electrospinning of the pure PLLA nor in the PLLA-PEO electrospun blends (figure 3.8).

After removal of the PEO polymer from the blend by immersing the scaffold in water for 24 h the infrared spectra of the sample only present the characteristic absorption bands of the PLLA, without any distinctive absorption band of the PEO polymer, which is in agreement with the thermal results, showing the poor miscibility of the PLLA and PEO and that the PEO is completely removed from the samples.

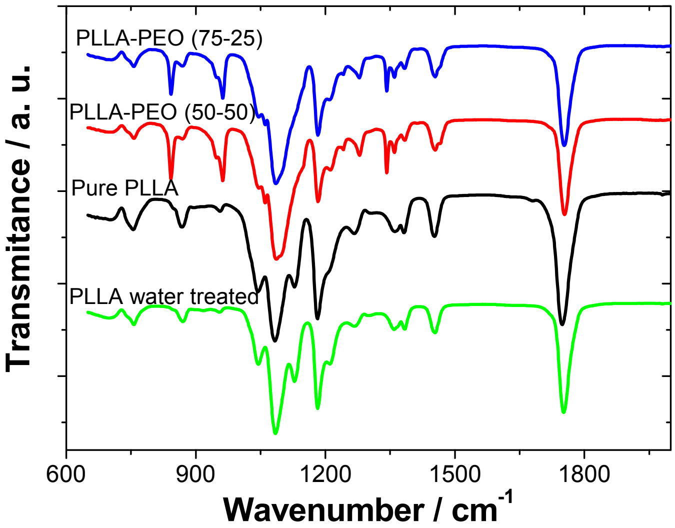

Figure 3.8 – Detail of FTIR spectra in the 650-2000 cm^{-1} region for the pure PLLA and for the PLLA-PEO blend membranes.

3.3.4 Hydrolytic degradation

The influence of morphology, fiber diameter and degree of crystallinity on the degradation of the obtained PLLA membranes was studied by placing the samples in PBS at 37 ºC over 20 weeks and evaluating regularly the variation of the sample characteristics.

The average fiber diameter of the membranes and the degree of porosity were measured at different hydrolytic degradation periods in order to study the effect of the swelling in the PLLA material. The porosity of the electrospun PLLA membranes remained unchanged during the thermal annealing process performed to obtain the desired crystalline fractions. As a general trend, a slight increase of the average fiber diameter is observed for the electrospun PLLA samples with increasing degradation time, this effect being independent of the degree of crystallinity of the samples. With respect to the average porosity, a decrease is observed in all samples and the decrease is larger for the samples with smaller mean diameter (∅ = 235 nm), where the porosity decreases almost 30% (from 79% before degradation to 48% after 20 weeks hydrolytic degradation). For the samples with higher average fiber diameter, just a slight decrease of the porosity is observed (Table 3.2).

Table 3.2 – Evolution of average fiber diameter and porosity for the samples after 20 weeks hydrolytic degradation.

Fiber diameter prior to degradation (nm)		**Fiber diameter for 20 weeks (nm)**		**Porosity prior to degradation (%)**	**Porosity after 20 weeks degradation (%)**
ΔX = 0%	**ΔX = 45%**	**ΔX = 0%**	**ΔX = 45%**	**ΔX= 0% and 45%**	**ΔX= 0% and 45%**
235 ± 70	315 ± 55	321 ± 76	353 ± 90	79	48
583 ± 225	737 ± 146	703 ± 139	826 ± 203	66	52
1883 ± 363	1859 ± 330	1844 ± 588	2133 ± 453	66	62

The influence of hydrolytic degradation on the samples surface and fiber morphology was analyzed by SEM and it was observed that sample structure remains unchanged for all fiber diameters and degrees of crystallinity (figure 3.9).

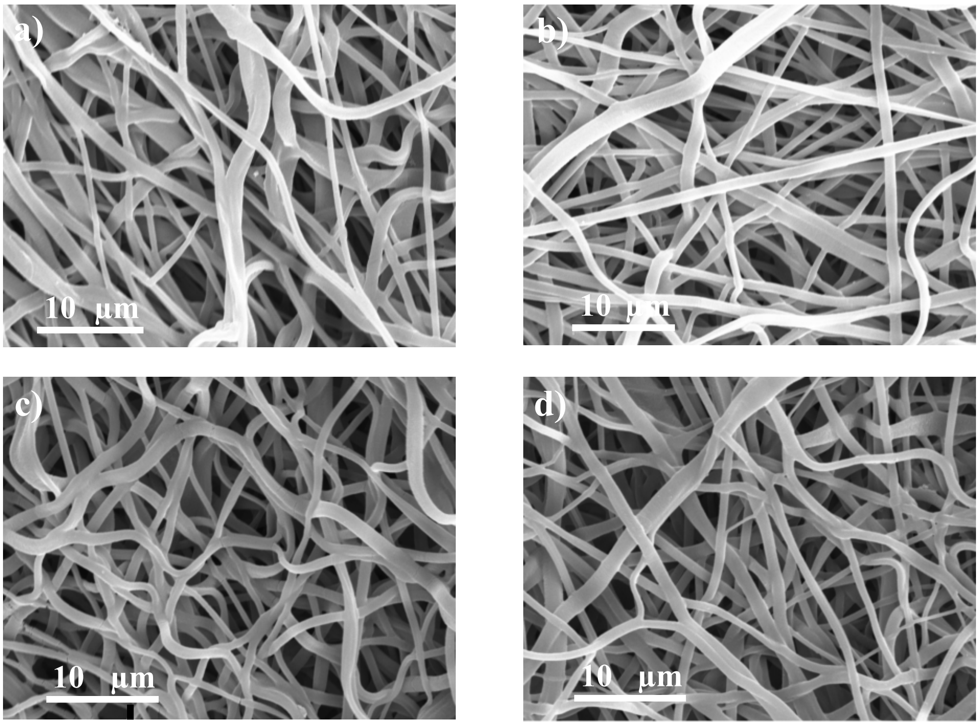

Figure 3.9 – SEM micrographs for the PLLA membranes with 583 nm average diameter and 45% crystallinity after different *in-vitro* degradation time: a) 2 days, b) 14 days, c) 28 days and d) 140 days.

Degradation of samples in PBS up to 20 weeks produced only a slight decrease in the sample mass and no variation in the degree of crystallinity. Nevertheless, polymer average molecular weight, as obtained by gel permeation chromatography, decreased clearly in amorphous fibers. The degradation effect in molecular weight is less important as the fiber crystallinity increases. Interestingly, as indicated before, morphological characteristics of the membranes are affected by degradation: average fiber diameter increases while membrane porosity decreases, i.e., the fibers are packed closer together, probably due to the release of internal tensions. The observed variations are just significant after 4 weeks, therefore, for the cell culture times used with these membranes, the degradation process has no effects on sample characteristics.

3.4 Conclusions

Electrospinning of PLLA-PEO blends can be achieved from the solution of both polymers in a common solvent: a mixture of MC and DMF. In this way, electrospun membranes can be prepared with tailored fiber diameter from some micrometers for pure PLLA membranes to few hundreds of nanometers by electrospinning of PLLA-PEO solution. The mean diameter of the fibrils in the electrospun mat decreases with increasing PEO content in the blend, which also broadens the diameter distribution. This fact is due both the larger interaction of PEO with the electric field, dragging also the PLLA material, and to the reduction of the solution viscosity with increasing PEO content. The PLLA-PEO membranes are composed by almost amorphous PLLA nanofibers and by high crystalline PEO electrospun nanofibers. PEO extraction from the electrospun blend is complete. This extraction decreases slightly the mean diameter of the fibers (from 260 nm to 235 nm for the PLLA-PEO 50/50 membrane) and increases membrane porosity (from 71% to 75% for the PLLA-PEO 50/50 membrane). These facts indicate that PEO and PLLA are phase separated and nearly randomly distributed along the nanofibers.

3.5 References

1. Seeram Ramakrishna, et al., *An introduction to electrospinning and nanofibers*. 2005, Singapore: World Scientific Publishing Co. Pte. Ltd.

2. Tan, S.H., et al., *Systematic parameter study for ultra-fine fiber fabrication via electrospinning process*. Polymer, 2005. **46**(16): p. 6128-6134.

3. Formhals, A., *Process and apparatus for preparing artificial threads*. 1934: United States. p. 4.

4. J. Venugopal, Y. Z. Zhang, and S. Ramakrishna, *Electropsun Nanofibers: Biomedical applications.* Proceedings of the institution of mechanical engineers, Part N: Journal of nanoengineering and nanosystems 2005. **218**(1): p. 35-45.

5. S. Ramakrishna, et al., *An introduction to electrospinning and nanofibers*. 2005, Singapore: World Scientific.

6. S. G. Kumbar, et al., *Recent Patents on Electrospun Biomedical Nanostructures: An overview* in *Recent Patents on Biomedical Engneering*. 2008. p. 68-78.

7. Pan, H., et al., *Continuous aligned polymer fibers produced by a modified electrospinning method.* Polymer, 2006. **47**(14): p. 4901-4904.

8. Tsuji, H., et al., *Electrospinning of Poly(lactic acid) Stereocomplex Nanofibers.* Biomacromolecules, 2006. **7**(12): p. 3316-3320.

9. Tomaszewski, W., et al., *Poly(L-lactide) Nano- and Microfibers by Electrospinning: Influence of Poly(L-lactide) Molecular Weight.* Macromolecular Symposia, 2008. **272**(1): p. 70-74.

10. Gu, S.-Y. and J. Ren, *Process Optimization and Empirical Modeling for Electrospun Poly(D,L-lactide) Fibers using Response Surface Methodology.* Macromolecular Materials and Engineering, 2005. **290**(11): p. 1097-1105.

11. Jun Zeng, et al., *Poly-L-lactide nanofibers by electrospinning - Influence of solution viscosity and electrical conductivity on fiber diameter and fiber morphology.* e-Polymers, 2003. **009**: p. 1-9.

12. Lu, X., C. Wang, and Y. Wei, *One-dimensional composite nanomaterials: synthesis by electrospinning and their applications.* Small, 2009. **5**(21): p. 2349-2370.

13. Xu, X., et al., *Preparation of core-sheath composite nanofibers by emulsion electrospinning.* Macromolecular Rapid Communications, 2006. **27**(19): p. 1637-1642.

14. Wei, M., et al., *Core-sheath structure in electrospun nanofibers from polymer blends.* Macromolecular Materials and Engineering, 2006. **291**(11): p. 1307-1314.

15. M. Spasova, et al., *Preparation of PLLA/PEG Nanofibers by Electrospinning and Potential Applications.* Journal of Bioactive and Compatible Polymers, 2007. **22**(1): p. 62-76.

16. Spasova, M., et al., *Electrospun Chitosan-Coated Fibers of Poly(L-lactide) and Poly(L-lactide)/Poly(ethylene glycol): Preparation and Characterization.* Macromolecular Bioscience, 2008. **8**(2): p. 153-162.

17. Younes, H. and D. Cohn, European Polymer Journal, 1988. **24**: p. 765.

18. Chitoshi Nakafuku and M. Sakoda, *Melting and Crystallization of Poly(L-lactid acid) and Poly(ethylene oxide) Binary Mixture.* Polymer Journal, 1993. **25**(9): p. 909 - 917.

19. Nakafuku, C. and M. Sakoda, *Melting and crystallization of poly (L-lactic acid) and poly (ethylene oxide) binary mixture.* Polymer journal, 1993. **25**(9): p. 909-917.

20. http://rsbweb.nih.gov/ij/index.html, *Image J.* 2009.

21. Bognitzki, M., et al., *Nanostructured Fibers via Electrospinning.* Advanced Materials, 2001. **13**(1): p. 70-72.

22. Huang, Z.-M., et al., *A review on polymer nanofibers by electrospinning and their applications in nanocomposites.* Composites Science and Technology, 2003. **63**(15): p. 2223-2253.

23. Zhou, H., T.B. Green, and Y.L. Joo, *The thermal effects on electrospinning of polylactic acid melts.* Polymer, 2006. **47**(21): p. 7497-7505.

24. Zeng, J., et al., *Enzymatic Degradation of Poly(L-lactide) and Poly(ε-caprolactone) Electrospun Fibers.* Macromolecular Bioscience, 2004. **4**(12): p. 1118-1125.

25. Inai, R., M. Kotaki, and S. Ramakrishna, *Deformation behavior of electrospun poly(L-lactide-co-ε-caprolactone) nonwoven membranes under uniaxial tensile loading.* Journal of Polymer Science Part B: Polymer Physics, 2005. **43**(22): p. 3205-3212.

26. Paul, D.R., *Polymer Blends*. Vol. 1. 1978, New York: Academic Press.

27. Kister, G., G. Cassanas, and M. Vert, *Effects of morphology, conformation and configuration on the IR and Raman spectra of various poly(lactic acid)s.* Polymer, 1998. **39**(2): p. 267-273.

28. Kang, S., et al., *A Spectroscopic Analysis of Poly(lactic acid) Structure.* Macromolecules, 2001. **34**(13): p. 4542-4548.

29. Mijovic, J. and J.-W. Sy, *Molecular Dynamics during Crystallization of Poly(l-lactic acid) As Studied by Broad-Band Dielectric Relaxation Spectroscopy.* Macromolecules, 2002. **35**(16): p. 6370-6376.

30. Urayama, H., S.-I. Moon, and Y. Kimura, *Microstructure and Thermal Properties of Polylactides with Different L- and D-Unit Sequences: Importance of the Helical Nature of the L-Sequenced Segments.* Macromolecular Materials and Engineering, 2003. **288**(2): p. 137-143.

4. Local piezoelectric activity of single poly(L- lactic acid) microfibers

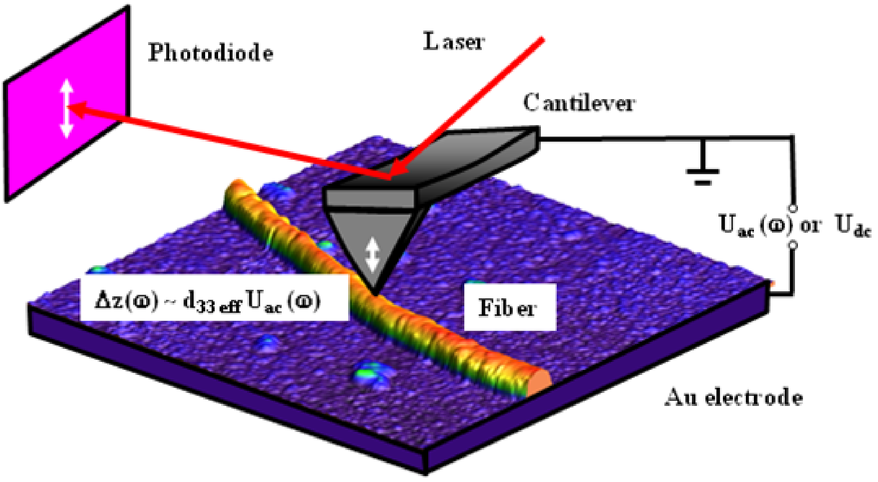
Photodiode
Laser
Cantilever
$U_{ac}(\omega)$ or U_{dc}
$\Delta z(\omega) \sim d_{33\,eff} U_{ac}(\omega)$
Fiber
Au electrode

This chapter is based on the following publication: V. Sencadas, C. Ribeiro, A. Heredia, I. K. Bdikin, A. L. Kholkin, S. Lanceros-Mendez. *Local piezoelectric activity of single poly(L- lactic acid) (PLLA) microfibers*. Submitted to Applied Physics A: Materials Science & Processing: Accepted; DOI: 10.1007/s00339-012-7095-z.

4.1 Introduction

One of the key aspects of biological systems is the intricate relationship between the biological response and relevant chemical/physical characteristics, including piezoelectricity, e.g. in amino acid derivatives and calcified tissues [1]. Traditionally, it has been believed that the polarization or more complex electromechanical responses in biological systems are unambiguously defined by the biological molecular structure, and cannot be tuned by the external electric fields. In other words, many biomaterials possess piezoelectricity, but ferroelectricity is rather rare. Somewhat contrary to this assumption, many of the early ferroelectrics are in fact partly organic. Rochelle salt is such an example as it comprises tartrate groups [2]. Since then, several crystalline organic materials have been identified as ferroelectrics but their polarization was too low to be used in practical applications [3]. Very recently, strong ferroelectricity was obtained in croconic acid crystals, showing a spontaneous polarization close to that of barium titanate ($\approx 20\ \mu C\ cm^{-2}$) at room temperature [4].

Piezoelectricity was observed in living tissues including bone [1, 5], dentin [6] and tendon [7], among others. It is known that physical exercise, which is associated with an applied stress to the material and translates into a piezoelectric signal from the bone to the living cells, thus helping bone regeneration, although the mechanisms involved bone mineralization and growth are unclear. The piezoelectric activity of the bone was attributed to the collagen and is dependent on the direction of the applied load, frequency and moisture [7-8]. Halperin *et al.* [5] reported that the piezoelectric coefficient for the human bone can go up to 7 $pC.N^{-1}$.

PLA is known to be one of the most used biomaterials, due its low density, low processing temperature, elastomeric behavior, corrosion resistance and versatile fabrication processes, among others [9]. The use of PLA in the medical field has increased due to its biocompatibility, bioresorption, biodegradation, low toxicity and strong mechanical performance. PLA is a synthetic biodegradable polyester obtained by the synthesis of a lactic acid (or lactide) which can be produced from renewable sources such as corn or sugar cane [10-11]. PLA belongs to the aliphatic polyesters derived from α-hydroxy acids. The building block of PLA, lactic acid (2-hydroxy proprionic acid), can exist as optically active D- or L-enantiomers, and their ratio will play an important role on the PLA properties. This allows the production of a wide range of PLA polymers to match performance requirements [12]. PLA is also known for its piezoelectric activity with a piezoelectric constant ranging up to approximately 10 $pC.N^{-1}$[13]. It consequently is considered as a promising material for bio applications that can also take advantage of its stress induced electroactivity, advantageous for bone growth and regeneration or neural recovery.

For many biological and biomedical applications it is an advantage to process the material in the form of fibers or fiber mats. Nanofibers can be produced by a variety of methods, such as drawing, template synthesis, self-assembly, wet spinning, electrospinning and phase separation [14]. In particular, electrospinning has been proven to be an excellent method for the synthesis of submicro- or nanofibers from polymer solutions for a wide range of polymeric materials [15]. When the diameter of the polymer fibers is downsized from micrometers to sub-micron or nanometer dimensions novel opportunities appear, such as very large surface area to volume ratio, flexibility in controlling surface functionalities, and superior mechanical performance (stiffness and strength) as compared to any other form of the same material [14].

Membranes and scaffolds of biodegradable polymers find numerous applications in tissue repair and regeneration. The tissue engineering approach relies upon the use of polymer scaffolds, which act as supports for cell adhesion, proliferation and differentiation, providing them mechanical reinforcement until the regenerated tissue is able to sustain the applied forces “in vivo”. In some cases scaffolds also help the organization of the produced extracellular matrix. Growth of cells on a polymeric scaffold using the principles of tissue engineering provides a viable “in vitro” model for biological experimentation [16].

Electrospun biodegradable polymer nanofibers are used in tissue engineering scaffold applications for nerve [17], cartilage [18], bone [19] and heart [20] regeneration. Electrospinning allows the production of polymeric nanofibers that closely mimic the fibers in the extra cellular matrix [21].

The present work demonstrates the piezoelectric activity of electrospun PLA nanofibers. Further, piezoelectricity is proven at a local level in single fibers, being this local electromechanical response a key issue for the development of membranes with tailored properties for applications in tissue engineering strategies.

4.2 Experimental

Materials: PLLA (Purasorb PL18, *Purac*) with an average molecular weight of 217.000 – 225.000 g.mol^{-1} was dissolved in a mixed solvent of DMF (*Merck*) and MC (*Sigma-Aldrich*) (3/7 volume ratio) to achieve a polymer concentration of 10 wt.% of the solution. The polymer solution was then dissolved at room temperature in a magnetic stirrer until complete polymer dissolution.

For the electrospinning process a glass substrate was previously coated with a gold (Au) thin layer in a Polaron SC502 Sputter coater. The polymer solution was placed in a commercial plastic syringe (10 mL) fitted with a steel needle with 500 µm of inner diameter. Electrospinning was conducted at 20 kV with a high voltage power supply (*Glassman,* model PS/FC30P04). A syringe pump (*Syringepump*) was used to feed the polymer solutions into the needle tip at 2 mL.h^{-1}. Single electrospun fibers were collected on the ground glass/Au substrate placed at 15 cm apart from the needle tip.

To characterize the piezoelectric and (possible) ferroelectric nature of the polycrystalline PLLA, PFM was used, a powerful tool for studying piezoelectric and ferroelectric phenomena at the micro- and nanoscale [22]. In this method, a sharp conductive Scanning Probe Microscopy tip in contact with the surface of the material is periodically biased and bias-induced surface displacements are translated into the mechanical motion of the tip. Both out-of-plane and in-plane displacements can be thus monitored to get insight into the nanoscale piezoelectric and ferroelectric properties [23].

The local piezoresponse measurements were performed with a commercial AFM (Ntegra Prima, NT-MDT) equipped with external function generator and lock-in amplifier as is described elsewhere [24]. Doped Si cantilevers were used with the spring constants of 0.5 - 1 N.m^{-1} driven at a frequency of 5 kHz. The experimental procedure for the electrical polarization and subsequent measurement of the electroactive properties of the PLLA nanofibers is shown in figure 4.1.

4.3 Results

Morphology and piezoresponse studies of a PLLA individual nanofiber (which including local poling) was performed by PFM, which is increasingly applied to analyze the local ferroelectric and piezoelectric properties of thin films [25-26]. This spatial resolution technique allows for a non-destructive characterization of the single nanofibers by the direct monitoring of the domain structures. This technique allows studying local properties such as polarization reversal and local piezoelectric activity [25, 27]. A schematic of the experimental setup is shown in figure 4.1.

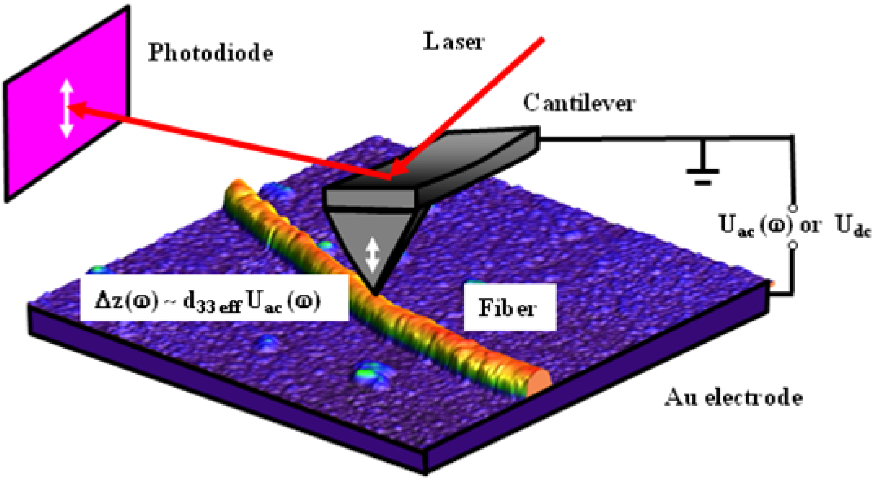
Photodiode
Laser
Cantilever
$U_{ac}(\omega)$ or U_{dc}
$\Delta z(\omega) \sim d_{33\,eff} U_{ac}(\omega)$
Fiber
Au electrode

Figure 4.1 – Design of the experimental arrangement for the measurement of the electroactive response of a single PLLA fiber.

Local studies of the piezoelectric response, the polarization switching and its time retention were carried out. The topography of a single PLLA fiber was routinely obtained (figure 4.2) indicating an average nanofiber diameter of ~ 800 nm. The fibers show notable roughness at the edge of the fibers, unseen by SEM reported in the past [28]. The surface of the fibers also reveals some roughness with RMS = 5.9 nm (figure 4.2), in particular at the center, resembling a drawing procedure induced by the applied electric field during the electrospinning process (figure 4.2). The small groove-like structures are also seen and attributed to the carrier solvent evaporation during the fiber polymer processing.

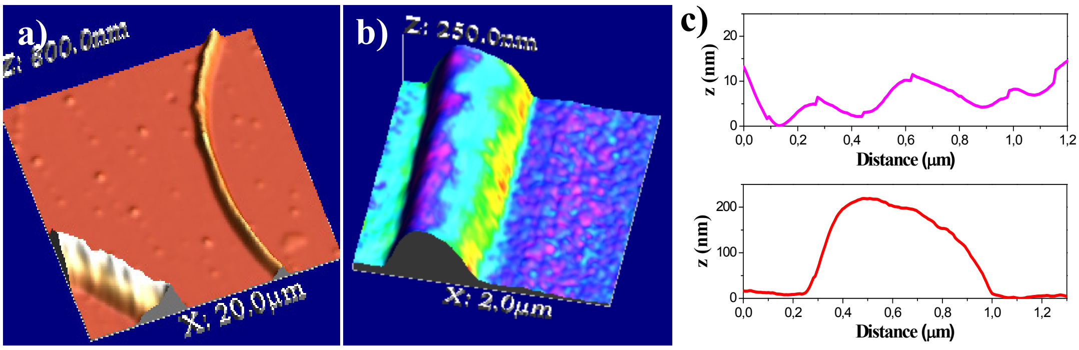

Figure 4.2 – a) 3D topography image; b) detailed 3D topography image; c) cross-section topography features of the fibers: roughness (above) and dimensions (below) of a single PLLA fiber.

In order to investigate the polarization response a dc bias was locally applied to the PLLA fiber through the AFM cantilever in order to polarize the sample. The piezoresponse signal was immediately recorded after the poling procedure with an ac bias of 5 V. PLLA nanofibers were poled with different dc bias amplitudes, ranging from ± 100 up to 200 V, in order to determine the maximum voltage required to switch the dipoles and saturate the induced polarization of the samples. The PLLA dipolar orientation corresponds to the internal rotation of the polar groups linked to asymmetric carbon atoms in the main chain and it can be induced by high enough electric field [29].

As it can be observed in figure 4.3, the unpoled polymer presents areas with different orientations of the polar phase that are distributed randomly along the fiber. The piezoelectric contrast does not follow directly the topographic shape (figure 4.3 a) and c)), indicating that the effect is due to the intrinsic piezoelectric properties of the PLLA and not originated from electrostatic effect and/or cross-talk with topography [30]. Magenta regions corresponds to the polarization oriented toward the substrate (φ = 180º) and the bright regions are referred to the polarization terminated at the free surface of the fiber.

Figure 4.3 b) and d) shows representative images of the poled PLLA nanofibers. The electrical poling was achieved by applying a bias of 100 and 200 V between the cantilever tip and grounded substrate, and verified by saturated hysteresis loops. For the poled spot of the PLLA nanofiber the piezoresponse image (figure 4.3 b) and d)) shows a homogeneous region with high contrast revealing that the dipole switching was achieved. The obtained data confirm that well-defined areas can be readily poled with high voltages applied the PLA nanofibers, allowing suitable electro active patterning of single fibers without their visible damage by positioning of the tip of the cantilever and application of the bias field in specific places of the fibers.

By positioning the tip of the cantilever in the poled region of figures 4.3 b) and d), a piezoelectric loop was then acquired. Figure 4.3 c) shows that the dipole switching is clearly observed resulting in the formation of a large single domain with net polarization aligned in the radial direction of the nanofibers with corresponding strong piezoelectric activity.

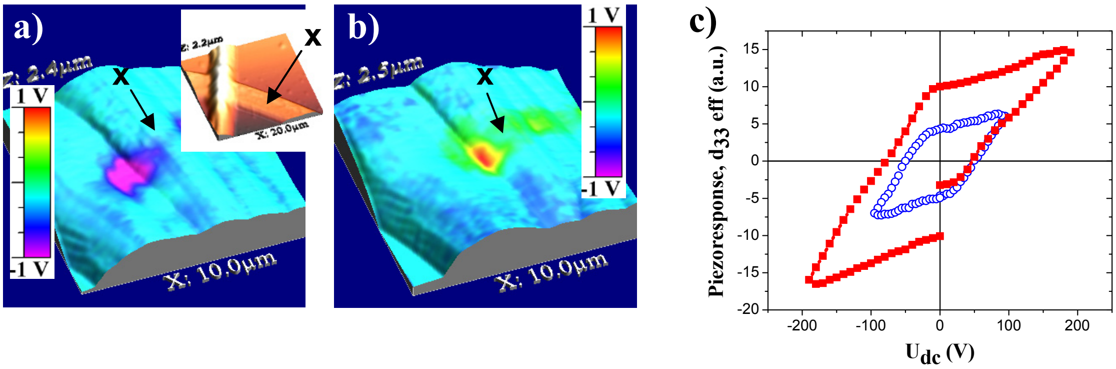

Figure 4.3 – PLLA fiber surfaces poled at a) 100 V and b) 200 V; well defined poled regions are obtained of fully poled material and c) measured hysteresis loops recorded in locations shown by x in a) and b).

PLLA is a simple which has flexible molecular chains containing C=O dipoles. The crystal structure of the PLA is characterized by the helical structure and in the PLLA crystal, three piezoelectric constants $d^C_{1,4}$, $d^C_{2,5}$, and $d^C_{3,6}$ were found. Fukada [31] shown that shear piezoelectricity at the molecular level is originated from the dipole that accompanies the asymmetric carbon. When the shear strain induced by the electric field is applied to the molecular chain of the PLA through its side chain, the displacement arises in all the atoms. The motions causing the change in polarization is the rotation of the plane defined by the C-O and C=O bond on the C–O bond of PLLA, which was reported that is perpendicular to the electric field [13, 31]. Accordingly, the change in polarization arises due to the applied stress.

It was observed that the material can be poled by applying biases in excess of ~100 V but the piezoresponse maximum achieved in PLA fibers is lower when compared to the one found in literature (10 pC.N^{-1} [13]). To increase the dipole alignment higher biases of about 200 V were applied in order to promote the polarization rotation and full dipole reversal (figure 4.3 c)) within the PLA fiber. As a result, the maximum value of the piezoelectric coefficient attained under local poling was similar to the found in the literature [13] and can be comparable to those of PVDF [32].

Piezoelectric effect on drawn PLA using films and rods has been investigated in the past [33], and it was demonstrated that the d_{14} increases with the drawing ratio, reaching values around 10 pC.N^{-1} [13]. This is due to the increasing of the PLA polymers chains alignment caused by stretching. During the electrospinning process, the applied electric field between the needle tip and the ground collector accelerates and drawn the polymer fiber during crystallization, probably giving origin high oriented polymer chains in longitudinal direction of the fibers.

4.4 Conclusions

The piezoelectric response of PLLA electrospun fibers has been proven and characterized by PFM. Domain switching and polarization patterning of individual fibers has been achieved in this important biomaterial, allowing interesting possibilities for novel tissue engineering and biomedical strategies, including sensor/actuator applications.

4.5 References

1. Fukada, E. and I. Yasuda, *On the Piezoelectric Effect of Bone.* J. Phys. Soc. Jpn., 1957. **12**(10): p. 5.

2. Valasek, J., *Piezo-Electric and Allied Phenomena in Rochelle Salt.* Phys. Rev., 1921. **17**(4): p. 475.

3. Horiuchi, S. and Y. Tokura, *Organic ferroelectrics.* Nature Mat., 2008. **7**: p. 357-366.

4. Horiuchi, S., et al., *Above-room-temperature ferroelectricity in a single-component molecular crystal.* Nature, 2010. **463**(7282): p. 789-792.

5. Halperin, C., et al., *Piezoelectric Effect in Human Bones Studied in Nanometer Scale.* Nano Letters, 2004. **4**(7): p. 1253-1256.

6. Wang, T., et al., *Piezoelectric properties of human dentin and some influencing factors.* Dental Materials, 2007. **23**(4): p. 450-453.

7. Ahn, A.C. and A.J. Grodzinsky, *Relevance of collagen piezoelectricity to "Wolff's Law": A critical review.* Medical Engineering & Physics, 2009. **31**(7): p. 733-741.

8. Maeda, H. and E. Fukada, *Effect of water on piezoelectric, dielectric, and elastic properties of bone.* Biopolymers, 1982. **21**(10): p. 2055-2068.

9. Garlotta, D., *A Literature Review of Poly(Lactic Acid).* Journal of Polymers and the Environment, 2001. **9**(2): p. 63-84.

10. Nijenhuis, A.J., D.W. Grijpma, and A.J. Pennings, *Lewis acid catalyzed polymerization of L-lactide. Kinetics and mechanism of the bulk polymerization.* Macromolecules, 2002. **25**(24): p. 6419-6424.

11. Tsuji, H., H. Daimon, and K. Fujie, *A New Strategy for Recycling and Preparation of Poly(l-lactic acid): Hydrolysis in the Melt.* Biomacromolecules, 2003. **4**(3): p. 835-840.

12. Lim, L.T., R. Auras, and M. Rubino, *Processing technologies for poly(lactic acid).* Progress in Polymer Science, 2008. **33**(8): p. 820-852.

13. Tsutomu Ochiai and E. Fukada, *Electromechanical Properties of Poly-L-Lactic Acid.* Japanese Journal Applied Physics, 1998. **37**: p. 3374-3376.

14. Seeram Ramakrishna, et al., *An introduction to electrospinning and nanofibers.* 2005, Singapore: World Scientific Publishing Co. Pte. Ltd.

15. Doshi, J. and D.H. Reneker, *Electrospinning process and applications of electrospun fibers.* Journal of Electrostatics, 1995. **35**(2-3): p. 151-160.

16. Sabir Muhammad, Xu Xiaoxue, and L. Li, *A review on biodegradable polymeric materials for bone tissue engineering applications.* Journal of Materials Science, 2009. **44**(21): p. 5713-5724.

17. Yang, F., et al., *Fabrication of nano-structured porous PLLA scaffold intended for nerve tissue engineering.* Biomaterials, 2004. **25**(10): p. 1891-1900.

18. Li, W.-J., et al., *A three-dimensional nanofibrous scaffold for cartilage tissue engineering using human mesenchymal stem cells.* Biomaterials, 2005. **26**(6): p. 599-609.

19. M. Shin , H. Yoshimoto, and J.P. Vacanti, *In vivo bone tissue engineering using mesenchymal stem cells on a novel electrospun nanofibrous scaffold.* Tissue engineering, 2004. **12**: p. 33.

20. Shin, M., et al., *Contractile cardiac grafts using a novel nanofibrous mesh.* Biomaterials, 2004. **25**(17): p. 3717-3723.

21. Yanzhong Zhang, et al., *Recent development of polymer nanofibers for biomedical and biotechnological applications.* Journal of Materials Science: Materials in Medicine, 2005. **16**(10): p. 933-946.

22. Kalinin, S.V., N. Setter, and A.L. Kholkin, *Electromechanics on the Nanometer Scale: Emerging Phenomena, Devices, and Applications.* MRS Bull., 2009. **34**(9): p. 634-642.

23. Isakov, D.V., et al., *Piezoresponse force microscopy studies of the triglycine sulfate-based nanofibers.* Journal of Applied Physics, 2010. **108**(4): p. 042011.

24. Kholkin, A.L., et al., *Review of Ferroelectric Domain Imaging by Piezoresponse Force Microscopy*, in *Scanning Probe Microscopy: Electrical and Electromechanical Phenomena at the Nanoscale*, S. Kalinin and A. Gruverman, Editors. 2006, Springer: New York. p. 173-214.

25. Christman, J.A., et al., *Piezoelectric measurements with atomic force microscopy.* Applied Physics Letters, 1998. **73**(26): p. 3851-3853.

26. Gruverman, A., et al., *Asymmetric nanoscale switching in ferroelectric thin films by scanning force microscopy.* Applied Physics Letters, 2001. **78**(18): p. 2751-2753.

27. Prashanthi, K., et al., *Local piezoelectric response of ZnO nanoparticles embedded in a photosensitive polymer.* physica status solidi (RRL) – Rapid Research Letters, 2012. **6**(2): p. 77-79.

28. Clarisse, R. and et al., *Tailoring the morphology and crystallinity of poly(L-lactide acid) electrospun membranes.* Science and Technology of Advanced Materials, 2011. **12**(1): p. 015001.

29. Sugita, A. and S. Tasaka, *Electric-field-induced chain orientation in poly(L-lactic acid).* Journal of Polymer Science Part B: Polymer Physics, 2004. **42**(24): p. 4433-4439.

30. Shin, J., et al., *Simultaneous elastic and electromechanical imaging by scanning probe microscopy: Theory and applications to ferroelectric and biological materials.* Journal of Vacuum Science & Technology B: Microelectronics and Nanometer Structures, 2005. **23**(5): p. 2102-2108.

31. E.Fukada, *History and recent progress in piezoelectric polymers.* IEEE Transactions Ultrasonic Ferroelectric and Frequency Control, 2000. **47**: p. 1277–1290.

32. Gomes, J., et al., *Influence of the β-phase content and degree of crystallinity on the piezo- and ferroelectric properties of poly(vinylidene fluoride).* Smart Materials and Structures, 2010. **19**(6): p. 065010.

33. Ikada, Y., et al., *Enhancement of bone formation by drawn poly(L-lactide).* Journal of Biomedical Materials Research, 1996. **30**(4): p. 553-558.

5. Influence of crystallinity on hydrophobicity and biological response of poly(L-lactide) electrospun mats

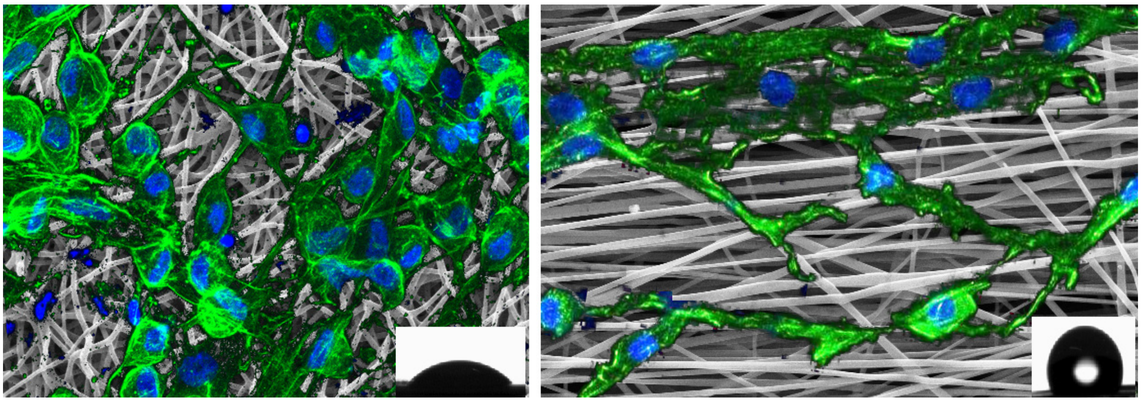

This chapter is based on the following publication: A.C. Areias, C. Ribeiro, V. Sencadas, N. Garcia-Giralt, A. Diez-Perez, J.L. Gómez Ribelles and S. Lanceros-Méndez. *Influence of crystallinity on hydrophobicity and biological response of poly(L-lactide) electrospun mats*. Soft Matter. 2012. 8: 5818-5825.

5.1 Introduction

The use of tissue engineering for restoring, maintaining or enhancing tissue and organ function is a rapid growing field of investigation [1] with important achievements both at “in vitro” and “in vivo” experimental levels. An important goal in this field is to improve the success rate of tissue engineering strategies by creating more sophisticated materials which can mimic the extra-cellular matrix, so that the body regenerates “neo-native” functional tissues [2]. One of the major challenges in tissue engineering is articular cartilage regeneration as current regeneration therapies fail producing functional hyaline cartilage and the regenerated tissue has the characteristics of fibrocartilage [3].

Biomaterials which mimic the ECM such as nanofibers have been pointed out as good scaffolds for cartilage regeneration [4]. ECM typically consists on a viscoelastic network with nanofibrous proteins that provide biological and chemical moieties as well as physical framework supporting cell attachment and growth [5]. Chondrocytes seeded on a scaffold should produce their own highly hydrated ECM which consists mainly in collagen fibrils, predominantly collagen type II, and proteoglycans [6]. These products will maintain the structural and functional integrity of chondrocytes such as shape, polarity, migration, differentiation, apoptosis and gene expression. Cartilaginous matrix is biosynthesized during the chondrogenic differentiation and can thus be used as a marker of their differentiation [7-8].

PLLA is a biodegradable and biocompatible material approved by U.S. Food and Drug Administration (FDA) for human clinical applications [9]. This polymer shows a wide range of applications and can be processed in a variety of ways and in different forms. PLLA nanofibers produced by electrospinning, the most common and versatile method used to produce nanofibers, have a large interest due to their structural similarity to the extracellular matrix of biological systems such as collagen fibers [10]. High surface area to volume ratio and the characteristics described above indicates that it may serve as effective tissue engineering scaffolds [11].

Electrospinning originates nanofibers with different morphology and hydrophobicity. Recent findings showed that mammalian cells do respond to nanosized features influencing the cellular behaviour, as for example, cell adhesion, proliferation, matrix production, cell morphology and orientation [9, 12-15]. Increasing evidences show that surface patterning or alignment of nanofibers influences the guide cell growth direction and morphology [5, 16-18]. Zhang *et al.* [19] show the contact guide of OP9 stroma cells on grooves patterned in polydimethylsiloxane (PDMS) surface. The cell movement velocity and cell number inside the microchannel, consisting in aligned nanofibers, influenced the cells migratory ability. Further, the surface topography can induce the cells to change their genetic code leaving them on tumor cell metastic form.

Several articles reported contradictory results about the effects of material topography, hydrophobicity and wettability on cell behaviour [20]. Some correlations between the wettability and cell behaviour have been reported showing that cells prefer to attach on hydrophilic surfaces. Further studies found that cells adhere, spread and grow more easily on substrates with moderate hydrophilicity [21]. To improve biomaterial surfaces to make them more suitable to cell attachment and spreading, methods such as enriching surfaces with ECM components or incorporation of natural polymers with synthetic polymers have been reported. Cui *et al.* [22] studied the effects of different biomimetic PLLA surfaces on articular chondrocytes *in vitro* in order to improve cytocompatibility. Gelatin was used to modify PLLA film surfaces by two different processes: physical entrapment and chemical coupling. The obtained surfaces showed different hydrophobicity and cell adhesion. Proliferation and differentiation were more efficient on the more hydrophilic surfaces which correspond to the PLLA films treated by chemical coupling. Similar works with electrospun PLLA nanofibers modified with cationized gelatin (CG) show the affinity of chondrocyte for the modified form instead of the virgin form. The chondrocytes seeded in nanofiber PLLA membranes displayed a dedifferentiated, fibroblast – like morphology, whereas chondrocytes seeded in CG–PLLA nanofibers mats maintained their chondrocytic phenotype.

The goal of this work is evaluate the human articular chondrocyte behaviour seeding on PLLA nanofiber scaffolds with different degree of crystallinity in order to assess the optimal environmental conditions for regenerate hyaline cartilage. Cell adhesion, proliferation and differentiation of chondrocytes, as well as their morphology and ECM production detection were studied in an *in vitro* environment.

5.2 Materials and methods

5.2.1 Preparation of PLLA electrospun membranes

Biodegradable PLLA electrospun membranes were prepared by electrospinning under the conditions indicated in [23]. Alignment of the fibril mats was obtained using a rotating collector while randomly oriented fiber mats were obtained with a flat collector. The mean diameter of the fibrils was 700 nm (standard deviation ± 235 nm). The polymer fibers obtained after electrospinning were nearly amorphous, as determined by DSC thermograms. Further isothermal annealing at temperatures in the range between 70 and 140 ºC allows controlled crystallization of the polymer without disturbing fibrils morphology [23]. In this way, oriented and non-oriented mats with approximately 0%, 8%, 27% and 50% of crystallinity were produced. The different PLLA samples used in present work are designed as listed in table 5.1.

Table 5.1 – Specification of the PLLA samples.

Morphology of PLLA fibers	Crystallinity	Symbol
Non-oriented	Amorphous	NO-PLLA-0
	8%	NO-PLLA-8
	27%	NO-PLLA-27
	50%	NO-PLLA-50
Oriented	Amorphous	O-PLLA-0
	8%	O-PLLA-8
	27%	O-PLLA-27
	50%	O-PLLA-50

For cell culturing, circular samples with 6-7 mm of diameter of oriented and non-oriented membranes with different degrees of crystallinity were cut and sterilized with ethylene oxide. PLLA samples were hydrated by Hanks' balanced salt solution (*Sigma-Aldrich*) overnight before cell culture and after that the samples were washed 1 time for 5 min in Dulbecoo's Modified Eagle's Medium (DMEM, *Invitrogen*).

5.2.2 Contact angle measurements

Contact angle measurements (sessile drop in dynamic mode) were performed at room temperature in a Data Physics OCA20 device using ultrapure water as test liquid. The contact angles were measured by depositing water drops (3 μL) on the sample surfaces using the software SCA20. At least 6 measurements in each PLLA electrospun membranes were performed in different sample locations and the average contact angle was taken for each sample.

5.2.3 Substrate topography measurements

The samples were measured using Tapping Mode with a MultiMode connected to a NanoScope III (*Veeco*) with non-contacting silicon (ca. 47 -76 kHz, k: 1.2 - 6.4 N.m^{-1}) from AppNano. All images (10 μm wide) were fitted to a plane using the 1st degree flatten procedure included in the NanoScope solftware version 4.43rd8. The surface roughness was calculated as Sq (root mean square from average flat surface) and Sa (average absolute distance from average flat surface).

5.2.4 Cell culture

Human primary chondrocytes were obtained from cartilage specimens extracted from knee samples otherwise discarded at the time of arthroplasty surgery in postmenopausal woman, as described previously [8, 24]. Briefly, the articular cartilage was separated from bone, cut into small fragments and treated with hyaluronidase at 0.5 mg.mL^{-1}, pronase at 1 mg.mL^{-1} and collagenase at 0.5 mg.mL^{-1}. The digested cartilage was filtered with 70 μm of pore size, centrifuged and finally placed on a tissue culture flask with DMEM supplemented with 10% fetal bovine serum (FBS) and 50 μg.mL^{-1} ascorbic acid. At confluence, the cells were subcultured maximum twice to obtain the desired cell number. The cells that were not used immediately in experiments were frozen in liquid nitrogen with 10% dimethyl sulfoxide (DMSO) until use.

Circular membranes of PLLA microfibers were placed in a 96-multi well plate and cultured with 140 000 cell/well in DMEM medium supplemented with 10% FBS and 50 μg.mL^{-1} ascorbic acid at 37 ºC and 5% CO_2. After two days of culture, the samples were changed to new wells and cultured with DMEM supplemented with 1% of Insulin, Transferin and Selenium (ITS; BD Biosciences), 50 µg.mL^{-1} ascorbic acid and 10 ng.mL^{-1} of transforming growth factor beta 1 (TGFβ1), corresponding this step to the zero time. The cell culture medium was replaced every 3 days during 28 days. The negative control was the biomaterial without cells and cells cultured on tissue culture polystyrene (TCPS) was used as a positive control.

5.2.5 Cell morphology

At 21 days of culture, chondrocytes were washed in Dulbecco's Phosphate Buffered saline (DPBS, *Invitrogen*) and fixed in 4% formaldehyde solution (*Sigma-Aldrich*) in PBS during 10 min at room temperature. The samples were then rinsed with DPBS and permeabilized with 0.1% Triton X-100 in PBS during 3 to 5 min at room temperature. Then, the samples were incubated with Alexa Fluor® 488 phalloidin (*Invitrogen*) at 6.6 µM during 20 min. Finally, samples were washed with PBS before being mounted in a coverslip with aqueous mounting medium containing DAPI (*Invitrogen*). Overall cell morphology was studied using a confocal laser scanning microscope (Leica TCS SP5 CFS) with an excitation at 495 nm and emission at 518 nm.

After cell proliferation for the desired period of culture, all samples were washed with PBS solution to remove the non-adherent cells and fixed with 0.25% of glutaraldehyde for 1 h at room temperature. Following, the samples were dehydrated through a series of graded alcohol series. The dried scaffolds were observed in SEM equipment (Leica Cambridge S360) at an accelerating voltage of 15 kV.

5.2.6 Cell viability and proliferation

Cell viability assay and proliferation analysis was performed at 0, 7, 14 and 28 days of culture on the material by (3,-(4,5-dymethylthiasol-2-yl)-2,5-diphenyltetrazolium bromide (MTT) kit (*Invitrogen*) and Live/Dead Viability/Cytotoxicity Kit (*Molecular Probes*).

MTT is an assay based on the cleavage of the tetrazolium salt in the presence of an electron coupling reagent intracellular in viable cells. The amount of formazan dye formed is directly correlated to the number of metabolically active cells in the culture and was measured at 550 nm using a plate reader (Biochrom Anthos 2010 Microplate Reader).

The Live/Dead Viability/Cytotoxicity Kit, which provides two color fluorescence cell staining, is based on the simultaneous determination of live and dead cells measuring recognized parameters of cell viability; intracellular esterase activity and plasma membrane integrity. The assay was evaluated by Confocal Fluorescent Microscope (Leica TCS SP5 CFS).

5.2.7 Cell differentiation

The chondrocyte differentiation was determined using enzyme-linked immunosorbent assay (ELISA) and immunohistochemical methods.

5.2.7.1 Human aggrecan

The quantitative measurement of human aggrecan (AGG) was evaluated at 7, 14 and 28 days by means of ELISA (KAP1461, DIAsource ImmunoAssays S.A., Belgium) in cell culture supernatants from experimental wells according to the manufacture protocol. The absorbance was measured at 450 nm by using a plate reader (Biochrom Anthos 2010 Microplate Reader).

5.2.7.2 Collagen type II

Specimens were fixed with 50/50 of ethanol/acetone during 10 min at 7 and 21 days of culture. The samples were rehydrated through washing with PBS during three times and then incubated with blocking solution (10% FBS, 0.1% Triton x-100 in PBS) at room temperature. Then, the samples were incubated with a mouse antibody anti-collagen type II (Ab-1), 1 μg mL^{-1} (Calbiochem®) during 1 h. The samples were washed with PBS and incubated with a secondary antibody Alexa Fluor® 488 anti-mouse (*Invitrogen*) (1:200). Finally, samples were washed 2 times for removing the excess of antibody before being mounted in a coverslip with mounting medium containing DAPI staining (*Invitrogen*). The assay was performed at Confocal Fluorescent Microscope (Leica TCS SP5 CFS) (ex/em ~495 nm/ ~515 nm for green fluorescence and ex/em ~358 nm/ ~461 nm for DAPI fluorescence).

5.2.8 Statistical analysis

All quantitative results were obtained from triplicate and were expressed as mean ± standard deviation. Statistical differences were determined by the analysis of variance (ANOVA) using F-test for the evaluation of different groups. P values < 0.05 were considered to be statically significant.

5.3 Results

5.3.1 Contact angle measurements

The wettability of different PLLA membranes was determined and is shown in figure 5.1. The amorphous non-oriented PLLA membrane shows to be the most hydrophilic sample, with a water contact angle (WCA) of 65,9º. The annealing treatment of non-oriented PLLA membranes produces a decrease of wettability in the surface of these samples, at the same time than crystallinity increases. In this way, a WCA of 118,1º was obtained for the NO-PLLA-50. A significant difference between oriented and non-oriented PLLA membranes for the same degree of crystallinity was observed.

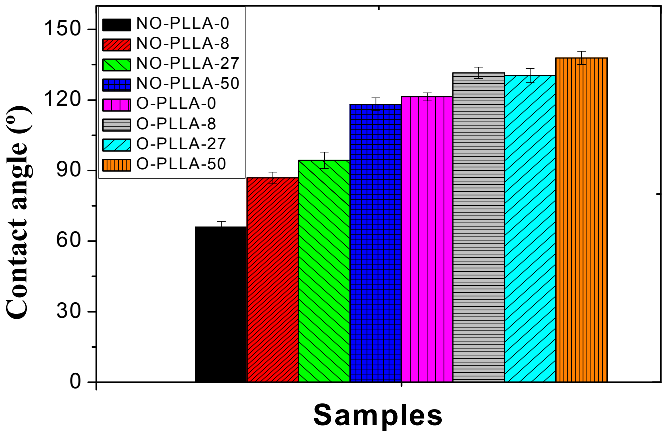

Figure 5.1 – Evaluation of water contact angle of PLLA membranes. Values are mean ± SD. No statistically significant difference in contact angle was found between non-oriented PLLA membrane with 50% of crystallinity and oriented PLLA membrane amorphous and also between oriented PLLA membrane with 8% and 27% of crystallinity.

Annealing oriented PLLA membranes also affects the wettability of the samples, but in a less effective way than in the non-oriented PLLA membranes is smaller. In this way, the WCA of O-PLLA-0 is 121,3º and for O-PLLA-50 is 137,8º.

It is important to notice in this sense that the annealing treatment does not change the morphology of the fiber mats [23], being the variations of the wettability to be fully ascribed to variations in the nanotopography of the fiber and in the stiffness due to the increase of the degree of crystallinity.

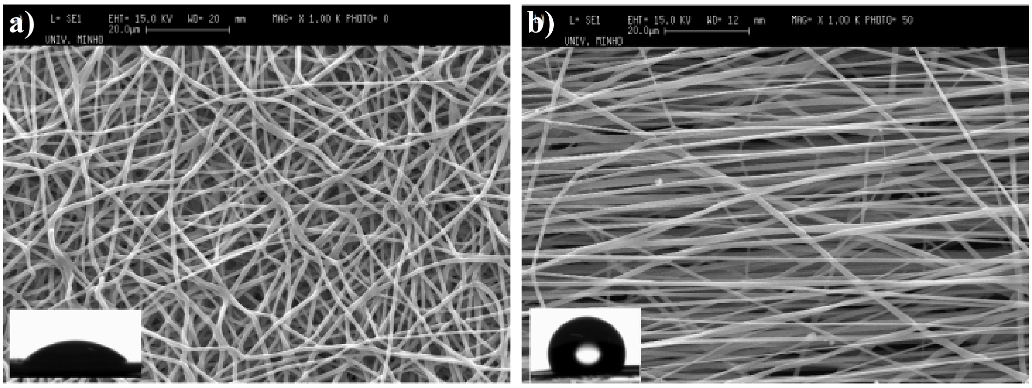
a)
L= SE1 EHT= 15.0 KV WD= 20 mm MAG= X 1.00 K PHOTO= 0
20.0µm
UNIV. MINHO
b)
L= SE1 EHT= 15.0 KV WD= 12 mm MAG= X 1.00 K PHOTO= 50
20.0µm
UNIV. MINHO

Figure 5.2 – a) Micrograph of static contact angle of non-oriented PLLA amorphous and b) Micrograph of static contact angle of oriented PLLA amorphous.

5.3.2 Substrate topography measurements

The results from AFM (figure 5.3) show no strong differences in the roughness between the samples. The RMS of NO-PLLA-0, NO-PLLA-50 and O-PLLA-0 were 14,410 nm, 14,408 nm and 22,110 nm, respectively.

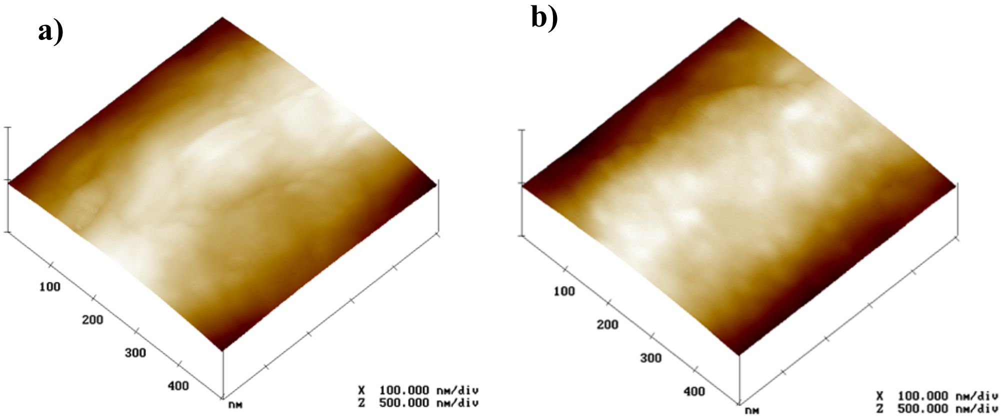

Figure 5.3 – AFM images of one nanofiber morphology on a) non-oriented PLLA amorphous and b) non-oriented PLLA with 50% of crystallinity.

5.3.3 Cell attachment and cell morphology

The overall morphology of chondrocytes seeded in PLLA membranes after 7, 14 and 28 days was visualized by SEM (figure 5.4) and after 21 days in confocal fluorescence microscopy after actin staining (figure 5.5). According to the evaluation form results similar to the ones presented in figure 5.3, a higher density of cells was observed on scaffolds at 14 days of cell culture independently of the degree of crystallinity of the membranes.

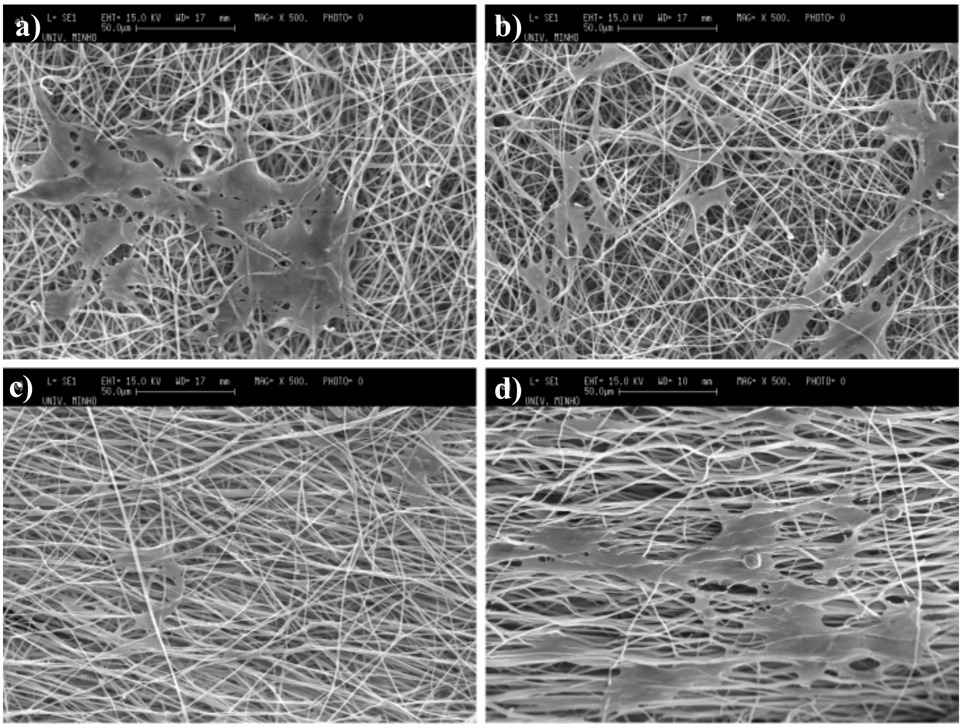

Figure 5.4 – Overall cell morphology of chondrocytes on PLLA membranes analyzed by SEM. a) amorphous non-oriented PLLA membrane for 14 days; b) non-oriented PLLA membrane with 27% of crystallinity for 7 days; c) oriented PLLA membrane with 27% of crystallinity for 7 days; d) amorphous oriented PLLA membrane for 14 days. The scale bar (50 µm) is valid for all the images.

With respect to the comparison of cell morphology between oriented PLLA membranes and non-oriented PLLA membranes, it was observed that cells exhibited a more elongated morphology in oriented PLLA scaffolds (figure 5.5). However, no significant differences were observed among cell cultures for a given fiber orientation of PLLA membranes with different degrees of crystallinity (data not shown).

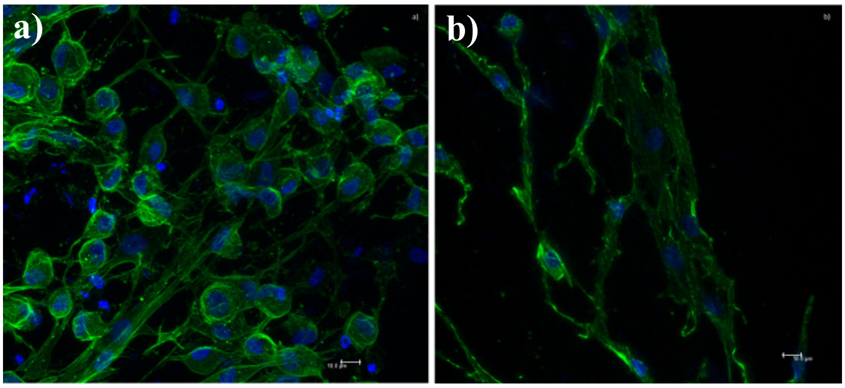

Figure 5.5 – Confocal fluorescence microscopy images of chondrocyte cells after 21 days of cell culture in PLLA membranes. a) non-oriented PLLA membrane amorphous; b) oriented PLLA membrane amorphous. The scale bar (10 μm) is valid for all the images (green: cytoskeleton; blue: nucleus).

5.3.4 Cell viability and proliferation

The proliferation and viability of the attached cells in the eight types of PLLA membranes after 7, 14 and 28 days in culture is shown in figure 5.6. For all the membranes, the viable cell number increased to 14 days of cell culture and decreased for longer cell culture time.

After 7 days of cell culture, cell viability and proliferation are similar for all the evaluated samples with a slight increase compared to time 0. At 14 days of cell culture, the amorphous PLLA membranes promote higher proliferation compared to crystalline PLLA membranes. Among crystalline PLLA membranes, cell viability is significantly lower in the case of the oriented PLLA membranes. Interestingly, the viability of the attached cells of the non-oriented PLLA membranes was higher in PLLA membranes with 27% of crystallinity than PLLA membranes with 8% and 50% of crystallinity. On the oriented PLLA membranes no significant differences are observed with the increase of crystallinity.

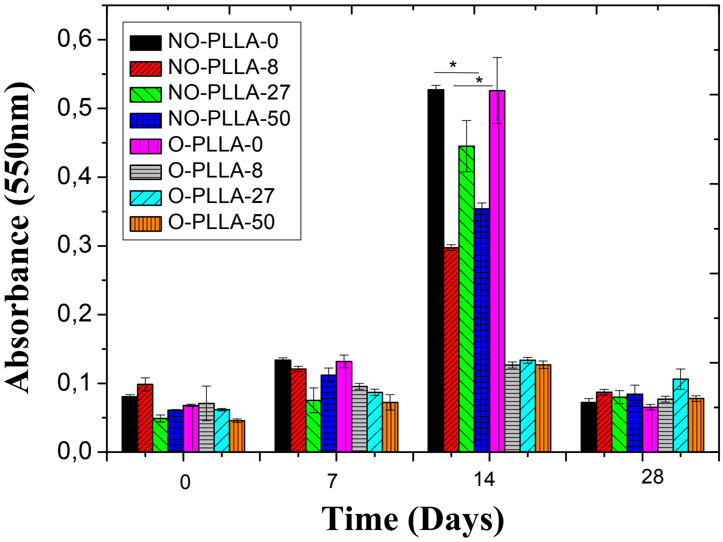

Figure 5.6 – MTT absorbance results after cells seeded for 0, 7, 14 and 28 days on different PLLA membranes. Values are mean ± SD. *Significantly different ($p<0.05$) PLLA samples.

To verify the viability of the chondrocytes on the material, a live/dead assay was also performed after 21 days of cell culture, confirming that most of adherent cells were viable (figure 5.7).

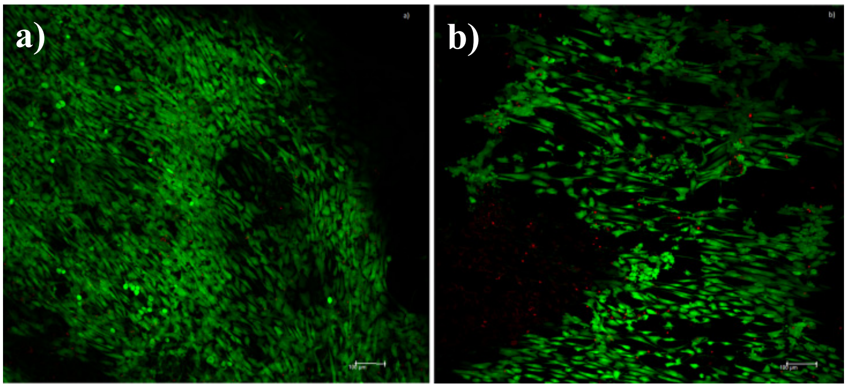

Figure 5.7 – Fluorescence micrographs of live/dead of cell culture with chondrocyte cells during 21 days in PLLA membranes. a) Non-oriented amorphous PLLA membrane; b) oriented amorphous PLLA membrane. The scale bar (100 μm) is valid for all the images.

5.3.5 Cell differentiation

The presence of two hyaline cartilage biomarkers as AGG and type II collagen was confirmed. The presence of type II collagen was observed at 21 days (figure 5.8) on the amorphous non-oriented PLLA membrane and the same sample demonstrated to have the higher AGG production (figure 5.9). However, no type II collagen was observed in the oriented PLLA membranes.

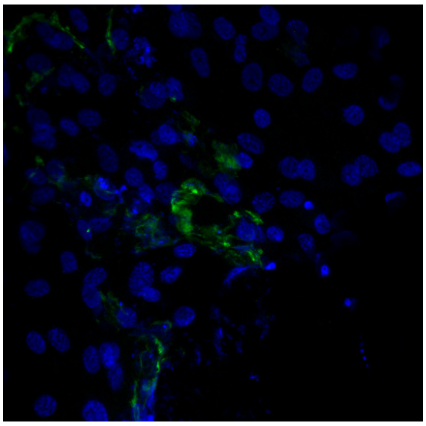

Figure 5.8 – Immunocytochemical visualization of type II collagen after 21 days of chondrocytes culture in amorphous non-oriented PLLA membrane.

Aggrecan is the most common proteoglycans of the cartilage matrix [25] and its content in supernatant after chondrocyte cells seeded for 7, 14 and 28 days is shown in figure 5.9.

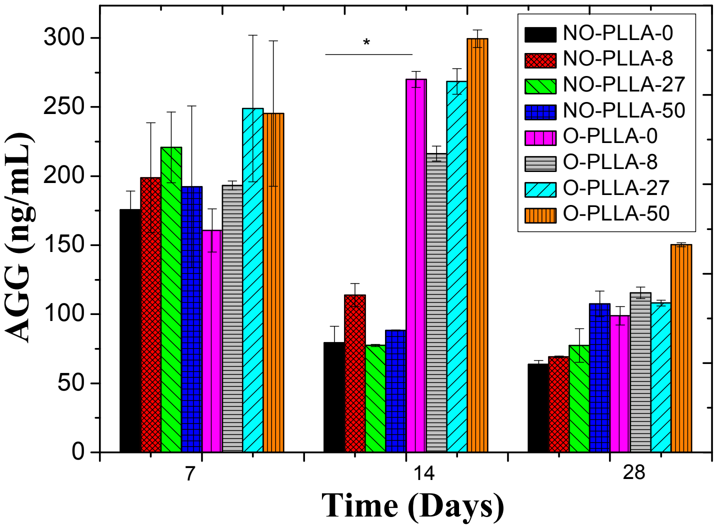

Figure 5.9 – Human aggrecan production in supernatant after cells seeded for 7, 14 and 28 days on different PLLA membranes. Values are mean ± SD. No statistically significant difference in concentration was found among samples after 7 and 28 days. At 14 days, significant differences between PLLA non-oriented and oriented membranes were found.

At 7 days, no differences are detected in the production of AGG between non-oriented and oriented PLLA membranes. At 14 days it is evident the strong difference between the non-oriented and oriented PLLA membranes. The NO-PLLA-0 shows the lowest AGG production in the supernatant and the O-PLLA-50 the highest. At 28 days, the same behaviour was observed with no strong differences between the main groups.

5.4 Discussion

Electrospinning is a powerful technique to produce micro- and nano-fibers and it is know that the different fibrous structures can result in a remarkable increase of surface hydrophobicity [26-28]. The present results show a large increase of water contact angle with increasing degree crystallinity in randomly oriented fiber mats and a higher hydrophobicity of the mats with aligned fibers with respect to the former ones.

Highly hydrophobous surfaces can be produced by introducing submicron roughness into an inherently hydrophobous surface [29-31]. Electrospinning is very adequate to generate roughness in the sub-micron range since both fibrils and fiber separation are in this order of magnitude. It should, thus be expected that water contact angle in electrospun mats depends on morphological parameters such as fiber orientation and porosity or fiber diameter [32-34]. The generation of topography in the nanometric scale on the submicron rough surface with an additional decoration of the electrospun fibrils or the space among them produces an increased tendency to water repulsion producing superhydrophobic surfaces. Thus, Li *et al.* found an important increase of hydrophobicity when combining in a mat polystyrene and nylon6 electrospun fibers with mean diameters quite different from each other [35]. The combination of thin and thick fibers mimics the superhydrophobic surfaces of living organisms such as lotus leaf [26]. Simultaneous contributions of chemical and topographical cues to hydrophobicity can be obtained by coating electrospun fibers with more hydrophobic polymers [36]. Pisuchpen *et al.* obtained mats with WCA above 150º with poly(vinyl alcohol) fibers coated with or silica or silanol nanoparticles. WCA as high as 178º were obtained with electrospun polystyrene or poly(vinyl chloride) incorporating nanoparticles that modify fibril surface roughness [37], or WAC above 140º in PVDF containing silica nanoparticles [38]. On the other hand the air retention at the surface also contribute to water repellency, an increase of the stiffness has been shown to favor air retention at the surface, too [39].

The development of crystallinity in PLLA films due to thermal treatments produces a surface roughness that highly depends on the size of the spherulites [40-41]. It is interesting to notice at this point that the variations in the degree of crystallinity in PLLA films does not imply significant variations either in the contact angle (74º +/- 3 for 10% and 67% crystalline samples) [42] nor in the stiffness (Young Modulus of 3.4 +/- 0.3 and 3.5 +/- 0.2 GPa for 7% and 40-50% crystalline samples) [43]. When the amorphous electrospun fibrils crystallize their stiffness and surface energy increase [23, 44], and at the same time surface nano-roughness is expected to be developed.

However, through the AFM images was possible to analyze at nanoscale the surface roughness in our fibers. This assay is not easy to perform due to the nanofibers proprieties. The membranes are soft materials and when the measurement is being done sometimes the nanofibers, due to the physics effects, attach to the AFM tip stopping the assay. The result shows a non existence of strong differences between the samples. The roughness of NO-PLLA-0 was quite similar to the NO-PLLA-50 suggesting that the crystallinity increase by annealing treatment has no effect in the surface roughness. On the other hand, the comparison between NO-PLLA-0 and O-PLLA-50 indicate that there also no changes in the roughness due to the orientation fibers, once the difference of values was not quite disparate.

The combination of all these effects has as a consequence the clear increase of water repellence of the mat surface. The effect is very apparent in randomly oriented fiber mats as the WCA is quite low, much smaller than in the mats with aligned fibers. The results reported in the literature with respect to the effect of fiber alignment are contradictory. Wang *et al.* found higher WCA in randomly oriented electrospun PLLA surfaces than in aligned ones [45], similar result was obtained by Kai *et al.* in electrospun polycaprolactone, although significant increase of WCA with alignment was found when the fibers were modified with gelatin [46-47]. In our case the high hydrophobicity of the mats with aligned fibers (values of WCA of 120º for the amorphous or 140º for the most crystalline mats) could be mainly due to the difference in the average pore size (or inter-fiber distance) with respect to randomly oriented mats that can be someway characterized by membrane porosity which is higher in randomly oriented mats [23]. The effect of the roughness seems to less important than compared to the other effects.

The topography created by the membrane features has a strong influence on the biological response of the cells seeded in its surface trough contact guidance. In spite of the porosity of the electrospun mats, they must be considered as a two dimensional substrates with respect to cell culture since inter-fiber spaces do not allow cell invasion of the three dimensional fiber structure. Cell-substrate interaction mediated by proteins adsorbed from the culture medium is crucial to control chondrocyte adhesion, proliferation and consequently gene expression in monolayer culture [5, 48-49]. It has been shown that nano-fibrilar substrates allow viable and proliferative chondrocyte culture [33, 50]. Mature chondrocytes are non-proliferative cells in hyaline cartilage. The first stage for chondrocytes proliferation when they are seeded on a flat substrate is the recognition by integrins of specific ligands in the proteins adsorbed on the substrate surface. Once adhered to these ligands, integrins cluster and form focal adhesions, which establish links in the cytoplasm with α-actin fibers. Development of the actin stress fibers of the cell cytoskeleton not only controls cell morphology but it establishes a cross-talk between the cell nucleus and the extracellular matrix which is an important signaling path regulating cell functions such as proliferation or gene expression. Chondrocytes seeded on a flat PLLA substrate spread and develop well defined focal adhesions and actin cytoskeleton. The peculiar morphology of electrospun mats imposes strong limitations to the formation of focal adhesions. This fact is responsible for the complex morphology of the cells cultured on electrospun mats [51] that can be observed in the SEM pictures of figure 5.4. Substrate morphology limits cell spreading [40] as can be observed in figure 5.5. Cells cultured in randomly aligned fiber mats have a non-fully extended morphology although the actin cytoskeleton is well developed (figure 5.5). Interestingly contact guidance makes that cells seeded in substrates with aligned fibers adopt an elongated morphology that has been observed many times when culturing different cell types on aligned electrospun membranes. Interestingly, the imposed restriction to spreading does not reduce the ability of chondrocytes to proliferate up to 14 days as can be seen by the MTT assays in the amorphous aligned or non-aligned mats. The decrease in viability for longer times is a consequence of the chondrogenic medium, without FBS, employed in cell culture. Nevertheless, cell numbers are still important up to 21 days culture as seen in the live-dead test shown in figure 5.7. Interestingly, fiber orientation and the hydrophobicity associated does not seem to affect cell proliferation in the case of amorphous fibers. The values of MTT tests are nearly identical in both supports. Crystallinity seems to decrease proliferation in the non-oriented supports, although dependence on crystallinity is not completely systematic. Proliferation drops sharply with the development of crystallinity in aligned fibers. It seems that proliferation is nearly suppressed when a limit in WCA is attained. Ballester-Beltran *et al.* [29] have recently shown that superhydrophobous surfaces can hinder the formation of focal adhesion. Suppression of proliferation in chondrocyte culture seems to be a requirement for the expression of the genes characteristic of the chondrocytes of hyaline cartilage and production of extracellular matrix. Interestingly, supports with crystalline aligned fibers induce active production of aggrecan by cells, collagen type II markers are positive only for several cells (figure 5.8). Lim *et al.* showed good performance of highly hydrophobous electrospun fiber mats in tissue production of bovine chondrocytes as well [33, 50, 52].

Some authors have been appointing the roughness as an important factor too on the cell behaviour [53-55]. In the 90s, Lincks *et al.* [56] studied at the microscale the influence of surface roughness and composition implants of pure titanium (Ti) and Ti-6Al-4V alloy implants on MG63 osteoblast-like cells behaviour. The samples were machined and either fine-polished or wet-ground, resulting in smooth and rough finishes, respectively. He reported that osteoblast-like cells respond in a differential manner to both surface roughness and material composition, which can be confirmed by decreased proliferation and increased ALPase and osteocalcein. In his study, one conclusion can be done that surface roughness may play one of the major roles in orthopedic implants and consequently the roughness should be present on the implants design. A recently study of Washburn *et al.* [57] investigated the crystallinity at nanoscale in cell response. A PLLA films with a gradient in crystallinity degree were developed lead changes in roughness from less than 1 to 13 nm. The most remarkable his finds suggests that the MC3T3-E1 proliferation rate on the smooth regions of the films is much greater than that on the rough regions.

However, our study shows that the roughness appears not to be the main factor on the cell behaviour, appointing the orientation and hydrophobicity affect overload the other factors, as already mentioned.

5.5 Conclusions

PLLA electrospun fibers are nearly amorphous after the electrospinning process. Aligned fiber mats are much more hydrophobous than randomly aligned ones. The fact that the fibers are aligned parallel to each other may be not crucial for the repellency to water. The inter-fiber void size can be also important and as detected by the difference in porosity, inter-fiber spacing is smaller in aligned fibers. Crystallization of the fibrils by thermal annealing at temperatures below melting does not affect membrane morphology, but produce an important increase of hydrophobicity what is ascribed to the tiny modification of the fiber roughness at nanometric scale and increase in fiber stiffness. Proliferation of human chondrocytes cultured in monolayer on these substrates is not different in aligned or non-aligned amorphous mats. However the differentiation rate seems to be higher on the non-aligned amorphous mats where it was possible observed amounts of aggrecan, characteristic of the extracellular matrix of hyaline cartilage. The crystallization of the aligned mats show nearly suppresses proliferation. The presence of collagen type II is only detected around part of the cultured cells, what is not unexpected in a monolayer culture even if culture medium is chondrogenic.

5.6 References

1. Huebsch, N. and D.J. Mooney, *Inspiration and application in the evolution of biomaterials.* Nature, 2009. **462**(7272): p. 426-432.

2. Place, E.S., N.D. Evans, and M.M. Stevens, *Complexity in biomaterials for tissue engineering.* Nat Mater, 2009. **8**(6): p. 457-470.

3. Rotter, N., et al., *Cartilage tissue engineering using resorbable scaffolds.* Journal of Tissue Engineering and Regenerative Medicine, 2007. **1**(6): p. 411-416.

4. Vasita, R. and D.S. Katti, *Nanofibers and their applications in tissue engineering.* International Journal of Nanomedicine, 2006. **1**(1): p. 15-30.

5. Kim, D.-H., et al., *Biomimetic Nanopatterns as Enabling Tools for Analysis and Control of Live Cells.* Advanced Materials, 2010. **22**(41): p. 4551-4566.

6. Gotting, C., et al., *Proteoglycan Biosynthesis during Chondrogenic Differentiation of Mesenchymal Stem Cells.* TheScientificWorldJOURNAL, 2007. **7**: p. 1207-1210.

7. Szivek, J.A., et al., *Selective cell proliferation can be controlled with CPC particle coatings.* Journal of Biomedical Materials Research Part A, 2007. **81A**(4): p. 939-947.

8. Izquierdo, R., et al., *Biodegradable PCL scaffolds with an interconnected spherical pore network for tissue engineering.* Journal of Biomedical Materials Research Part A, 2008. **85A**(1): p. 25-35.

9. Yaszemski, M.J., et al., *Evolution of bone transplantation: molecular, cellular and tissue strategies to engineer human bone.* Biomaterials, 1996. **17**(2): p. 175-185.

10. Murugan, R. and S. Ramakrishna, *Nano-Featured Scaffolds for Tissue Engineering: A Review of Spinning Methodologies.* Tissue Engineering, 2006
12(3): p. 435-447

11. Chen, J.-P. and C.-H. Su, *Surface modification of electrospun PLLA nanofibers by plasma treatment and cationized gelatin immobilization for cartilage tissue engineering.* Acta Biomaterialia, 2011. **7**(1): p. 234-243.

12. Lampin, M., et al., *Correlation between substratum roughness and wettability, cell adhesion, and cell migration.* Journal of Biomedical Materials Research, 1997. **36**(1): p. 99-108.

13. Anselme, K., et al., *The interaction of cells and bacteria with surfaces structured at the nanometre scale.* Acta Biomaterialia, 2010. **6**(10): p. 3824-3846.

14. Martínez, E., et al., *Effects of artificial micro- and nano-structured surfaces on cell behaviour.* Annals of Anatomy - Anatomischer Anzeiger, 2009. **191**(1): p. 126-135.

15. Yim, E.K.F. and K.W. Leong, *Significance of synthetic nanostructures in dictating cellular response.* Nanomedicine: Nanotechnology, Biology and Medicine, 2005. **1**(1): p. 10-21.

16. Yang, Y. and K.W. Leong, *Nanoscale surfacing for regenerative medicine.* Wiley Interdisciplinary Reviews: Nanomedicine and Nanobiotechnology, 2010. **2**(5): p. 478-495.

17. Jeon, H., et al., *The effect of micronscale anisotropic cross patterns on fibroblast migration.* Biomaterials, 2010. **31**(15): p. 4286-4295.

18. Yim, E.K.F., S.W. Pang, and K.W. Leong, *Synthetic nanostructures inducing differentiation of human mesenchymal stem cells into neuronal lineage.* Experimental Cell Research, 2007. **313**(9): p. 1820-1829.

19. Zhang, X., et al., *Nanofiber-modified surface directed cell migration and orientation in microsystem.* Biomicrofluidics, 2011. **5**(3).

20. Gümüşderelioğlu, M., F. Betül Kaya, and I.G. Beşkardeş, *Comparison of epithelial and fibroblastic cell behavior on nano/micro-topographic PCL membranes produced by crystallinity control.* Journal of Colloid and Interface Science, 2011. **358**(2): p. 444-453.

21. Ma, Z., et al., *Chondrocyte behaviors on poly-l-lactic acid (PLLA) membranes containing hydroxyl, amide or carboxyl groups.* Biomaterials, 2003. **24**(21): p. 3725-3730.

22. Cui, Y.L., et al., *Biomimetic surface modification of poly (L-lactic acid) with gelatin and its effects on articular chondrocytes in vitro.* Journal of Biomedical Materials Research Part A, 2003. **66A**(4): p. 770-778.

23. Ribeiro, C., et al., *Tailoring the morphology and crystallinity of poly(L-lactide acid) electrospun membranes.* Science and Technology of Advanced Materials, 2011. **12**(1).

24. Pérez Olmedilla, M., et al., *Response of human chondrocytes to a non-uniform distribution of hydrophilic domains on poly (ethyl acrylate-co-hydroxyethyl methacrylate) copolymers.* Biomaterials, 2006. **27**(7): p. 1003-1012.

25. Rahman, M.S. and T. Tsuchiya, *In vitro culture of human chondrocytes (1): A novel enhancement action of ferrous sulfate on the differentiation of human chondrocytes.* Cytotechnology, 2001. **37**(3): p. 163-169.

26. Wang, X.F., et al., *Engineering biomimetic superhydrophobic surfaces of electrospun nanomaterials.* Nano Today, 2011. **6**(5): p. 510-530.

27. Kong, J., et al., *Wettability of Polyethylene Micropatterns with Aligned One-Dimensional Nanostructures.* Journal of Macromolecular Science Part B-Physics, 2010. **49**(4): p. 711-722.

28. Chen, H.C., C.H. Tsai, and M.C. Yang, *Mechanical properties and biocompatibility of electrospun polylactide/poly(vinylidene fluoride) mats.* Journal of Polymer Research, 2011. **18**(3): p. 319-327.

29. Ballester-Beltran, J., et al., *Role of superhydrophobicity in the biological activity of fibronectin at the cell-material interface.* Soft Matter, 2011. **7**(22): p. 10803-10811.

30. Erbil, H.Y., et al., *Transformation of a simple plastic into a superhydrophobic surface.* Science, 2003. **299**(5611): p. 1377-1380.

31. Shi, L., et al., *Effect of additives on the fabrication of poly (vinylidene fluoride-co-hexafluropropylene) (PVDF-HFP) asymmetric microporous hollow fiber membranes.* Journal of Membrane Science, 2008. **315**(1-2): p. 195-204.

32. Cho, D., et al., *Structural properties and superhydrophobicity of electrospun polypropylene fibers from solution and melt.* Polymer, 2010. **51**(25): p. 6005-6012.

33. Lim, G.T., et al., *Highly Hydrophobic Electrospun Fiber Mats from Polyisobutylene-Based Thermoplastic Elastomers.* Biomacromolecules, 2011. **12**(5): p. 1795-1799.

34. Zheng, J., et al., *Studies on the controlled morphology and wettability of polystyrene surfaces by electrospinning or electrospraying.* Polymer, 2006. **47**(20): p. 7095-7102.

35. Li, X.H., et al., *Enhanced Mechanical Properties of Superhydrophobic Microfibrous Polystyrene Mats via Polyamide 6 Nanofibers.* Journal of Physical Chemistry C, 2009. **113**(47): p. 20452-20457.

36. Ma, M.L., et al., *Superhydrophobic fabrics produced by electrospinning and chemical vapor deposition.* Macromolecules, 2005. **38**(23): p. 9742-9748.

37. Asmatulu, R., M. Ceylan, and N. Nuraje, *Study of Superhydrophobic Electrospun Nanocomposite Fibers for Energy Systems.* Langmuir, 2010. **27**(2): p. 504-507.

38. Wang, S., et al., *Preparation of a durable superhydrophobic membrane by electrospinning poly (vinylidene fluoride) (PVDF) mixed with epoxy–siloxane modified SiO2 nanoparticles: A possible route to superhydrophobic surfaces with low water sliding angle and high water contact angle.* Journal of Colloid and Interface Science, 2011. **359**(2): p. 380-388.

39. Pisuchpen, T., et al., *Tuning Hydrophobicity and Water Adhesion by Electrospinning and Silanization.* Langmuir, 2011. **27**(7): p. 3654-3661.

40. Costa Martinez, E., et al., *Effect of poly(L-lactide) surface topography on the morphology of in vitro cultured human articular chondrocytes.* Journal of Materials Science-Materials in Medicine, 2007. **18**(8): p. 1627-1632.

41. Costa Martinez, E., et al., *Human Chondrocyte Morphology, Its Dedifferentiation, and Fibronectin Conformation on Different PLLA Microtopographies.* Tissue Engineering Part A, 2008. **14**(10): p. 1751-1762.

42. Park, A. and L.G. Cima, *In vitro cell response to differences in poly-L-lactide crystallinity.* Journal of Biomedical Materials Research, 1996. **31**(1): p. 117-130.

43. Sarasua, J.R., et al., *Crystallinity and mechanical properties of optically pure polylactides and their blends.* Polymer Engineering and Science, 2005. **45**(5): p. 745-753.

44. Salgado, A.J., et al., *Influence of molecular weight and cristallinity of poly(L-lactic acid) on the adhesion and proliferation of human osteoblast like cells,* in Advanced Materials Forum Iii, Pts 1 and 2, P.M. Vilarinho, Editor. 2006. p. 1020-1024.

45. Wang, B., et al., *The effect of poly (L-lactic acid) nanofiber orientation on osteogenic responses of human osteoblast-like MG63 cells*. Journal of the Mechanical Behavior of Biomedical Materials, 2011. **4**(4): p. 600-609.

46. Kai, D., et al., *Guided orientation of cardiomyocytes on electrospun aligned nanofibers for cardiac tissue engineering*. Journal of Biomedical Materials Research Part B-Applied Biomaterials, 2011. **98B**(2): p. 379-386.

47. Feng, L., et al., *Super-hydrophobic surface of aligned polyacrylonitrile nanofibers*. Angewandte Chemie-International Edition, 2002. **41**(7): p. 1221-1223.

48. Torres, A.J., et al., *Nanobiotechnology and Cell Biology: Micro- and Nanofabricated Surfaces to Investigate Receptor-Mediated Signaling*. Annual Review of Biophysics, 2008. **37**(1): p. 265-288.

49. Zhang, X., et al., *Nanofiber-modified surface directed cell migration and orientation in microsystem*. Vol. 5. 2011: AIP. 032007.

50. Li, W.J., et al., *Biological response of chondrocytes cultured in three-dimensional nanofibrous poly(epsilon-caprolactone) scaffolds*. Journal of Biomedical Materials Research Part A, 2003. **67A**(4): p. 1105-1114.

51. Luong, T.H.N., et al., *The role of nanofibrous structure in osteogenic differentiation of human mesenchymal stem cells with serial passage*. Nanomedicine, 2011. **6**(6): p. 961-974.

52. Subramanian, A., et al., *Preparation and evaluation of the electrospun chitosan/PEO fibers for potential applications in cartilage tissue engineering*. Journal of Biomaterials Science-Polymer Edition, 2005. **16**(7): p. 861-873.

53. Rim, N.G., et al., *Mussel-inspired surface modification of poly(l-lactide) electrospun fibers for modulation of osteogenic differentiation of human mesenchymal stem cells*. Colloids and Surfaces B: Biointerfaces, 2012. **91**(0): p. 189-197.

54. Flemming, R.G., et al., *Effects of synthetic micro- and nano-structured surfaces on cell behavior*. Biomaterials, 1999. **20**(6): p. 573-588.

55. Meredith, J.C., et al., *Combinatorial characterization of cell interactions with polymer surfaces*. Journal of Biomedical Materials Research Part A, 2003. **66A**(3): p. 483-490.

56. Lincks, J., et al., *Response of MG63 osteoblast-like cells to titanium and titanium alloy is dependent on surface roughness and composition*. Biomaterials, 1998. **19**(23): p. 2219-2232.

57. Washburn, N.R., et al., *High-throughput investigation of osteoblast response to polymer crystallinity: influence of nanometer-scale roughness on proliferation*. Biomaterials, 2004. **25**(7-8): p. 1215-1224.

6. Influence of processing conditions on polymorphism and nanofiber morphology of electroactive poly(vinylidene fluoride) electrospun membranes

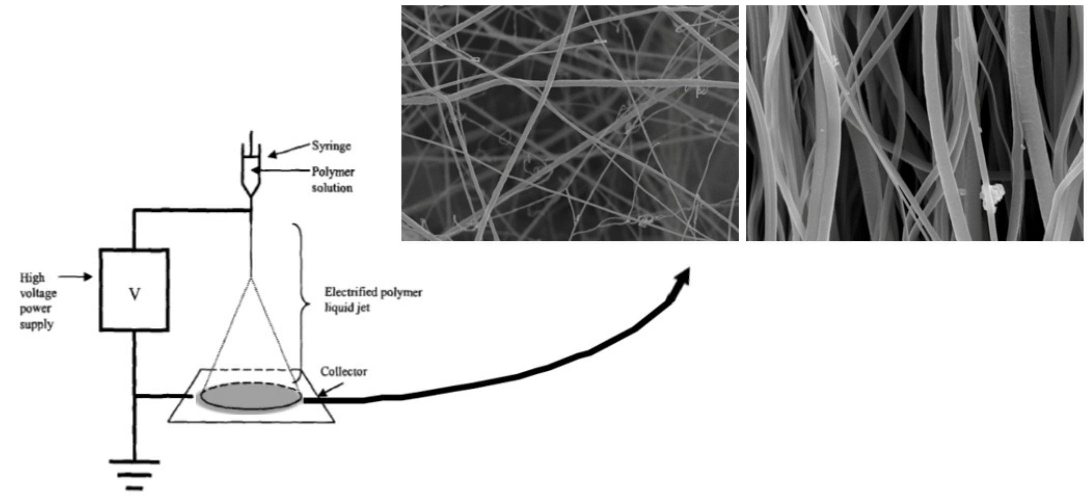
Syringe
Polymer solution
High voltage power supply
V
Electrified polymer liquid jet
Collector

This chapter is based on the following publication: C. Ribeiro, V. Sencadas, J.L. Gómez Ribelles and S. Lanceros-Méndez. *Influence of Processing Conditions on Polymorphism and Nanofiber Morphology of Electroactive Poly(vinylidene fluoride) Electrospun Membranes*. Soft Materials. 2010. 8: 274-287.

6.1 Introduction

Nanofibers can be produced by a variety of methods, such as drawing, template synthesis, self-assembly, wet spinning, electrospinning and phase separation. Most of these techniques present important drawbacks because sometimes processes are not scalable and not specific for certain polymers or have no control over the diameter and orientation of the fibers [1]. Electrospinning has demonstrated to be a unique method for the synthesis of submicron- or nanofibers from polymer solutions, suitable for a broad set of polymeric materials. This technique is relatively versatile, simple, fast and efficient. Electrospinning of PVDF has attracted interest for the production of membranes for various applications, including filtration, biomedical applications, sensors, batteries, cell phones, for chemical warfare protection, among others [2-6].

The PVDF is a material with particular scientific and technological interest due to its excellent properties including chemical resistance, good mechanical properties and, in particular, excellent electrical properties, such as piezo-, pyro and ferroelectricity [7].

The PVDF is a semi-crystalline polymer known by its polymorphism. Depending on the conditions of processing four different crystal structures: α, β, γ, and δ can be obtained [7-8]. The all trans, TTTT, planar zig-zag configuration confers to the β-phase the highest resulting permanent dipole and consequently the best piezoelectric and pyroelectric properties. Electroactive properties are also present in the γ and δ phases in a lesser extent. The TGTG' configuration of the α crystals makes the consecutive permanent dipoles of the monomer units to orient in opposite directions, resulting in no net dipole and therefore neutral polymer chain [7]. The β−phase is not formed by crystallization from the melt, whereas the α−phase is obtained in a broad range of crystallization temperatures [7-10]. Nevertheless, the β-phase can be produced by thermal and mechanical treatments of samples initially in the α-phase [11-13] and also by casting from solutions in several solvents [10]. These procedures produce the coexistence of several crystalline phases. In this way, the electroactive properties of PVDF heavily depend on the β-phase content, microstructure, and degree of crystallinity of the samples, which in turn depend on the processing conditions. Interestingly enough, it has been shown that the electrospinning conditions, namely solution parameters, processing, and environmental conditions strongly affect not only fiber morphology but also the phase in which PVDF crystallizes. In this way electrospinning seems to be a preferred technique for the development of electroactive membranes from PVDF.

Thus, Zheng *et al.* [14] found that electrospinning at lower temperatures of the chamber or fast evaporation of the solvent favor the formation of the β-phase. Further, high voltage or high stretching ratio of the jets also benefits crystallization in the β-phase, as well as the alignment of the electrospun fibers by using a rotating collector also favoured formation of β-phase [15]. It has been shown that the processing conditions and the solvent used influenced the crystalline fraction [14-15], as well as fiber average diameter [14-17], specific surface [17], surface tension [17], and mechanical properties [15] of the membrane.

Despite previous investigations, there is a lack of systematic information and understanding on how the different membranes processing parameters influence crystallinity, electroactive phase content and morphology, which are the key issues for tailoring membranes for specific applications. In this work we present a systematic study of the influence of electrospinning parameters such as the applied voltage, flow rate, needle diameter, and collecting procedure on the fiber morphology and orientation, the ratio of β- to α-phase and the total crystalline fraction present in the electrospun fibers.

6.2 Experimental

Materials: PVDF (Solef 1100, *Solvay*) was dissolved in DMF (*Merck*) with a concentration of 20% (w/w) of PVDF. The polymer was dissolved at room temperature in a magnetic stirrer. The viscosity of the solution was measured in a rheometric apparatus ViscoStar L plus.

Electrospinning: The polymer solution was placed in a plastic syringe (5 mL) fitted with a steel needle of tip-diameter between 250 and 500 μm. Electrospinning was conducted in a range of 15 to 30 kV with a high voltage power supply (*Glassman*, model PS/FC30P04). A syringe pump (*Syringepump*) was used to feed the polymer solutions into the needle tip at rate between 0.5 and 4 mL.h^{-1}. The electrospun fibers were collected in an aluminum and in a rotating drum that was placed at 15cm from the needle, to obtain random and oriented nanofibers, respectively.

Characterization: Electrospun fibers were coated with gold using a sputter coating and their morphology was observed by scanning electron microscopy (model JSM-6300, *JEOL*) with an accelerating voltage of 20 kV and a magnification of 1000-10000X. The size of nanofibers was measured on 4000X magnified SEM images using the Scion Imaging software (*Scioncorp*).

FTIR measurements were performed at room temperature in a Perkin-Elmer Spectrum 100 apparatus in ATR mode from 4000 to 650 cm^{-1}. Differential scanning calorimetry measurements were performed in a Mettler-Toledo DSC823e apparatus at a heating rate of 10 ºC.min^{-1}. The samples for the DSC studies were cut into small pieces from the middle region of the electrospun membranes and placed into 40 µL aluminum pans. All experiments were performed under a nitrogen purge.

The local piezoresponse measurements of single PVDF fiber were performed with a AFM (*Ntegra Prima, NT-MDT*). Doped Si cantilevers were used with spring constants of 0.5 - 3 N.m^{-1} driven at a frequency of 5 kHz. The experimental setup for the measurement of the electroactive properties of the PVDF fibers is shown in figure 6.1.

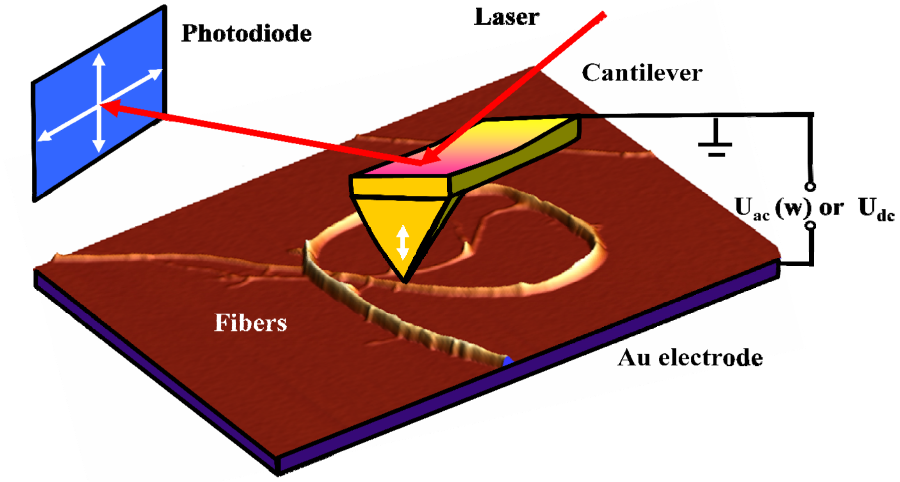

Figure 6.1 – Experimental setup for the measurement of the local piezoelectric response of single PVDF electrospun fibers (the fiber in the figure is a real polymer fiber).

6.3 Results and discussion

The main processing parameters that influence the morphology and properties of the electrospun fibers are those corresponding to the initial polymer solution. Among these parameters, the most relevant are the solvent used (its dielectric constant, volatility, boiling point, and others), the solution concentration (that controls its viscosity), and the molecular weight of the polymer (that must allow polymer entanglement). The main parameters that control the jet formation and solvent evaporation are the flow rate through the needle, the needle diameter, distance from the needle to the collector, temperature, and applied voltage. Finally the collection procedure, static or rotating collector, and the rotating collector speed are important parameters to determine the fiber diameter and orientation [1].

The number of parameters that influence the process is thus quite high and the study must fix some of them. In this work, we have used solutions of PVDF in DMF. The high polarity of the solvent facilitates the fiber formation. When the polymer content of the solution was lower than 20% microfibers did not form on the collector due to the low viscosity of the solutions (e.g., for polymer concentrations of 15% the viscosity is 191.5 cP). The results obtained for lower concentrations suggest that the entanglement of the molecules was not strong enough to overcome the repulsion of positive charge arising from the applied external voltage.

Solutions with 20% of PVDF were successfully electrospun on aluminized flat plates, and this concentration was fixed in all the study, the travelling distance between the needle and the collector was fixed at 15 cm. The viscosity for this solution was 831.91 cP and perfect fibers were formed. The influence of different parameters influencing jet formation: applied voltage, flow rate, and needle diameter was studied, as they are the ones most strongly influencing the phase present in the polymer. On the other hand, membranes of oriented fibers were obtained using a rotating collector and the influence of the rotation speed was characterized.

6.3.1 Influence of applied voltage

The influence of applied high voltage was investigated keeping constant the value of the needle diameter of 0.25 mm, flow rate of 4 $mL.h^{-1}$, and travelling distance of 15 cm.

The SEM pictures of figure 6.1 show the influence of applied voltage on the size of the electrospun fibrils. A histogram of fiber diameter was determined from SEM images and figure 6.2 shows the average ± standard deviation.

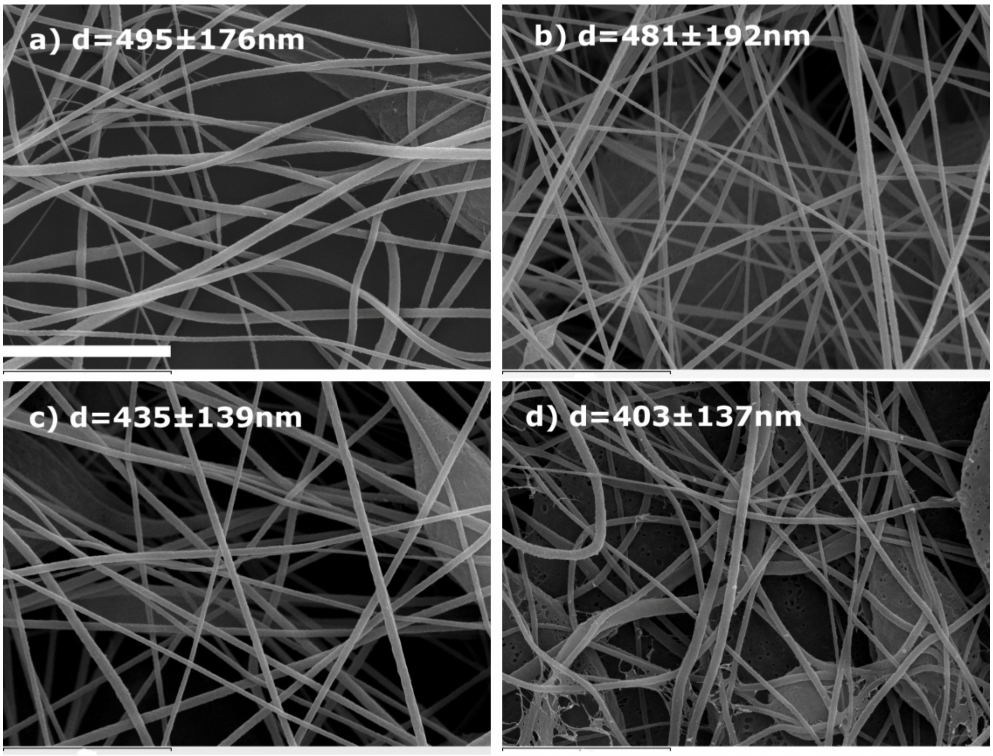

Figure 6.2 – SEM image of PVDF electrospun nanofibers obtained from a solution of 20/80 (20% PVDF + 80% DMF by w/w) at a traveling distance of 15cm, needle diameter of 0.25 mm and flow rate of 4 mL.h^{-1}, with an applied voltage of a) 15 kV, b) 20 kV, c) 25 kV and d) 30 kV.

It can be observed that the average fiber diameter of the polymeric electrospun membranes decreases from 495 nm to 403 nm with increasing voltage from 15 to 30 kV. In electrospinning, the high voltage is the drive of the electrospinning processing. The formation of ultra fine fibers is mainly achieved by the stretching and acceleration of the jets in a high electric field [18-19]. High applied voltages can result in a higher charge density on the surface of the ejected jets, thus the jet velocity increases and higher elongation forces are imposed to the jet. Consequently, it has been generally reported that the diameter of the final fibers becomes gradually smaller with increasing applied voltages [20-24]. The result is not general since changes in the applied voltage also affects other parameters of the process such as the traveling time of the jet with the opposite effect on the fiber diameter [1], thus in some cases no clear effect of the applied voltage has been found [25]. In fact the changes in the fiber diameter with the electric field in our case are quite modest. At the same time, an increase in the applied voltage also enhances the degree of the instability of the jets during the travel from the needle tip to the metal collector, which result in a broader distribution of the fiber diameters [23].

The influence of the voltage on the crystalline phase of the polymer was characterized by infrared FTIR spectroscopy. Figure 6.3 shows the FTIR spectra obtained for the different electrospun scaffolds.

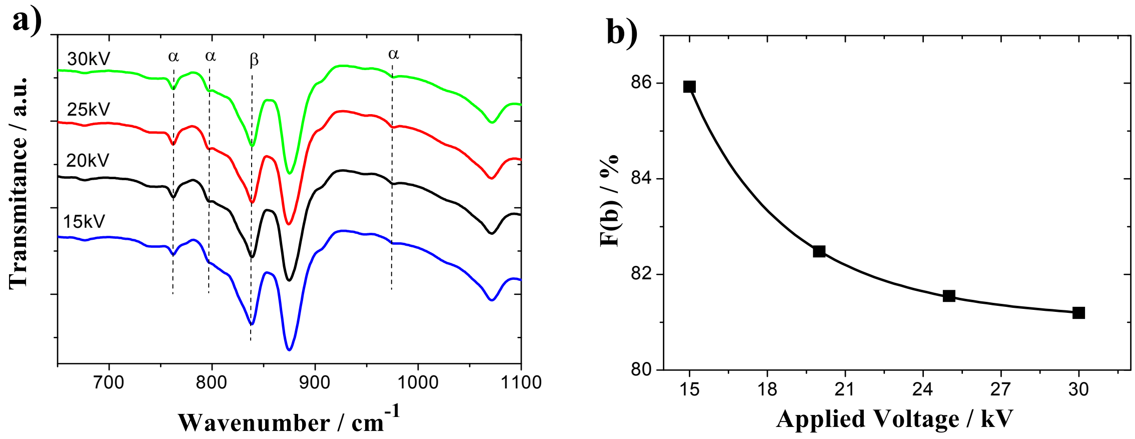

Figure 6.3 – a) Detail of the FTIR spectra for the PVDF electrospun scaffolds obtained at different applied voltages (lines indicates the absorption bands characteristics of the α- and β-phase), b) Crystalline phase content of the polymeric membranes.

Figure 6.3 a) shows the characteristic absorption modes for the α-phase (855, 766, 615 and 531 cm^{-1}) and β-phase (510 and 840 cm^{-1}) without traces of the γ-phase (431, 776, 812 and 833 cm^{-1}) [6, 26]. The general appearance of the spectra is similar for all samples: neither vibrational modes are totally suppressed nor new modes seem to appear due the increasing of the applied voltage. The evolution of the phase with applied voltage was also studied by FTIR on these samples. The method explained elsewhere [26] was applied to calculate the relative amount of α- and β-phase present in the different samples (Eq. 6.1).

$$F(\beta) = \frac{A_\beta}{(K_\beta / K_\alpha) A_\alpha + A_\beta} \qquad \text{(Eq. 6.1)}$$

Here, F(β) represents the β-phase content; A_α and A_β the absorbance at 766 and 840 cm^{-1}, corresponding to the α and β-phase of the material; K_α and K_β are the absorption coefficient at the respective wavenumber. The value of K_α and K_β are 6.1x10^4 and 7.7x10^4 cm^2.mol^{-1}, respectively [26]. The results obtained for the non-polar α-phase and for the electroactive β-phase amount present in each sample is illustrated in figure 6.3 b).

Figure 6.3 b) demonstrates that the crystalline main phase in the polymeric scaffolds is the β-phase, and the amount of the electroactive phase slightly decreases with increasing the applied electrical voltage. The maximum fraction of β-phase present in the scaffolds is ≅ 86%, obtained for V = 15 kV. For increasing voltages, the stretching effect by the field is counterbalanced by the enhancement in the degree of the instability of the jets, which result in not further increasing the amount of electroactive phase but even an small decrease of the β-phase content.

In order to determine possible modifications in crystal structure and melting behavior, DSC measurements were performed on raw PVDF and in the electrospun scaffolds with different average fiber diameters. Figure 6.4 a) shows the DSC thermograms of the samples. All samples showed similar endothermic peaks. It is to notice that the DSC curves show two melting peaks. The melting point of the α-phase of PVDF is several degrees lower than that of the β-phase and since FTIR results probe the presence of both phases in the sample, the two melting peaks that superpose in the DSC thermogram could be ascribed to the melting of both phases. Nevertheless this kind of results has to be consider with care since the DSC heating thermograms recorded at low heating rates can present more than one endotherm due to recrystallization taking place during the scan itself after the first melting, and also a distribution of crystal sizes could produce the same effect. So, a PVDF sample consisting of only α-phase could present a thermogram similar to the ones shown in figure 6.4 a). In the present case, contributions of the two existing phases (proven by FTIR) and a distribution of crystal sizes must be the main reasons for the observed thermograms.

The crystallinity degree of each sample was determined from the DSC curves using Eq. 6.2:

$$\Delta X_c = \frac{\Delta H}{x\Delta H_\alpha + y\Delta H_\beta} \tag{Eq. 6.2}$$

where ΔH is the melting enthalpy of the sample under consideration; ΔH_α and ΔH_β are the melting enthalpies of 100% crystalline sample in the α- and β-phase, respectively, and x and y are the amount of the α- and β-phase present in the sample, respectively. In this study, a value of 93.07 J.g^{-1} and 103.4 J.g^{-1} was used for the ΔH_α and ΔH_β, respectively [26-27] and x and y were obtained from the FTIR measurements as explained earlier (figure 6.3 b)).

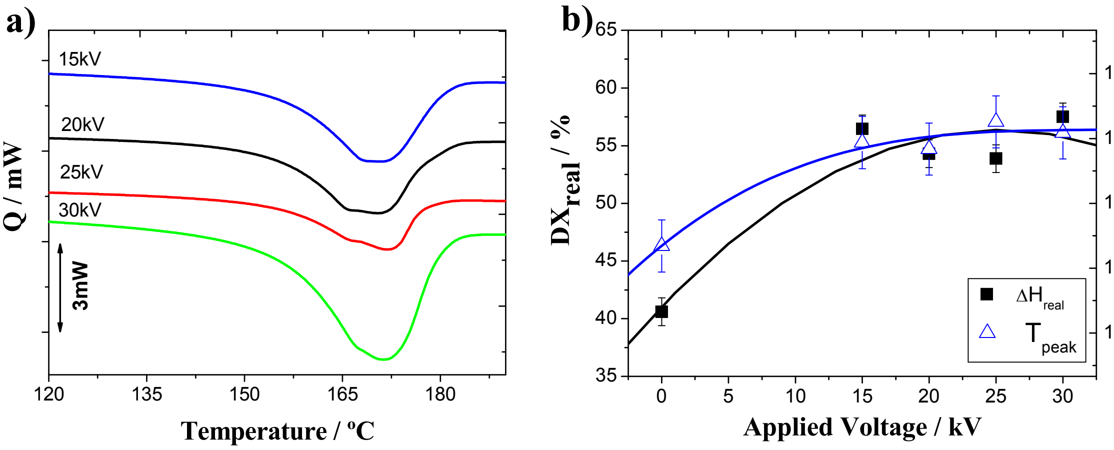

Figure 6.4 – a) DSC thermograms for the electrospun PVDF scaffolds processed at different applied voltages and b) crystallinity degree and melting peak temperature of the obtained electrospun mats.

Compared to α-PVDF films prepared by the conventional stretching method [6, 26], all electrospun samples show higher crystallinity content, corresponding to higher melting enthalpy. The solidification of the polymer molecular chains under high elongational rate during the spinning process may enhance the development of the polymer crystallinity. In other words, the molecular chains of PVDF partially crystallize under elongation before they are immobilized in the collector, where the final crystallization steps occur.

The peak temperature of the DSC thermograms (figure 6.4 b)), also show that samples of PVDF obtained by electrospinning have higher melting temperature than the PVDF films. Melting temperature and crystallinity of the electrospun samples on the other hand does not suffer significant changes with the applied voltage.

6.3.2 Influence of flow rate and needle diameter

When needle diameter is increased with respect to that used in the experiments explained in the former section, the fraction of β-phase decreased sharply. With a voltage of 20 kV, a traveling distance of 15 cm and a flow rate of 4 mL.h^{-1}, the increase of the needle diameter from 0.25 mm to 0.50 mm results in a decrease of the β-phase fraction from 86% to 53% as determined from the FTIR spectra. The fiber diameter significantly decreased, as can be observed by comparing the SEM picture of figure 6.2 b) with that of figure 6.5 d). The literature shows contradictory results in this point, thus Macossay *et al.* [28] found no influence of the needle diameter on the diameter of PMMA electrospun fibers, while Katti *et al.* reports that the fiber diameter decrease with decreasing needle diameter [22].

The influence of flow rate was investigated keeping constant the value of the voltage of 20 kV and needle diameter of 0.5 mm. Figure 6.5 shows that increasing the flow rate in the range from 0.5 to 4 mL.h^{-1} produces small changes in the fiber morphology, the increase of the fiber diameter with increasing flow rate that should be expected according to some authors [1, 29] was not found in this case. Some beads appeared when low flow rates were used with this larger needle diameter as also reported in PVDF [15]. The increase in surface tension can be main responsible for the formation of beads and loss of uniformity of the on the electrospun fibers. For a molecule within the solution, there is a uniform attractive force exerted on it by other molecules surrounding it. However, for a molecule at the surface of a solution, there is a net downward force as the molecules below exert a larger attractive force. Thus, the surface is in tension and this causes a contraction at the surface of the solution, which is balanced by repulsive forces that arise from the collisions of the molecules from the interior of the solution. The net effect of the pulling of all surface liquid molecules causes the liquid surface to contract thereby reducing the surface area [1].

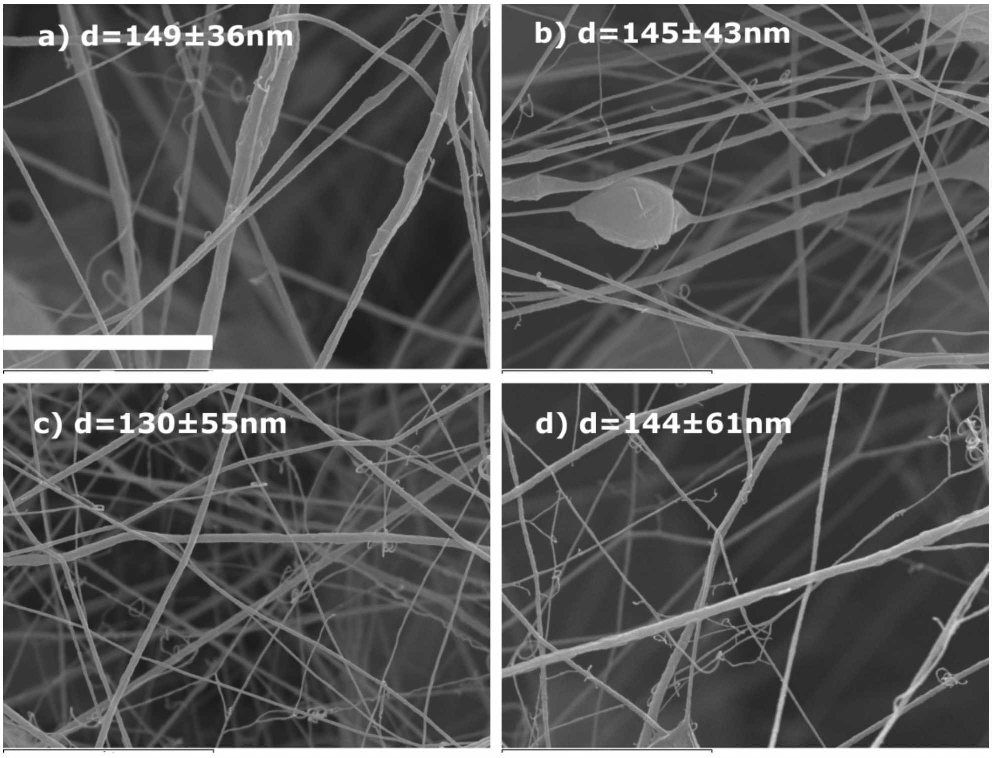

Figure 6.5 – SEM image of PVDF electrospun nanofibers obtained from a solution of 20/80 (20% PVDF + 80%DMF by w/w) at a traveling distance of 15cm, needle diameter of 0.5 mm and voltage of 20 kV, with an increase of flow rate from 0,5 to 4 mL.h^{-1} (a) 0,5 mL.h^{-1}, b) 1 mL.h^{-1}, c) 2 mL.h^{-1}, d) 4 mL.h^{-1}). The scale bar corresponds to 10 μm.

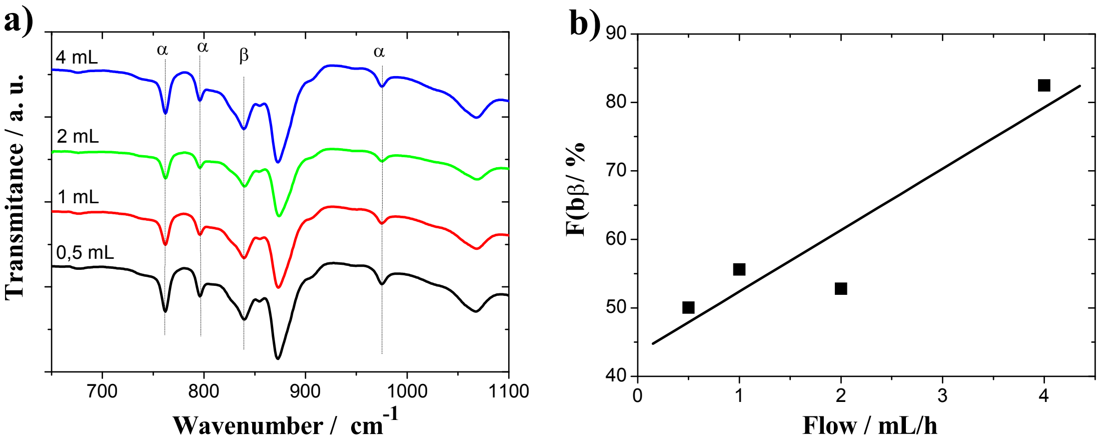

Figure 6.6 – a) Detail of the FTIR spectra for the PVDF electrospun membranes obtained at different flow rates (lines indicates the absorption bands characteristics of the α- and β-phase), b) Crystalline phase content of the polymeric membranes.

The fraction of β-phase is almost stable for the flow rates under consideration, indicating just a slight increasing trend with increasing flow rate (figure 6.6). This point can be compared to the findings of Zheng *et al.* [14] that compared electrospun fibers obtained from a solution of PVDF in a mixture of DMF and acetone at flow rate 75 mL.h^{-1} with those obtained at 5 mL.h^{-1}: the observed variations of the β-phase content with increasing flow are only significant for much higher rates than the ones used in the present investigation. Finally, neither the total crystalline fraction, considering both α- and β-phases according to Eq. 6.2, nor the melting peak temperature change significantly with the variation of the flow rate (figure 6.7).

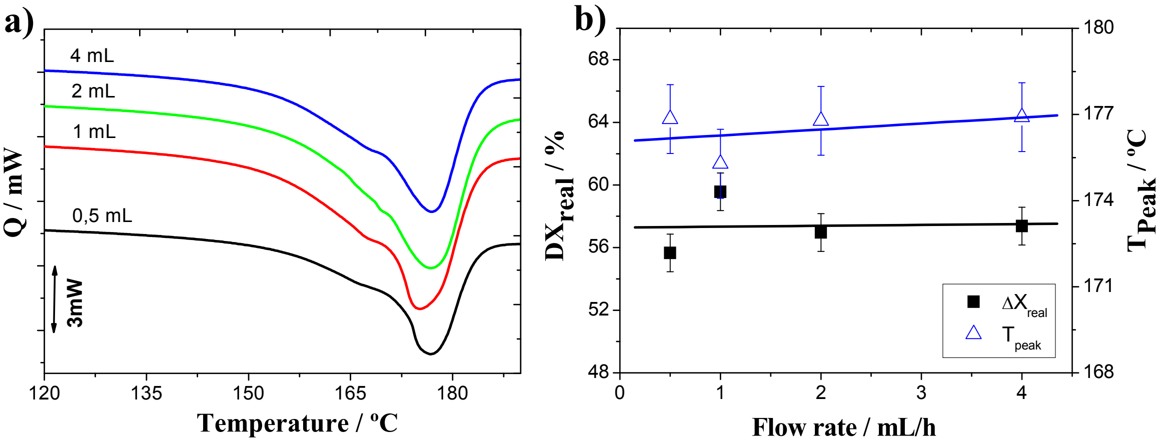

Figure 6.7 – a) DSC thermograms for the electrospun PVDF membranes processed at different flow rate, b) Influence of the flow rate on the crystallinity degree and melting peak temperature of the electrospun membranes.

The enhancement of the crystallization of PVDF in β-phase by decreasing needle diameter or increasing flow rate can be related to the increase of the jet stretching produced by both factors, favoring the ordering of the polymer chains in the *all trans* conformation.

6.3.3 Fibrils orientation using a rotating collector

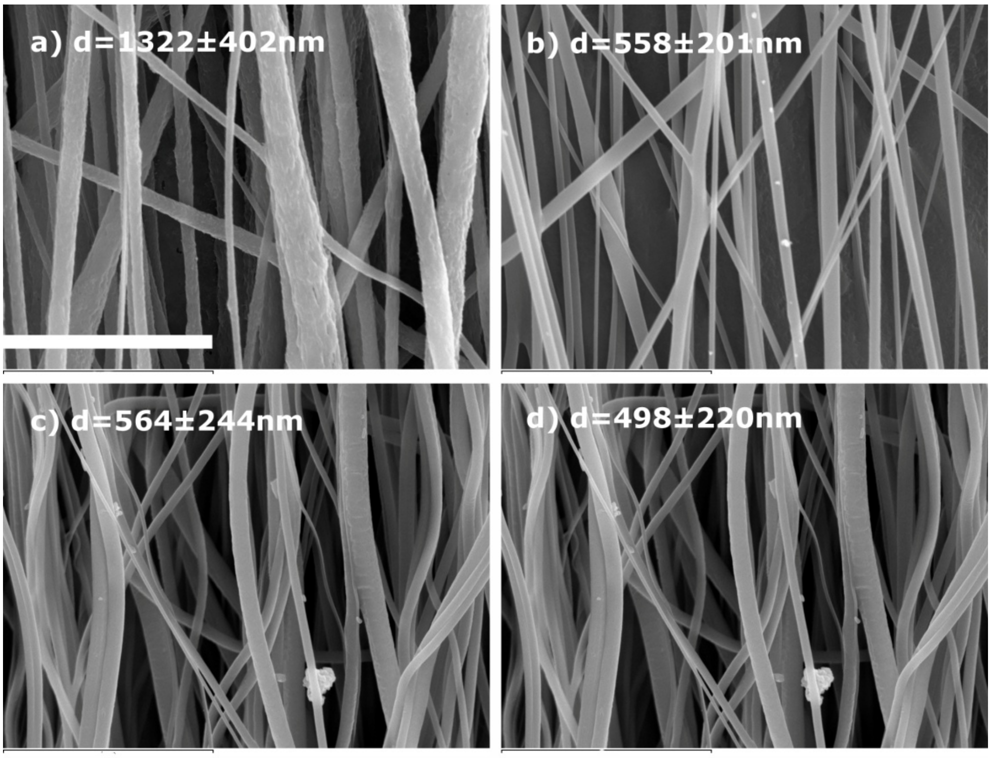

Figure 6.8 – SEM image of PVDF electrospun nanofibers obtained from a solution of 25/75 (25% PVDF + 75% DMF by w/w) at a traveling distance of 15 cm, needle diameter of 0.5 mm, voltage of 20 kV and flow rate of 4 mL.h^{-1}, with an increase of rotation from 750 to 2000 rpm: a) 750 rpm, b) 1000 rpm, c) 1500 rpm, d) 2000 rpm.

The electrospun fibrils could be effectively oriented using a rotating collector even at quite low rotation speed. The effect of the rotation speed on the fiber diameter is quite apparent as shown in figure 6.8. The influence of rotation was investigated keeping the value of the constant voltage of 20 kV, a flow rate of 4 mL.h^{-1} and needle diameter of 0.5 mm. As was explained in the former section, electrospun fibers obtained with 0.5 mm diameter needle contained around 50% of PVDF crystalline fraction in the β-phase, and a similar result is obtained in the case of the aligned fibers collected at low rotating speed. Interestingly, higher rotation speeds yield fibers with the same β- to α-phase ratios that can be obtained with narrower needles (figure 6.9). The effect of chain orientation during collection can be observed in the DSC traces as well (figure 6.10). After considering the differences in the mass of the samples, no significant change in the total crystal fraction can be observed when varying the rotation speed from 500 to 2000 rpm. On the other hand, the shape of the melting endotherm changes slightly, the characteristic double peak shown by PVDF (see figure 6.4 a)) appears in the electrospun fibers collected at 500 rpm but it disappears to form a single broad peak for higher rotation speed and the maximum shifts towards lower temperatures. The diameter of the fibrils is larger in the oriented fibers than in those produced using a flat collector using the same parameters (compare figure 6.5 d) and 6.8 a)), the reason can be that each oriented fiber rather than a monofilament is formed by more than one aligned fibrils that crystallize simultaneously [30]. Crystallization process during the electrospinning processing is an open research area both from the experimental and theoretical points of view, depending also on the polymer type [1]. The present investigation supports the arguments that, for PVDF, the crystallization process initiates in the travelling jet and finishes once the fibers are in the collector, as factors related to the jet and the collector influence the amount of β-phase content.

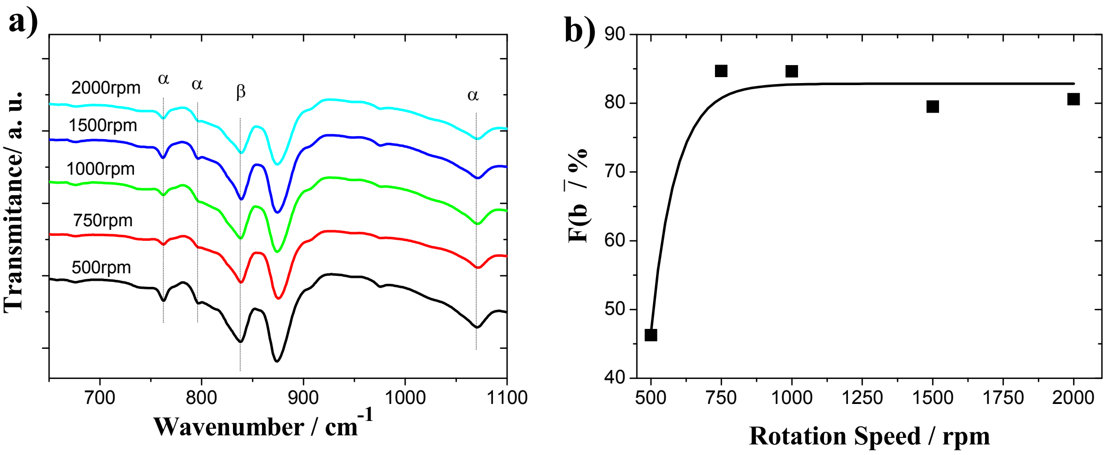

Figure 6.9 – a) Detail of the FTIR spectra for the PVDF electrospun membranes obtained at different rotations (lines indicates the absorption bands characteristics of α- and β-phase), b) Crystalline phase content of the polymeric membranes.

The influence of the different processing parameters on the crystalline morphology of electrospun fibers can be related to the well-known α- to β-phase transformation that takes place when an α-PVDF film is deformed at strain ratios approximately 500% in the temperature range ranging between 80 and 140 ºC [11-13]. Under the tension loading, after yield, not only the lamellae shifts with respect to each other and orient, but they can be effectively melted and then recrystallization takes place under the applied tension. In this way, the formation of the β-phase is favored by the amorphous chain orientation under irreversible flow. In the case of PVDF processed by electrospinning the key factor that seems to determine crystal organization is the ability of jet straining to orient polymer chains. Further, also the straining of the fibers during collection at the same time than the solvent evaporates is able to enhance the all-trans conformation of the polymer chains and their crystallization in β-phase.

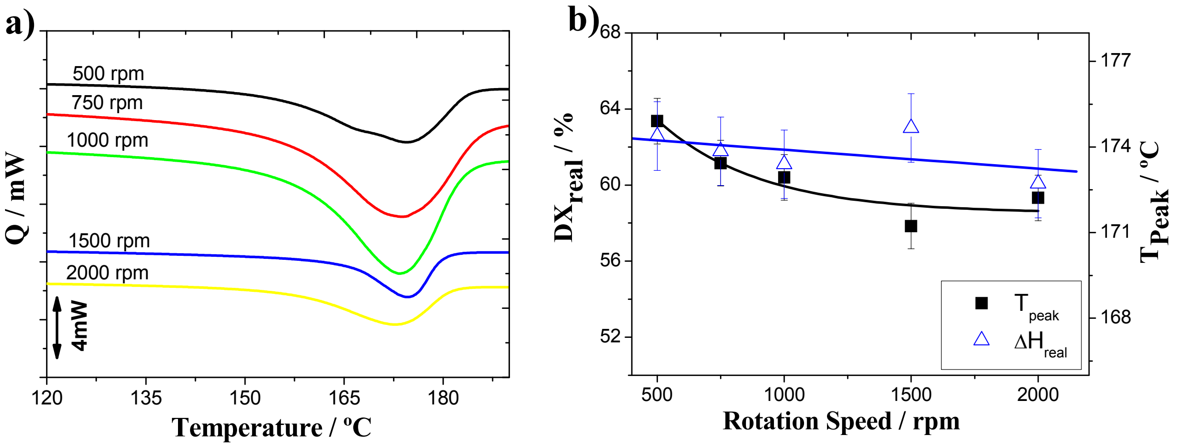

Figure 6.10 – a) DSC thermograms for the electrospun PVDF membranes processed at different rotations, b) Influence of the applied voltage in the crystallinity degree and melting peak temperature of the electrospun membranes.

6.3.4 Local piezoelectric response of a single PVDF electrospun fiber

The piezoelectric characteristics of single fibers was demonstrated and evaluated by PFM. The influence of the time of the applied electric field in the area and length of the domain switching was studied and the nanofibers were submitted at an electric field of + 20 V during different time intervals (figure 6.11). A complete saturation was obtained for this applied electric field, and as it can be observed in figure 6.11, the poled area increases linearly with increasing poling time for the poling times under consideration. It was also noticed that the minimum voltage measured for the poled sample is independent of applied time (figure 6.11 c)). The domain area (figure 6.11 e)) and domain length (figure 6.11 f)) increase almost linearly with increasing poling time. This linear behavior, attributed to the semi crystalline nature of the polymer, allows precise control of the poled dimensions within the fibers which is of large advantage for patterning active areas on the fibers for applications such as data storage and sensors and actuators.

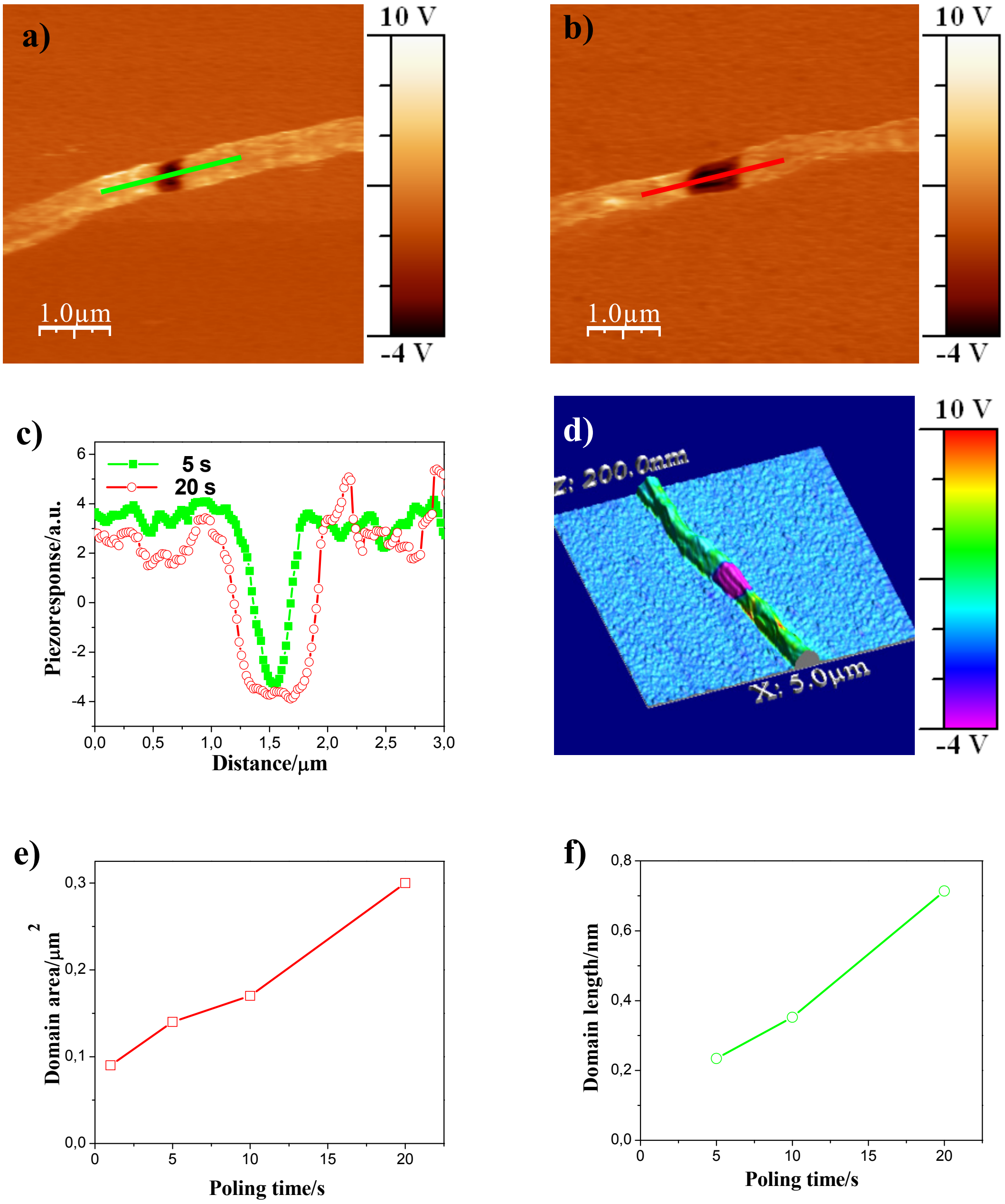

Figure 6.11 – PFM images of the patterns obtained for the E = 20 V: a) t = 5 s, b) t = 20 s, c) electrical response of the fiber for the different time intervals of the applied electric field, d) poled area, e) domain area as a function of the applied time and f) domain length for the different time of the applied electrical field.

6.4 Conclusions

Polyvinyl fluoride can be electrospun from a solution in DMF if the polymer concentration is above 20% w/w. For lower concentrations, the density is too low to allow an stable electrospinning process with fiber formation. In present work, the influence of different parameters influencing jet formation: applied voltage, flow rate, and needle diameter on the morphology, β-phase, and crystallinity content of the membranes was studied. Their parameters were chosen as they are the ones most strongly influencing the phase present in the polymer, and therefore, its electroactivity. Further, membranes of oriented fibers were obtained using a rotating collector and the influence of the rotation speed on the morphology, β-phase content and crystallinity was also characterized.

The fraction of β-phase can range between more than 85% to around 50% in the parameter window explored in this work. Those parameters leading to a higher stretching of the jet or straining of the fibrils during collection favor the formation of β-phase. In this way, increasing rotating speeds and decreasing needle diameters, improves strongly the β-phase content. On the other hand, the range voltages and flow rates used in the present investigations do not show large influence in the electroactive phase content. The total crystalline fraction depends only slightly on the electrospinning conditions but it is higher than in PVDF produced by other conventional methods from the melt or casting from a solution.

Piezoelectric response, polarization switching and nanoscale patterning of the fibers have been demonstrated and a function of applied field and poling time. In this way, both the direct implementation of as electrospun fibers into electroactive applications and the possibility of tailored patterning for specific applications have been demonstrated.

6.5 References

1. Ramakrishna, S., et al., *An Introduction to Electrospinning and Nanofibers*. 2005: World Scientific Publishing Company.

2. Cheng, L.P., et al., *PVDF membrane formation by diffusion-induced phase separation-morphology prediction based on phase behavior and mass transfer modeling.* Journal of Polymer Science Part B-Polymer Physics, 1999. **37**(16): p. 2079-2092.

3. Xiao, Q., et al., *Macroporous polymer electrolytes based on PVDF/PEO-b-PMMA block copolymer blends for rechargeable lithium ion battery.* Journal of Membrane Science, 2009. **334**(1–2): p. 117-122.

4. Choi, S.W., et al., *Characterization of electrospun PVdF fiber-based polymer electrolytes.* Chemistry of Materials, 2007. **19**(1): p. 104-115.

5. Laroche, G., et al., *Polyvinylidene fluoride monofilament sutures - can they be used safely for long term anastomoses in the thoracic aorta.* Artificial Organs, 1995. **19**(11): p. 1190-1199.

6. Klinge, U., et al., *PVDF as a new polymer for the construction of surgical meshes.* Biomaterials, 2002. **23**(16): p. 3487-3493.

7. Lovinger, A.J., *Developments in crystalline polymers*. Vol. vol. 1. 1982, London: Elsevier Applied Science.

8. Nalwa, H.S., *Ferroelectric polymers: chemistry, physics and applications*. Vol. vol. 1. 1995, New York: Marcel Dekker, Inc.

9. Gregorio, R. and R.C. Capitao, *Morphology and phase transition of high melt temperature crystallized poly(vinylidene fluoride).* Journal of Materials Science, 2000. **35**(2): p. 299-306.

10. Gregorio, R. and M. Cestari, *Effect of crystallization temperature on the crystalline phase content and morphology of poly(vinylidene fluoride).* Journal of Polymer Science Part B-Polymer Physics, 1994. **32**(5): p. 859-870.

11. Sencadas, V., R. Gregorio, and S. Lanceros-Mendez, *alpha to beta Phase Transformation and Microestructural Changes of PVDF Films Induced by Uniaxial Stretch.* Journal of Macromolecular Science Part B-Physics, 2009. **48**(3): p. 514-525.

12. Gregorio, R. and E.M. Ueno, *Effect of crystalline phase, orientation and temperature on the dielectric properties of poly (vinylidene fluoride) (PVDF).* Journal of Materials Science, 1999. **34**(18): p. 4489-4500.

13. Matsushige, K., et al., *The II-I crystal transformation of poly(vinylidene fluoride) under tensile and compressional stresses.* Polymer, 1980. **21**(12): p. 1391-1397.

14. Zheng, J., et al., *Polymorphism Control of Poly(vinylidene fluoride) through Electrospinning.* Macromolecular Rapid Communications, 2007. **28**(22): p. 2159-2162.

15. Yee, W.A., et al., *Morphology, polymorphism behavior and molecular orientation of electrospun poly(vinylidene fluoride) fibers.* Polymer, 2007. **48**(2): p. 512-521.

16. Zhao, Z.Z., et al., *Preparation and properties of electrospun poly(vinylidene fluoride) membranes.* Journal of Applied Polymer Science, 2005. **97**(2): p. 466-474.

17. Huang, L.H., et al., *Synthesis of biodegradable and electroactive multiblock polylactide and aniline pentamer copolymer for tissue engineering applications.* Biomacromolecules, 2008. **9**(3): p. 850-858.

18. Reneker, D.H., et al., *Bending instability of electrically charged liquid jets of polymer solutions in electrospinning.* Journal of Applied Physics, 2000. **87**(9): p. 4531-4547.

19. Qin, X.H., et al., *Effect of LiCl on electrospinning of PAN polymer solution: theoretical analysis and experimental verification.* Polymer, 2004. **45**(18): p. 6409-6413.

20. Megelski, S., et al., *Micro- and nanostructured surface morphology on electrospun polymer fibers.* Macromolecules, 2002. **35**(22): p. 8456-8466.

21. Demir, M.M., et al., *Electrospinning of polyurethane fibers.* Polymer, 2002. **43**(11): p. 3303-3309.

22. Katti, D.S., et al., *Bioresorbable nanofiber-based systems for wound healing and drug delivery: Optimization of fabrication parameters.* Journal of Biomedical Materials Research Part B-Applied Biomaterials, 2004. **70B**(2): p. 286-296.

23. Gao, K., et al., *Crystal structures of electrospun PVDF membranes and its separator application for rechargeable lithium metal cells.* Materials Science and Engineering: B, 2006. **131**(1–3): p. 100-105.

24. Zhao, S., et al., *Electrospinning of ethyl–cyanoethyl cellulose/tetrahydrofuran solutions.* Journal of Applied Polymer Science, 2004. **91**(1): p. 242-246.

25. Casper, C.L., et al., *Controlling surface morphology of electrospun polystyrene fibers: Effect of humidity and molecular weight in the electrospinning process.* Macromolecules, 2004. **37**(2): p. 573-578.

26. Lanceros-Mendez, S., et al., *FTIR and DSC studies of mechanically deformed beta-PVDF films.* Journal of Macromolecular Science-Physics, 2001. **B40**(3-4): p. 517-527.

27. Doshi, J. and D.H. Reneker, *Electrospinning process and applications of electrospun fibers.* Journal of Electrostatics, 1995. **35**(2-3): p. 151-160.

28. Macossay, J., et al., *Effect of needle diameter on nanofiber diameter and thermal properties of electrospun poly(methyl methacrylate).* Polymers for Advanced Technologies, 2007. **18**(3): p. 180-183.

29. Zong, X., et al., *Structure and process relationship of electrospun bioabsorbable nanofiber membranes.* Polymer, 2002. **43**(16): p. 4403-4412.

30. Moon, S. and R.J. Farris, *How is it possible to produce highly oriented yarns of electrospun fibers?* Polymer Engineering & Science, 2007. **47**(10): p. 1530-1535.

7. Fibronectin adsorption and cell response on electroactive poly(vinylidene fluoride) films

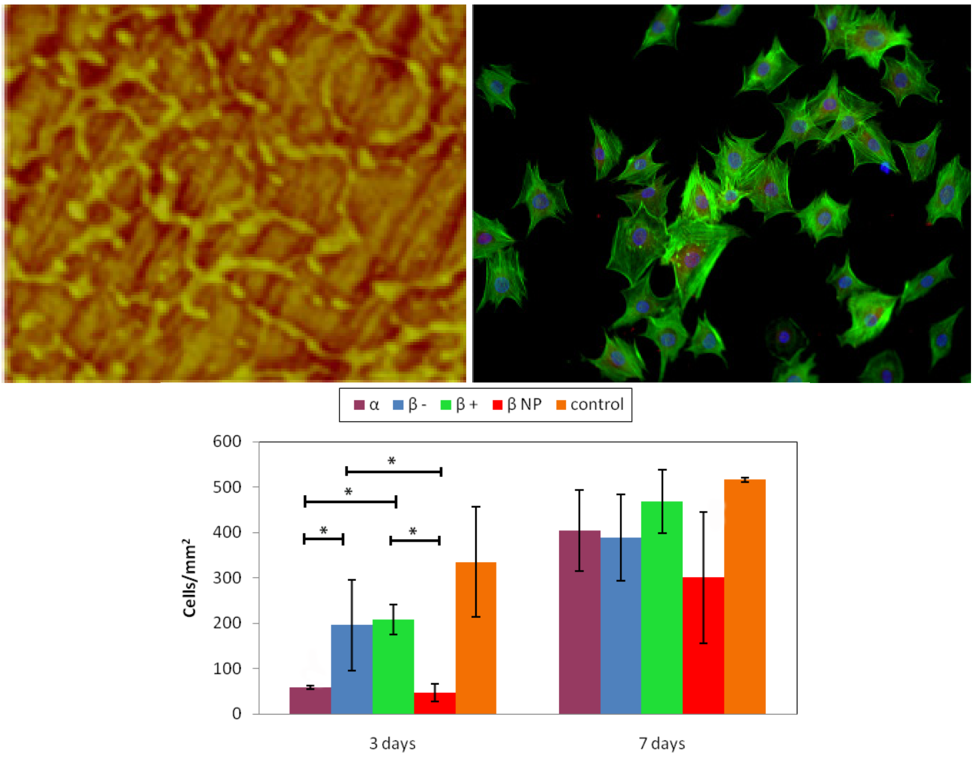

This chapter is based on the following publication: C. Ribeiro, J.A. Panadero, V. Sencadas, S. Lanceros-Méndez, M.N. Tamaño, D. Moratal, M. Salmerón-Sánchez, J.L. Gómez Ribelles. *Fibronectin adsorption and cell response on electroactive poly(vinylidene fluoride) films*. Biomedical Materials. 2012. 7: 035004

7.1 Introduction

In the last decades, a wide variety of biomaterials with different properties have been studied and developed for biomedical applications. The cell/biomaterial interaction is a complex multi-step process that consists of several events. The first observable event *in vivo* or in a culture medium *in vitro* is the adsorption of proteins [1-2]. Then, cell adhesion is mediated by cell-surface receptors that interact with specific ligands recognized in the layer of proteins previously adsorbed on the biomaterial surface [3-4]. This protein layer is then reorganized and substituted by matrix proteins produced by the cells [5-7]. The quality of this first phase of cell/biomaterial interactions will influence the ability of the cells for proliferation and differentiation [8-9].

The adsorption of matrix proteins such as fibronectin (FN) on substrate surfaces has been shown to be of large importance when culturing a variety of cells *in vitro* [10-11]. The activity of adsorbed proteins (*i.e.* the distribution, concentration, conformation and motility) plays an important role in the biofunctionality of the biomaterial and allows understanding the biological response in cell culture in the laboratory [4, 10]. The surface characteristics such as chemical composition, topography, viscoelastic properties, electric charge distribution and others determine how biological molecules will be absorbed by the surface and, more particularly, it will also determine the conformation of adsorbed molecules [8, 12]. In this way, the behavior of cells cultured on substrates is highly dependent on these characteristics.

Previous studies have shown that electrically charged surfaces can influence cell behavior in different aspects such as growth, adhesion or morphology of cells. Beyond this, an electrically charged base for tissue engineering applications can be an interesting and promising approach [13]. Electroactive polymers, in particular piezoelectric PVDF, have attracted interest for biomedical applications in the fabrication of sensors and actuators and supports for cell culture. PVDF shows good biocompatibility, chemical resistance, and, in particular, excellent electroactive properties, such as piezo-, pyro-, and ferroelectricity [14]. This polymer can be obtained in four different crystalline phases, known as α, β, γ and δ, depending on the processing conditions. The β-phase is the one with the best piezoelectric and pyroelectric properties [14-15].

The processing conditions optimizing the electroactive properties of β-PVDF have been previously studied both for films obtained from solvent evaporation [16-17] and for films obtained by mechanical stretching [18-19]. Particularly relevant for the present work are previous studies by scanning force microscopy in a piezoresponse mode on the variations in the topological morphology and piezoelectric surface response of PVDF [20]. The piezoelectric activity at a mesoscale reflects the semicrystalline nature of the polymer: the piezoelectric activity of the *β*-phase at a mesoscopic scale is formed by dispersed nanoregions instead of classical domains. Clear differences in the poled region distribution and size, as well as in the local piezoactivity, have been identified in the different forms of PVDF: in the poled *β*-PVDF samples, the piezoelectric activity is more evident than before poling, the piezoelectric activity of *β*-PVDF being independent of the processing method and morphology. No local piezoelectric activity is obtained in *α*-PVDF, corresponding to the non-polarity of the macromolecule and the absence of macroscopic piezoelectric response.

Due to the potential of electroactive materials in the biological and biomedical field, as they respond to electrical and mechanical solicitations, the aim of this work is to understand the role of the crystalline phase and polarity (i.e. surface charge) of electroactive supports on the cell response. With this purpose, the polymer with the largest electroactive response, β-phase PVDF, is investigated. As a first step fibronectin from human plasma was adsorbed on the different PVDF films from solutions of varying protein concentration. The surface density of adsorbed FN was quantified by the ELISA technique and the protein distribution and conformation was observed by AFM. Thereafter, the effect of polymer phase (α or β) and surface polarization on preosteoblasts morphology, viability and proliferation was studied.

7.2 Materials and methods

7.2.1 Preparation of polymer films

PVDF films with thickness of around 30 μm were obtained by casting a 20% solution of PVDF in DMF on a glass slide, applying the procedure reported in [16, 18]. Briefly, a glass slide with the spread solution was kept inside an oven at a controlled temperature of 120 ºC for 60 min in order to assure the removal of the solvent and the isothermal crystallization of PVDF. After evaporation of the solvent, the sample was melted at 220 ºC for 10 min. Then, the samples were removed from the oven, cooled to room temperature and removed from the glass. The polymer obtained by this procedure is predominantly α-PVDF. These films were then uniaxially drawn in a tensile machine at a stretching velocity of ~ 1 mm.min^{-1} at a temperature of 80 ºC and a draw ratio ($R = L_{fnal}/\ L_{initial}$) of 5. After this procedure, the β-phase content of the samples is maximized up to ~85% [18-19]. The α to β phase transformation is accompanied by a morphological transition from a spherulitic microstructure typical of the α- PVDF to a microfibrilar microstructure [18].

The electrical poling of the β-PVDF films was performed by a corona discharge inside of a home-made chamber and the piezoelectric response (d_{33}) of the poled samples was analyzed with a wide range d_{33}-meter (model 8000, *APC Int Ltd*). The obtained value of the piezoelectric d_{33} coefficient for the poled samples was ~ -32 pC.N^{-1} [16].

For cell culturing, circular PVDF films with 11 mm diameter were cut from the prepared films and sterilized by immersing several times in 70% ethanol for 15 min. Before cell seeding, the samples were washed 5 times for 5 min in phosphate-buffered saline solution.

The films used in this study were α-PVDF, non-poled β-PVDF, “poled +” β-PVDF (cell culture on the positively charged side of the sample) and “poled –” β-PVDF (cell culture on the negatively charged side of the sample).

7.2.2 Contact angle measurements

The contact angle measurements (sessile drop in static mode) were performed at room temperature in a Data Physics OCA 20 device using distilled water as test liquid. All the micrographs were taken at the same focal distance (20 cm) and the volume of the drops was of 20 µl. The contact angles were determined after six repetitions for each sample by using image analysis software (Image J) taking into account the entire drop shape.

7.2.3 Fibronectin adsorption

FN distribution on the different substrates was observed by AFM. Fibronectin from human plasma (*Sigma-Aldrich*) was adsorbed on the different PVDF films (α-PVDF, non-poled β-PVDF, "poled +" β-PVDF and "poled –" β-PVDF) by immersing the material sheets in FN solutions with different concentrations (1, 2 and 5 μg.mL^{-1}) in modified saline (0.4% NaCl) for 10 min. After protein adsorption, the samples were rinsed in saline solution to eliminate the non-adsorbed protein. After that, the samples were dried by exposing their surface to a nitrogen flow for a few minutes. AFM experiments were performed in tapping mode in air immediately after sample preparation, using a Multimode AFM equipped with NanoScope IIIa controller (*Veeco*), at ambient conditions. Si-cantilevers with a constant force of 2,8 N.m^{-1} and a resonance frequency of 75 kHz were used. All the samples were characterized using a set-point amplitude ratio of around 0.9. The NanoScope 5.30r2 software version was used for the simultaneous recording of the height, phase and amplitude magnitudes of the images.

FN conformation was characterized by ELISA using monoclonal antibodies directed to cell adhesion domains. FN was adsorbed on all samples from a solution of 5 μg.mL^{-1} for 1 h at 37 ºC. The same samples without FN were used as controls. After FN adsorption, the surfaces of PVDF films were washed a few times in DPBS solution to remove non-adsorbed protein. After the FN adsorption, the nonspecific binding sites of the PVDF surface were blocked with DPBS with bovine serum albumin (DPBS++/BSA) 1% for 30 min at room temperature. Then, the samples were incubated in the presence of monoclonal antibody IgG1 (*DSHB University of Iowa*), directed against the synergic site, in the FN repeat III$_{9,}$ in dilution 1:4000 for 1h at 37 ºC. Following the incubation, each substrate was washed a few times with DPBS++/Tween 20. After being rinsed, a secondary antibody, antimouse alkaline phosphatase (Jackson Immuno Research), in dilution 1:5000 was added to the PVDF substrates for 1h at 37 ºC and then washed again as described above. The 4-methylumbelliferyl phosphate (4-MUP; *Sigma-Aldrich*) was added to the samples for 45 min at 37 ºC. The optical density (absorbance) of the wells at a wavelength of 465 nm was measured using a standard plate reader (Victor III, Perkin Elmer). Each experiment was performed in triplicate.

7.2.4 Cell adhesion and overall morphology

MC3T3-E1 cells (Riken cell bank, Japan) were cultivated in DMEM 1 g.L^{-1} glucose (Gibco) containing 10% FBS (Fisher) and 1% penicillin/streptomycin (P/S) at 37 ºC in CO_2 incubator. To investigate the initial cell adhesion and overall cell morphology, osteoblast-like cells suspended in 400 μL of serum-free DMEM were seeded on the substrates (PVDF samples disks and control glass covers) in 24-well TC plates at a cell density of 1×10^4 cells/well. All samples (three repetitions per sample) were previously coated with FN (20 $\mu g.mL^{-1}$) for 1 h at 37 °C. After 2 h of incubation, the cells were rinsed with DPBS and fixed with formalin solution 10%, neutral buffered (*Sigma-Aldrich*) (1 h at 4 ºC). After that, the substrates were washed with DPBS, permeabilized with Triton X-100 (5 min at room temperature) and incubated with a monoclonal mouse antibody against vinculin (*Sigma-Aldrich*) (1:400 in 1% DPBS/BSA, at room temperature for 1h in agitation). The samples were rinsed a few times with 0.5% DPBS/Tween 20. Thereafter, it was added Alexa Fluor 633-conjugated rabbit anti-mouse secondary antibody (Invitrogen) (1:200 in 1% DPBS/BSA, at room temperature for 1h in agitation) and, at the same time, Bodipy FL Phallacidin (Invitrogen) for actine cytoskeleton (10 μL/sample). At last, the substrates were washed with 0.5% DPBS/Tween 20 and mounted with Vectashield containing DAPI. Focal adhesions were visualized by immune-fluorescence staining of vinculin. Images of adhered cells were taken with a fluorescence microscope (Leica DM6000B). Cytoplasma observed by cytoskeleton images were processed and analyzed using an in house software developed under MATLAB R2009b (The MathWorks, Inc., Natick, MA, USA). Mean cell area was calculated for every sample.

To determine the area covered by each cell, the processing of the cytoplasm images consisted firstly in grayscaling and equalization. Afterwards, the images were binarized using the Otsu's method [21] and the existing gaps were filled using an erosion morphological operator followed by a dilation one, using both a diamond structuring element of size 3. The resulting image was size-filtered using an opening morphological operator to eliminate remaining isolated pixels. In this way, a binary image stating the cytoplasm coverage was obtained, allowing the calculation of the total area covered by the cells or the mean area covered by each cell.

7.2.5 Cell viability and proliferation

For the study of cell viability and proliferation, the cells were seeded in 24-well TC plates with PVDF films and glass covers used as control at a cell density of 10^4 cells/well for 3 days and 7 days, and incubated at 37 ºC and 5% CO_2. All samples (three repetitions for each sample) were previously immersed in a fibronectin solution 20 μg.mL^{-1} for 1 h at 37 ºC. After washing all samples with DPBS, cells were suspended in DMEM without serum and seeded in the samples for 2 h at 37 ºC and 5% CO_2. Finally, medium was replaced with DMEM containing 10% FBS.

For the quantification of cell viability and proliferation, 3-(4,5-dymethylthiazol-2-yl)-5-(3-carboxymethoxyphenyl)-2(4-sulfopheny)-2H tetrazolium (MTS) assay (CellTiter 96^{TM} Aqueous One Solution Cell Proliferation Assay, Promega) was carried out. In this assay, the samples were washed a few times with DPBS. Then, 600 μL of MTS solution (prepared with DMEM low glucose without FBS, in a relation 1:5) was added to the substrates and it was incubated for 3 h at 37 ºC in a 5% CO_2 incubator. At the end of the incubation period, 100 μL of each sample were transferred (in triplicate) into a 96 well-plate. Finally, the absorbance at 490 nm, representing the proportion of viable cells, was measured by an optical spectrometer (Victor III, Perkin Elmer).

For cell number quantification, after fixation with a formalin buffered solution, the cell –supports constructs were mounted with Vectashield containing DAPI for fluorescence microscopy (Leica DM6000B). For cell counting, the previously described software was used. Cell nuclei images were firstly grayscaled and equalized, providing an output grayscale image with its intensity values evenly distributed throughout the intensity range. These new images were then binarized through the Otsu's method and size-filtered using an opening morphological operator. The cell nuclei were finally labeled and counted. Thus, cell number per mm^2 was calculated.

7.2.6 Statistical analysis

The results were expressed in mean ± standard deviation. Statistical comparisons were made by ANOVA and F-tests were used for the evaluation of different groups. The differences were considered significant when $p<0.05$.

7.3 Results

7.3.1 Contact angle measurements

Surface wettability (generally referred to as hydrophobicity/hydrophilicity) is one of the most important parameters affecting the biological response. According to the literature, wettability affects protein adsorption and cell adhesion [22-23]. The wettability of the different PVDF film surfaces was determined showing that (figure 7.1) the non-poled β-PVDF film is the more hydrophobic, with a contact angle of 76.8º, significantly higher than that measured in α-PVDF. Corona treatment produces an increase of the wettability of the β-PVDF films surface. The "poled +" β-PVDF film is the most hydrophilic material with a contact angle of 31.8 °C, lower than that of the negatively charged surface.

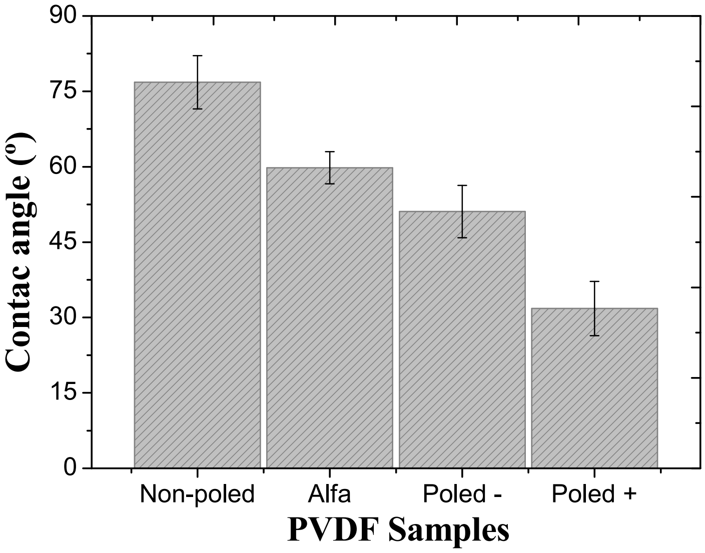

Figure 7.1 – Evaluation of water contact angle of different PVDF films (Alfa, Beta non-poled, poled + and poled -).

7.3.2 Surface topography

The processing conditions of PVDF influence the phase content, morphology and electroactivity [20]. PVDF adopts an spherulitic morphology in the α phase [15], that can be observed in the AFM pictures (figure 7.2 a), b)). Crystal lamellae are apparent both in amplitude and phase images. The α-PVDF is a non-electroactive phase and the mean roughness measured in 2 x 2 microns surface areas (average of 3 measurements) was around 68.5 nm. The topography of β-PVDF is quite different, being characterized by an oriented microfibrilar microstructure [18] (figure 7.2 c), d)). When the β-PVDF sample is poled there are no significant differences in morphology. With the AFM analysis of the local piezoresponse data of the non-poled β-PVDF and poled samples, it is shown [20] that a clear piezoresponse signal exists in both samples, being therefore the domain contrast more pronounced in the poled samples. The mean roughness of the non-poled β-PVDF is approximately 42 nm. The poling process does not affect the topography of the samples which maintain the same mean roughness [20]. The analysis of the line profiles of the topographic image and the corresponding domain contrast image confirm that there is no relationship between the surface piezoelectric response and the topography [20].

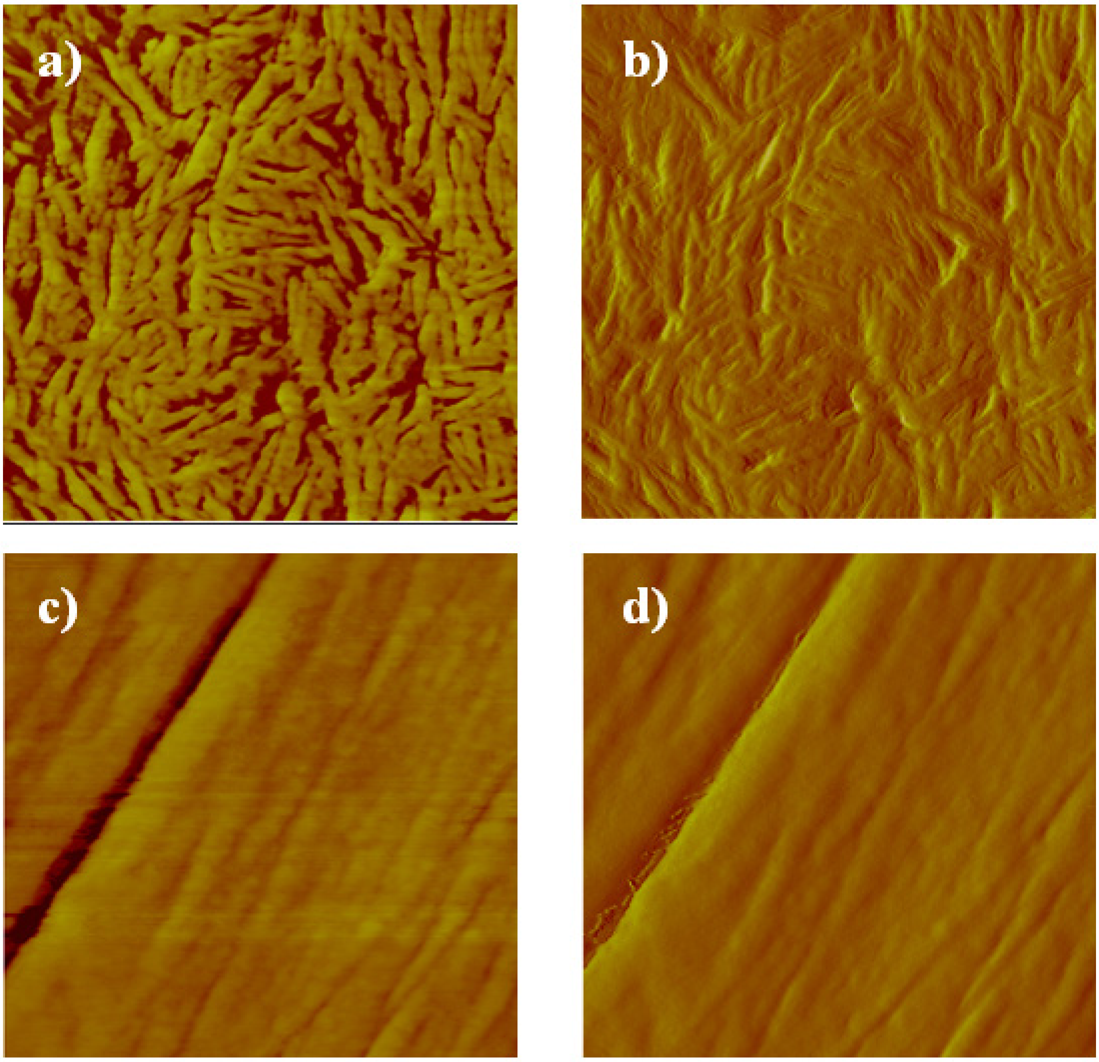

Figure 7.2 – AFM images recorded in a 1 x 1 μm area of: a) - b) α-PVDF and c) - d) non-poled β-PVDF surfaces. a) - c) Phase and b) - d) amplitude pictures.

7.3.3 Protein adsorption

The distribution of fibronectin adsorbed on the substrate can be observed by AFM provided the surface density of protein molecules is low enough. If the amount of protein adsorbed is too high, a continuous coating is formed preventing the observation of single protein molecules as well as their distribution at the material interface. This is the reason why FN was adsorbed on the substrates from aqueous solutions of varying concentration. Figure 7.3 shows AFM images (height, phase and amplitude) of non-poled β-PVDF films after FN adsorption from a 2 μg.mL^{-1} solution.

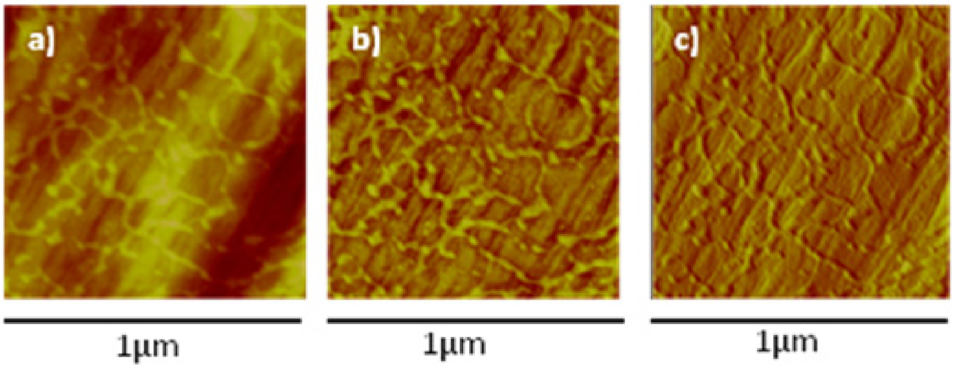

Figure 7.3 – AFM images of non-poled β-PVDF with fibronectin adsorbed form a solution with a concentration of 2 μg.mL^{-1}. a) Height, b) phase and c) amplitude magnitudes respectively.

Figure 7.4 shows the AFM images of the adsorbed proteins on the different PVDF films. FN distribution and organization on the surface depends significantly on the type of substrate and the concentration of the protein solutions.

The influence of the crystalline phase of the polymers is quite apparent when comparing α-PVDF and non-poled β-PVDF films. In both cases at the lower solution concentrations (1 – 2 μg.mL^{-1}), homogeneously distributed FN molecules on the substrates are observed. When FN was adsorbed from a 2 μg.mL^{-1} solution, a well defined fibrillar distribution is found on β-PVDF, with the incipient formation of a protein network. On the other hand, a more homogeneous FN distribution is found on α-PVDF. Higher concentration of the FN solution (5 μg.mL^{-1}) gives rise to the formation of a FN continuous protein coating that, in the case of α-PVDF, completely covers the spherulitic topography of the polymer. Likewise, α- and β-PVDF surfaces display similar appearance when they are completely covered by the protein layer.

In the poled β-PVDF films, the situation is quite different: a dense coating is formed already when FN is adsorbed from the 1 µg.mL^{-1} solution. By increasing FN concentration, some changes in the topography of the protein surface are observed with no observable differences between the “poled +” and “poled –” β-PVDF substrates.

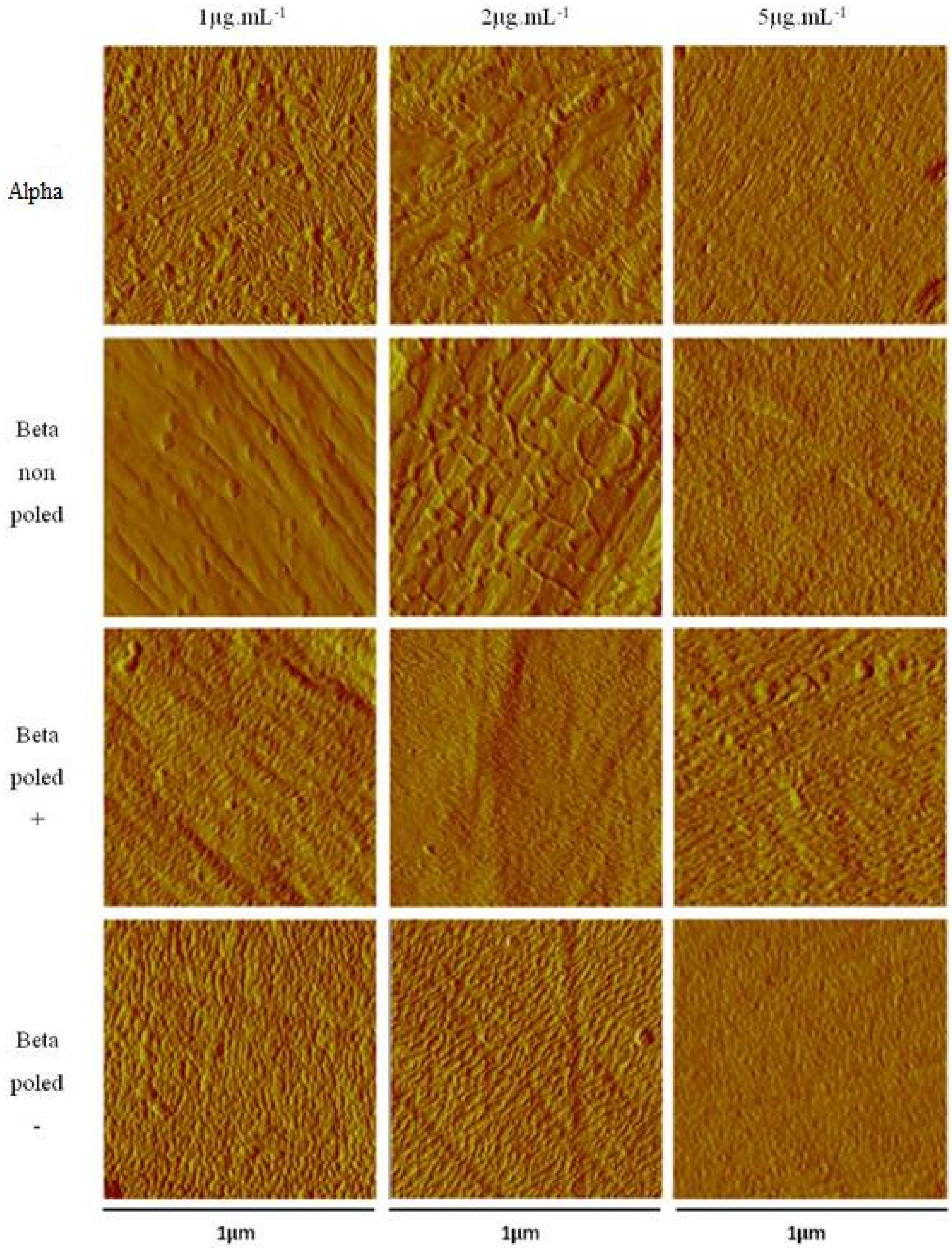
1µg.mL-1
2µg.mL-1
5µg.mL-1
Alpha
Beta non poled
Beta poled +
Beta poled -
1µm
1µm
1µm

Figure 7.4 – Fibronectin distribution as observed by the amplitude magnitude in AFM on the different substrates (α–PVDF, β-PVDF non-poled, “poled +” β-PVDF and “poled –” β-PVDF). Fibronectin was adsorbed for 10 min from solutions of different concentrations (1µg.mL^{-1}, 2 µg.mL^{-1}, 5µg.mL^{-1}).

Single molecules could not be distinctly observed by AFM even in smaller scans areas. However, it can be inferred from FN adsorption from solution of concentration 2 μg.mL^{-1} that approximately the same amount of FN is adsorbed on the different surfaces. Further, the differences in protein distribution observed at the lower concentrations suggest surface-induced changes in FN conformation [24]. Thus, an ELISA assay was performed to quantify differences in FN conformation, using antibodies against adhesion related domains, in order to obtain information about domain exposition. Figure 7.5 shows the results of the ELISA experiments for the different PVDF films and the control substrate. These results confirm that adhesion domains in poled β-PVDF films are more available for cell adhesion than in either non poled β-PVDF or α-PVDF films. These domains are significantly masked in non-poled β-PVDF. Nevertheless, the difference between positively or negatively charged surfaces is not significant.

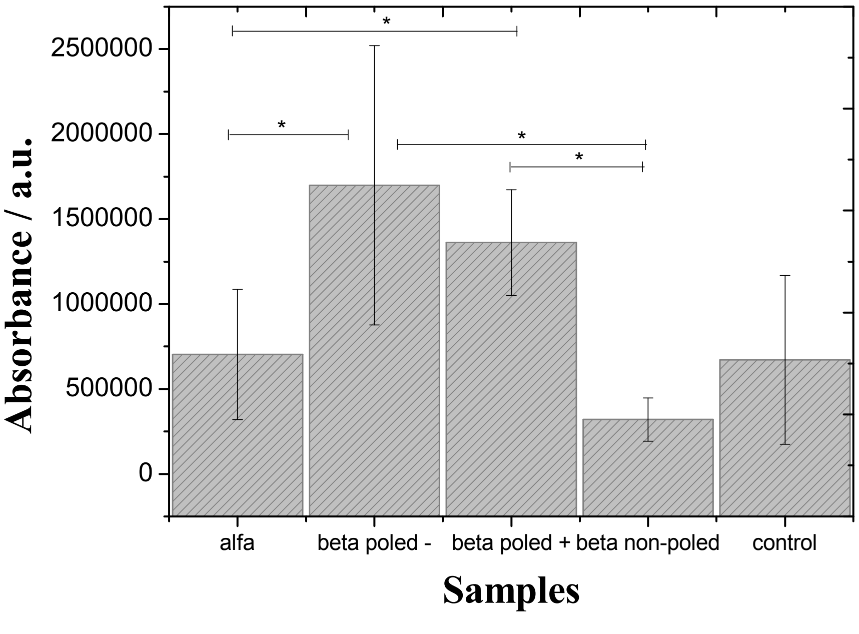

Figure 7.5 – Monoclonal antibody binding for HFN7.1 monoclonal antibody on the different PVDF samples after FN adsorption from a solution of concentration 5 μg.mL^{-1}. * Significantly different ($p<0.05$) PVDF samples.

7.3.4 Cell attachment and cell proliferation

The overall morphology of the cells after 2 h is observed in figure 7.6. With respect to cell morphology and cell area, no significant differences were detected between poled and non-poled films, as well as between films in different phases and the control glass.

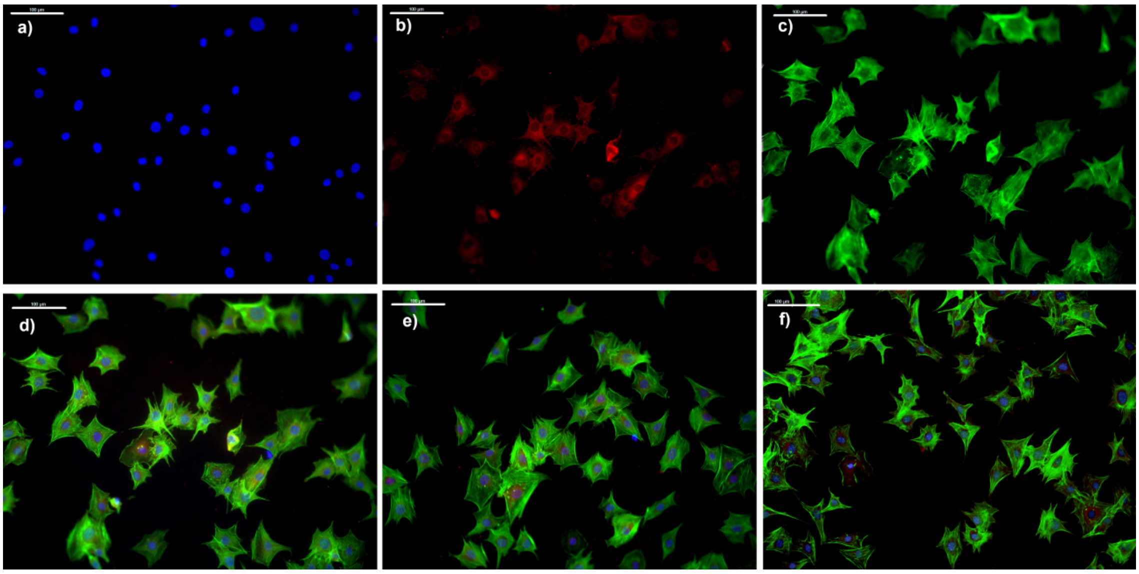

Figure 7.6 – Cell culture with pre-osteoblast cells during 2 h in negative poled β-PVDF film (DAPI stained nuclei are shown in a), vinculin expression in b) and F-actin staining in c), overlay d)) For comparison the overlay images of α-PVDF film and control glass are shown in e) and f) respectively. The scale bar (100µm) is valid for all the images.

Figure 7.7 shows the viability of the attached osteoblast cells in PVDF films and control after 3 and 7 days of culture. For all substrates, the number of viable cells increased with cell culture time. The substrates that seem to promote more active proliferation are α-PVDF and both positive and negative poled β-PVDF films, with no significant differences with respect to the control and among them. Cell viability is significantly lower in the case of non-poled PVDF as shown by the MTS test. Nevertheless, when cell nuclei were stained with DAPI and counted from fluorescence microscopy images no significant differences in cell density between poled and non-poled β-PVDF substrates was found (figure 7.8).

The shapes of the cells attached on the different substrates are quite similar to each other and also similar to the control, as shown in figure 7.6. Cells are extended on the substrates and form well defined and developed actin cytoskeleton. Using image analysis, the average surface covered by a cell was found to be 4475 ± 349 μm^2 with no significant differences among the substrates.

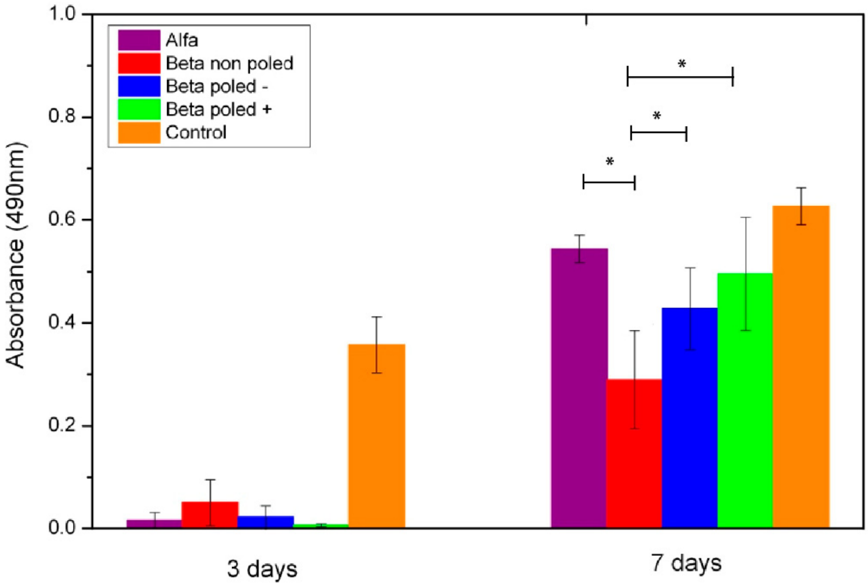

Figure 7.7 – MTS absorbance results after cells seeded for 3 and 7 days on different PVDF films and control substrate. * Significantly different ($p<0.05$) PVDF samples.

Cell density on the different substrates is represented in figure 7.8. After 3 days, all samples show low number of cells. After 7 days of cell culture, the samples show significant differences in the number of cells. Also, it can be also observed that the cell distribution in the samples is not uniform. The control substrate shows the highest number of cells mm^{-2}, but comparing just the different PVDF films, the non-poled β-PVDF films show the lowest cell number and the poled α -PVDF films the highest number, with no significant differences with both poled β-PVDF, positive and negative .

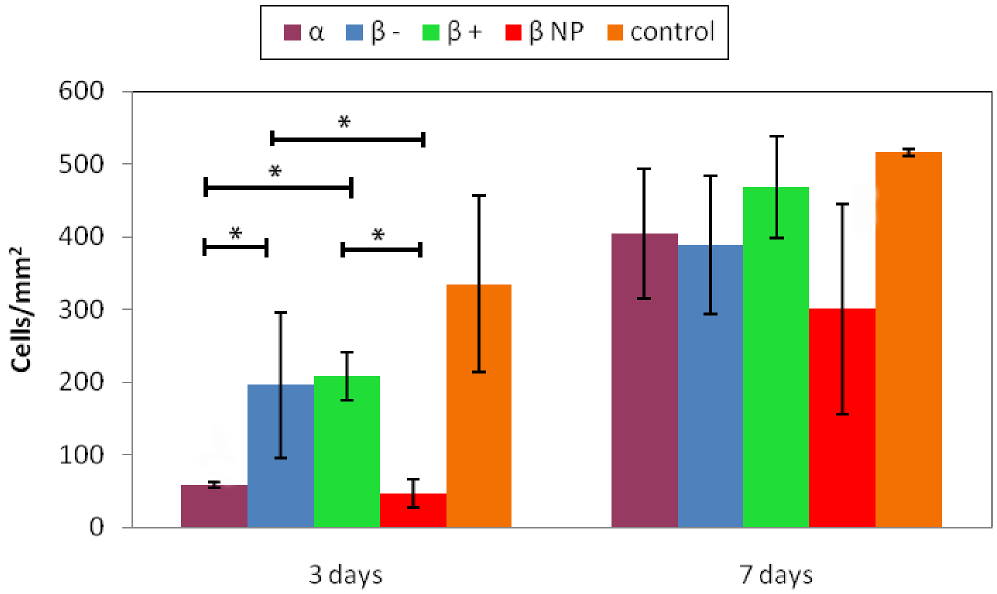

Figure 7.8 – Cell density after for 3 and 7 days on different PVDF films and control substrate. * Significantly different ($p<0.05$) PVDF samples.

7.4 Discussion

The surface properties of PVDF are influenced by its crystalline phase, not only because of the different arrangement of crystal lamellae that, as shown in figure 7.2, leads to a different roughness and surface topography, but also due to a different surface energy leading to a quite hydrophobic material in the case of non-poled β-PVDF and to a more hydrophilic one in the case of α-PVDF. The reason for these differences is related to the different ordering of the permanent dipoles along the polymer chains in one and another crystalline order. The configuration of PVDF chains crystallized in α-phase is a non-polar trans-gauche-trans-gauche', TGTG', configuration, leading the consecutive permanent dipoles of the monomer units to orient in opposite directions, resulting in no net dipole per unit cell [14, 25]. The crystalline β-phase has an all trans planar zigzag configuration, TTT, which confers to this crystalline phase the highest resulting permanent dipolar moment and consequently the best electroactive properties [14, 25]. Note, nevertheless, that the non-poled β-phase PVDF shows a random distribution of the dipolar moments, and therefore, the overall surface charge will be zero. Just by poling the samples and alignment of the dipolar moments and an overall surface distribution will be achieved [20].

FN adsorption has been studied on different synthetic substrates. A straightforward correlation between substrate hydrophilicity and FN adsorption does not exist since other surface properties such as surface chemistry [26-27], the presence of particular functional groups [28], roughness or the presence of patterning cues [27] also have an important effect on FN adsorption. While many studies have shown that larger amounts of protein get adsorbed on hydrophobic surfaces than on hydrophilic ones, as it is the case with other matrix proteins as laminin, fibrinogen or vitronectin [29-30], the literature also shows many important examples of higher activity of FN on hydrophilic surfaces [31-32]. On the other hand, the conformation of FN on the substrate is also highly influenced by other surface characteristics. It seems that an important characteristic of FN with respect to cell adhesion is its ability to intermolecular linkage forming a fibrillar structure (fibrillogenesis) or a protein network. Cell activity seems to be essential for fibrillogenesis but it has been observed in some synthetic substrates in absence of cells. This is the case of hydrophobous poly(ethyl acrylate) substrates [33-34].

When the electroactive β-PVDF is poled by corona discharge, introducing a positive or negative electric charge density, the wettability of the surface increase significantly as shown in figure 7.1.

In the PVDF substrates of this work the observed behavior by adsorbed fibronectin is peculiar in some aspects. Although the AFM images of figure 7.4 give no quantitative information about protein adsorption, they suggest that adsorbed protein quantity is higher in poled β-PVDF than in non-poled β-PVDF or in α-PVDF but only when adsorbed from low FN concentration solutions. When FN is adsorbed from a 5 $\mu g.mL^{-1}$, the FN layer observed in all samples looks similar. When dispersed protein domains are observed, the images suggest differences in distribution. The visual aspect in non-poled β-PVDF is clearly different than in α-PVDF when immersed in the same FN solution. Association in fibrils seems to appear only in non-poled β-PVDF, which can be related to the lower hydrophilicity of its surface. Randomly distributed FN aggregates can be observed in α-PVDF or in the poled samples at very low FN concentration.

Data from the ELISA experiments complement the information obtained from the AFM images. ELISA experiments were performed on samples after adsorption from a 5 $\mu g.mL^{-1}$ FN solution, in which the surface appearance in AFM is that of a homogeneous coating of the PVDF surface (figure 7.4). The exposition of cell adhesion domains is significantly higher in the poled β-PVDF samples with respect to non-poled samples and also with respect to the control. It seems that the presence of a surface distribution of electric charges overcomes the effect of other surface properties. On the one hand, exposition of adhesion ligands in poled samples is higher than in non-poled β-PVDF, that shows the same topography, despite the later having much lower wettability. In the same way, it is higher than in α-PVDF.

MC3T3-E1 pre-osteoblasts were seeded on the substrates previously coated with FN and in a culture medium in absence of serum in order to avoid the modification of the protein layer adsorbed on the substrate. In order to allow long-term culture, medium with FBS was added after initial adhesion. Cells adhere to all the substrates, develop focal adhesions and organize the actin cytoskeleton. The shape of the cells and the average surface covered per cell for the shortest times of cell culture seems to be equal in the four substrates under study. Some of the differences in MC3T3-E1 pre-osteoblasts are just shown after several days of culture and are in accordance with the differences shown in protein adsorption and conformation. The low absorbance in MTS experiments at 3 days culture does not allow us to detect significant differences among the different samples due to the small signal, the absorbance being much lower than in the control surface. Nevertheless, the cell numbers counted from fluorescence microscope images clearly show that cell numbers are higher in the poled β-PVDF samples what correlates with availability of cell adhesion sequences of the adsorbed fibronectin, as determined by ELISA tests. At 7 days culture, the cell number and MTS absorbance in non-poled β-PVDF sample seems still to be smaller than those in the samples with a surface density of electric charges. MC3T3-E1 are highly proliferative cells, reaching confluence in few days in tissue culture polystyrene or in the glass slides used as controls in our experiments. This is shown by the high cell numbers and MTS signal after 3 days culture in the controls in contrast with the slower culture proliferation in all the PVDF substrates. Nevertheless, after relatively short times of culture cells reach confluence in all substrates and at 7 days culture the cell numbers and MTS signal tends to be the same in the α and positively or negatively poled β-PVDF samples and also nearly the same as that of the controls. Only non-poled β-PVDF shows significantly smaller MTS absorbance and small mean cell numbers than the rest culture surfaces at day 7. For longer culture time, this sample shows the same cell number than the others.

These experiments show that the presence of electrical charge on the surface of the piezoelectric material influences the distribution and conformation of adsorbed protein layers on the material surface and in turn on cell adhesion. In this sense, the difference between poled and non-poled states of the electroactive β-phase of PVDF is particularly significant. If this material is deformed by the action of mechanical forces, the piezoelectric effect will produce the variation of the electrical charge density at the interfaces with the biological tissue. Thus, this type of substrate can be used for simultaneous mechanical and electric stimulation of cells in culture.

7.5 Conclusions

It is shown that polarization of a PVDF electroactive crystalline phase to create both a negative or positive electrical charge surface density modifies the conformation of adsorbed FN at the material surface and therefore cell adhesion on the FN-coated substrates. As a consequence, cell numbers on the substrate are significantly higher in poled than in non-poled samples. Differences in FN adsorption between α- and non-poled β-crystalline phases due to different surface topography, wettability and ordering of polymer chain groups are detectable but can be considered less important. In this way, these results open the possibility of developing active substrates for cell culture and tissue engineering, influencing cell response through variation of the surface electrical charge density when a mechanical solicitation is applied.

7.6 References

1. Ratner, B.D., *Biomaterials science : an introduction to materials in medicine*. 2004, Amsterdam; Boston: Elsevier Academic Press.
2. Shard, A.G. and P.E. Tomlins, *Biocompatibility and the efficacy of medical implants.* Regenerative Medicine, 2006. **1**(6): p. 789-800.
3. Klee, D., et al., *Surface modification of poly(vinylidenefluoride) to improve the osteoblast adhesion.* Biomaterials, 2003. **24**(21): p. 3663-3670.
4. Guerra, N.B., et al., *Subtle variations in polymer chemistry modulate substrate stiffness and fibronectin activity.* Soft Matter, 2010. **6**(19): p. 4748-4755.
5. Altankov, G. and T. Groth, *Reorganization of substratum-bound fibronectin on hydrophilic and hydrophobic materials is related to biocompatibility.* Journal of Materials Science: Materials in Medicine, 1994. **5**(9): p. 732-737.
6. Avnur, Z. and B. Geiger, *The removal of extracellular fibronectin from areas of cell-substrate contact.* Cell, 1981. **25**(1): p. 121-132.
7. Altankov, G., et al., *Morphological evidence for a different fibronectin receptor organization and function during fibroblast adhesion on hydrophilic and hydrophobic glass substrata*. Vol. 8. 1997. 721-40.
8. Anselme, K., *Osteoblast adhesion on biomaterials.* Biomaterials, 2000. **21**(7): p. 667-681.
9. Wilson, C.J., et al., *Mediation of biomaterial-cell interactions by adsorbed proteins: A review.* Tissue Engineering, 2005. **11**(1-2): p. 1-18.
10. Whittle, J.D., et al., *Adsorption of vitronectin, collagen and immunoglobulin-G to plasma polymer surfaces by enzyme linked immunosorbent assay (ELISA).* Journal of Materials Chemistry, 2002. **12**(9): p. 2726-2732.
11. Barrias, C.C., et al., *The correlation between the adsorption of adhesive proteins and cell behaviour on hydroxyl-methyl mixed self-assembled monolayers.* Biomaterials, 2009. **30**(3): p. 307-316.
12. Okada, S., et al., *Adhesion of osteoblast-like cells on nanostructured hydroxyapatite.* Acta Biomaterialia, 2010. **6**(2): p. 591-597.
13. Weber, N., et al., *Characterization and in vitro cytocompatibility of piezoelectric electrospun scaffolds.* Acta Biomaterialia, 2010. **6**(9): p. 3550-3556.
14. Lovinger, A.J., *Developments in crystalline polymers*. Vol. vol. 1. 1982, London: Elsevier Applied Science.

15. Nalwa, H.S., *Ferroelectric polymers: chemistry, physics and applications*. Vol. vol. 1. 1995, New York: Marcel Dekker, Inc.

16. Branciforti, M.C., et al., *New technique of processing highly oriented poly(vinylidene fluoride) films exclusively in the beta phase.* Journal of Polymer Science Part B-Polymer Physics, 2007. **45**(19): p. 2793-2801.

17. Sencadas, V., R. Gregorio Filho, and S. Lanceros-Mendez, *Processing and characterization of a novel nonporous poly(vinilidene fluoride) films in the [beta] phase.* Journal of Non-Crystalline Solids, 2006. **352**(21-22): p. 2226-2229.

18. Sencadas, V., R. Gregorio, and S. Lanceros-Mendez, *alpha to beta Phase Transformation and Microestructural Changes of PVDF Films Induced by Uniaxial Stretch.* Journal of Macromolecular Science Part B-Physics, 2009. **48**(3): p. 514-525.

19. Gomes, J. and et al., *Influence of the β-phase content and degree of crystallinity on the piezo- and ferroelectric properties of poly(vinylidene fluoride).* Smart Materials and Structures, 2010. **19**(6): p. 065010.

20. Nunes, J.S., et al., *Relationship between the microstructure and the microscopic piezoelectric response of the alpha- and beta-phases of poly(vinylidene fluoride).* Applied Physics a-Materials Science & Processing, 2009. **95**(3): p. 875-880.

21. Otsu, N., *Threshold selection method from gray-level histograms.* Ieee Transactions on Systems Man and Cybernetics, 1979. **9**(1): p. 62-66.

22. Sigal, G.B., M. Mrksich, and G.M. Whitesides, *Effect of surface wettability on the adsorption of proteins and detergents.* Journal of the American Chemical Society, 1998. **120**(14): p. 3464-3473.

23. Vanwachem, P.B., et al., *Interaction of cultured human-endothelial cells with polymeric surfaces of different wettabilities.* Biomaterials, 1985. **6**(6): p. 403-408.

24. Hernandez, J.C.R., et al., *Substrate chemistry-dependent conformations of single laminin molecules on polymer surfaces are revealed by the phase signal of atomic force microscopy.* Biophysical Journal, 2007. **93**(1): p. 202-207.

25. Bar-Cohen, Y., *Electroactive Polymer (EAP) Actuators as Artificial Muscles - Reality, Potential, and Challenges (2nd Edition)*, SPIE.

26. Roach, P., et al., *Modern biomaterials: a review—bulk properties and implications of surface modifications.* Journal of Materials Science: Materials in Medicine, 2007. **18**(7): p. 1263-1277.

27. Tsapikouni, T.S. and Y.F. Missirlis, *Protein–material interactions: From micro-to-nano scale.* Materials Science and Engineering: B, 2008. **152**(1-3): p. 2-7.

28. Michael, K.E., et al., *Adsorption-Induced Conformational Changes in Fibronectin Due to Interactions with Well-Defined Surface Chemistries.* Langmuir, 2003. **19**(19): p. 8033-8040.

29. Schmidt, D.R., H. Waldeck, and W.J. Kao, *Protein Adsorption to Biomaterials Biological Interactions on Materials Surfaces*, D.A. Puleo and R. Bizios, Editors. 2009, Springer New York. p. 1-18.

30. Comelles, J., et al., *The role of surface energy of technical polymers in serum protein adsorption and MG-63 cells adhesion.* Nanomedicine: nanotechnology, biology, and medicine, 2010. **6**(1): p. 44-51.

31. Garcia, A.J., M.D. Vega, and D. Boettiger, *Modulation of cell proliferation and differentiation through substrate-dependent changes in fibronectin conformation.* Molecular Biology of the Cell, 1999. **10**(3): p. 785-798.

32. Llopis-Hernandez, V., et al., *Role of Surface Chemistry in Protein Remodeling at the Cell-Material Interface.* Plos One, 2011. **6**(5).

33. Salmeron-Sanchez, M., et al., *Role of material-driven fibronectin fibrillogenesis in cell differentiation.* Biomaterials, 2011. **32**(8): p. 2099-2105.

34. Gugutkov, D., et al., *Biological Activity of the Substrate-Induced Fibronectin Network: Insight into the Third Dimension through Electrospun Fibers.* Langmuir, 2009. **25**(18): p. 10893-10900.

8. Enhanced viability of pre-osteoblastic cells by dynamic piezoelectric stimulation

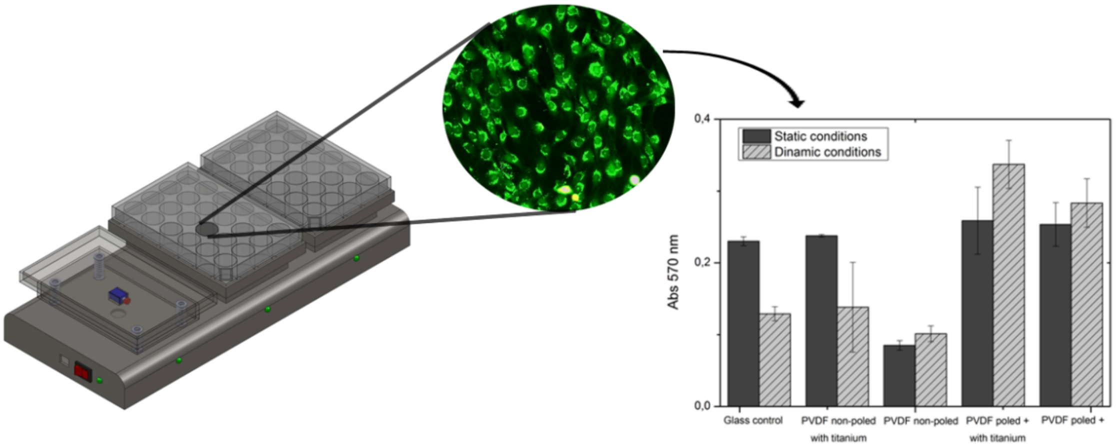

This chapter is based on the following publication: C. Ribeiro, S. Moreira, V. Correia, V. Sencadas, J.G. Rocha, F. M. Gama, J.L. Gómez Ribelles and S. Lanceros-Méndez. *Enhanced viability of pre-osteoblastic cells by dynamic piezoelectric stimulation*. Submitted to Soft Matter.

8.1 Introduction

Cell/biomaterial compatibility and cell response are strongly influenced by the surface properties of the biomaterial, such as surface charge, chemical composition and surface energy [1-2]. In particular, surface charge and therefore electric field have been proved to influence growth and differentiation of some cells types [3-4]. The cell/biomaterial quality interactions influence cell adhesion, migration and proliferation, thus playing a decisive role for tissue engineering applications [2, 5]. Further, the different cells may behave differently on materials, according to surface morphology, hydrophobicity and roughness [1, 5-6]. For instance, Huag *et al.* [5] found that osteoblast (hFOB1.19) and fibroblast (L929) exhibit different responses on surfaces with different morphologies. In general, it can be stated that osteoblastic cells prefer rougher surfaces, whereas fibroblasts, the most common cell type found in connective tissue, favor smoother ones [7-8]. Furthermore, the surface charge influence the cell attachment and behavior [6].

Indeed, it has been shown that electrically charged surfaces can influence cell behavior in different aspects such as growth, adhesion or morphology of different cells types including osteoblast, nervous and cardiac cells [3, 5, 9]. In this respect, piezoelectric materials have the interesting ability to vary surface charge when a mechanical load is applied [10], without the need of an external power source or connection wires, property that can be taken to advantage in novel tissue engineering strategies. Verma *et al.* [11] verified that surface charge is a critical factor for osteoblast adhesion, it was shown that positively charged surfaces promote higher adhesion [12]. Schneider *et al.* [13] observed that charged poly(hydroxyethyl methacrylic) acid promotes higher osteoblast attachment and spreading, and positive charged scaffold supported higher cell attachment and spreading than neutral charges.

Many body tissues react to mechanical and electrical stimulus, thus the use of electroactive films, membranes and scaffolds shows a novel and potentially interesting approach for tissue engineering applications [14]. PVDF is a semi-crystalline and biocompatible polymer with the largest piezoelectric response [15-16], good mechanical properties and excellent electroactive properties such as piezo-, pyro and ferroelectricity [10]. The material can be prepared in the form of films, fibers [17] or porous structures [18], allowing the production of materials with customized microstructure for biomedical applications, among others. Depending on the processing conditions, four different crystalline structures can be obtained, known as α, β, γ and δ, being the β-phase the one with the higher piezoelectric and pyroelectric properties [10, 19]. The semicrystalline nature of PVDF is reflected by the piezoelectric activity at the mesoscale. At mesoscopic scale, the piezoelectric activity of β-PVDF is formed by dispersed nanoregions instead a classical regions [16]. So, the charge distribution is not totally homogeneous on the PVDF film. It has been proven that the charge surface of PVDF influence the cell viability and proliferation, being higher in poled (larger net surface charge) than in non-poled samples [14, 20].

Considering the PVDF suitability, two challenges remain to make possible the exploitation of electrical stimulus for cell culture purposes: evaluation of cell response when a thin metal layer is deposited on top of polymer surface, which is needed in order to get a more homogeneous surface charge and to eventually use the material as *in-body* sensor and/or actuator, and to evaluate the effect under dynamical conditions. In this sense, the aim of present work is to give answer to the aforementioned issues by evaluating the cells cultured directly on the polymer or on the polymer coated with a conductive thin titanium layer. Further, experiments were performed both under static and dynamical conditions. MC3T3-E1 osteoblast where selected for this work, since physiologically these cells are subjected to mechanical solicitations an can therefore be stimulated by the corresponding varying charge density on the surface of the materials, to evaluate cell adhesion, viability and proliferation in an *in vitro* environment.

8.2 Materials and methods

8.2.1 Preparation of PVDF samples

PVDF films were prepared as described previously in [21-22]. Briefly, PVDF (Solef 1010, *Solvay*) was mixed with DMF (20 wt.% PVDF), and films were obtained by spreading the solution on a glass slide than was then kept inside an oven at a controlled temperature of 120 ºC for 60 min, to ensure the solvent removal by evaporation and the isothermal crystallization of PVDF. Then, the sample was melted at 220 ºC for 10 min, removed from the oven and cooled down at room temperature. The polymer obtained by this procedure is predominantly α-PVDF and the transformation into β-phase was achieved by the conventional stretching procedure [15, 22]. Corona discharge was used to obtain the electrical poling of β-PVDF inside a home-made chamber and the piezoelectric response (*d*33) verified with a wide range d_{33}-meter (model 8000, *APC Int Ltd*). The obtained value of the piezoelectric d_{33} coefficient for the poled samples was ~ -32 pC.N^{-1} [15].

A thin titanium layer (approximately 30 nm) was deposited on top of some of the non-poled and "poled +" β-PVDF samples by magnetron sputtering.

For the *in vitro* assays, circular PVDF films with 13 mm diameter were cut from the prepared films and sterilized by immersing several times in 70% ethanol for 30 min. Then, the samples were washed 5 times for 5 min in sterile PBS to eliminate any residual ethanol.

The films used in the present study were non-poled β-PVDF, “poled +” β-PVDF (cell culture on the positively charged side of the material), non-poled β-PVDF with titanium (titanium deposited on the side in which the cell were cultured) and “poled +” β-PVDF with titanium.

8.2.2 Substrate topography and contact angle measurements

The samples were measured using Tapping Mode with a MultiMode connected to a NanoScope III (*Veeco*), with non-contacting silicon (ca. 47-76 kHz, k: 1.2 -6.4 N.m^{-1}) from AppNano. All images (10 µm wide) were fitted to a plane using the 1st degree flatten procedure included in the NanoScope software version 4.43rd8. The surface roughness was calculated as Sq (root mean square from average flat surface) and Sa (average absolute distance from average flat surface).

Contact angle measurements (sessile drop in dynamic mode) were performed at room temperature in a Data Physics OCA20 set up using ultrapure water as test liquid. Water drops (3 µL) were placed onto the surface of the PVDF samples. The contact angles were measured using the software SCA20. Each sample was measured at six different locations and the contact angle was taken as the average obtained for each sample.

8.2.3 Cell culture

MC3T3-E1 osteoblasts (Riken cell bank, Japan) were cultivated in DMEM containing 1 g.L^{-1} glucose (*Gibco*) supplemented with 10% FBS (*Biochrom*) and 1% P/S, at 37 ºC in a 95% humidified air containing 5% CO_2. The medium was changed every 3 days.

Circular PVDF samples and glass covers used as control were placed in a 24-well tissue culture polystyrene plate and 0.5 mL of cell suspension (3×10^4 cells.mL^{-1}) was added to each well and incubated at 37 ºC. Also, after 3 h of static culture, part of the cell-cultured membranes was transferred onto a home-made bioreactor system.

A dynamic culture was performed with MC-3T3 E1 osteoblast on the same samples on a home-made bioreactor system with mechanical stimulation by placing the culture plate on a vertical vibration module at frequency of 1 Hz with amplitude of ~1 mm (figure 8.1).

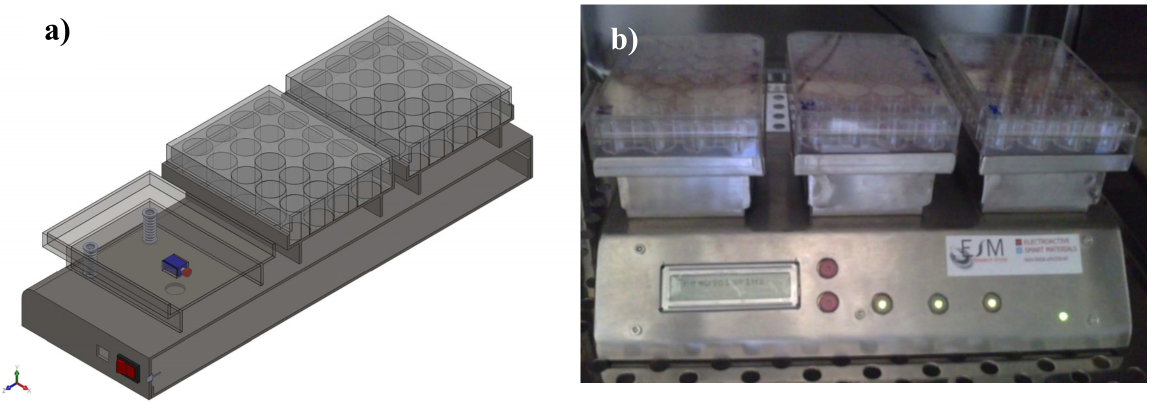

Figure 8.1 – Home-made bioreactor system used for dynamic cell culture at 1 Hz: a) schematic system and b) system photography.

8.2.4 Cell viability and proliferation

The viability of MC-3T3 E1 osteoblasts on the different PVDF films under static conditions was analyzed by Live/Dead Viability/Citotoxicity kit (Invitrogen, CA), by observation in a fluorescence microscope (Olympus BX51 Microscope).

The evaluation of the cells viability/proliferation was also carried out by MTT assay. The MTT assay measures the cell's mitochondrial activity, which reflects the viable cell number, and was carried out after 1, 3 and 5 days for the experiments performed under static conditions and dynamic conditions. At each time point, the cell/films were transferred to new wells and fresh medium containing MTT was added. After 3 h of incubation, the MTT crystals were dissolved and optical density was measured at 570 nm.

8.2.5 Statistical analysis

All quantitative results were obtained from triplicate samples. The results were expressed as mean ± standard deviation. Statistical differences were determined by ANOVA using F-test for the evaluation of different groups. P values < 0.05 were considered to be statically significant.

8.3 Results

8.3.1 Surface topography

The phase content, morphology and electroactivity of PVDF films depend on the processing conditions [16]. The topography of the β-PVDF obtained after stretching from α-PVDF is characterized by an oriented microfibillar microstructure. The poling process of PVDF films induce no significant differences on morphology [22] and sample topography, which maintains the same mean roughness [16]. The AFM analysis of the local piezoresponse data of the non-poled β-PVDF and poled samples show [16] that a clear piezoresponse signal exists in both samples, being therefore the domain contrast more pronounced in the poled ones.

The AFM pictures of β-PVDF samples with and without titanium are displayed in figure 8.2 keeping the same scale and scan size for comparison. The deposition of a titanium thin layer on PVDF films increases the mean roughness (rms) of the samples, as can be observed on figure 8.2, from 20,79 nm and 24,60 nm for the non-coated samples (non-poled β-PVDF, “poled +” β-PVDF, respectively) to 29,72 nm and 26,06 nm, in average, for the coated ones (non-poled β-PVDF with titanium and “poled +” β-PVDF with titanium, respectively). Considering the titanium coated films, it can be observed that the mean roughness is lower on "poled +" β-PVDF films (26,06 nm vs 29,72 nm, for the poled and non-poled ones, respectively). This is explained by the fact that the positive polymer charge promotes the titanium adhesion during the first deposition steps, leading to a more homogeneous and therefore less rough surface.

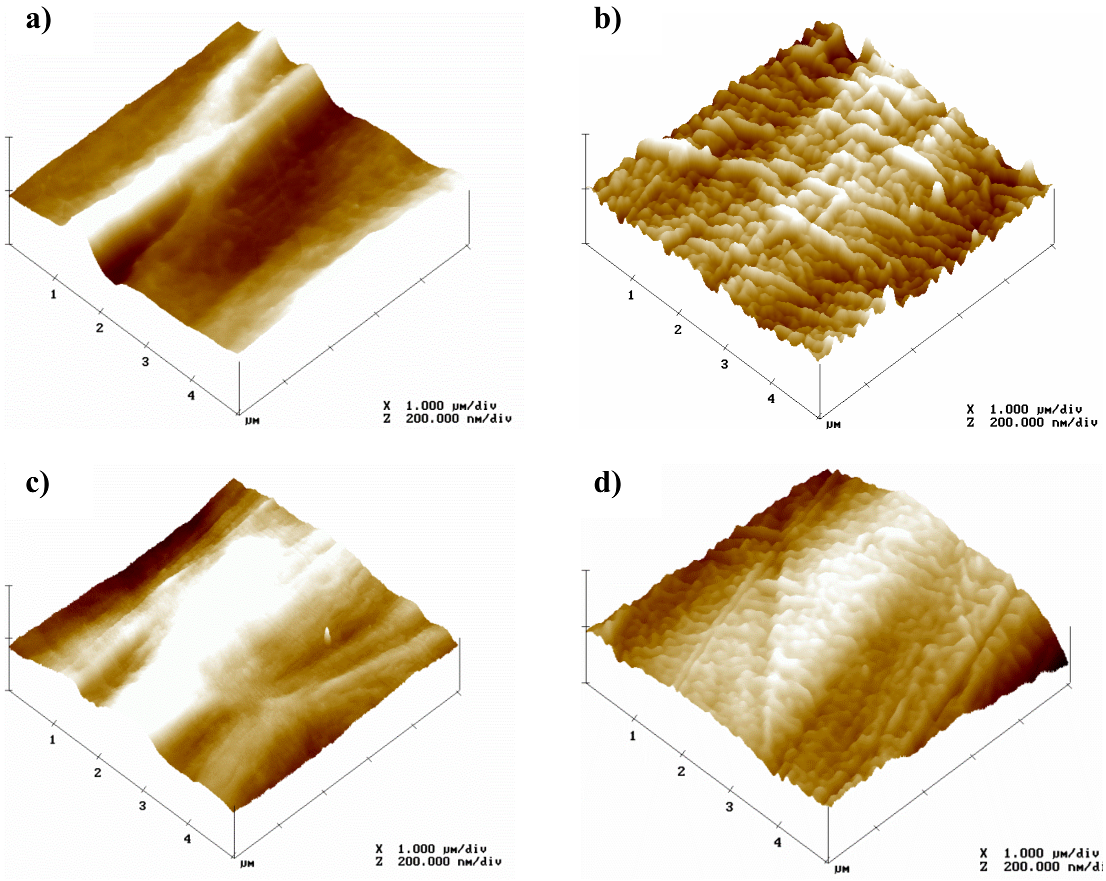

Figure 8.2 – AFM pictures recorded in a 5×5 μm area of different PVDF sample: a) non-poled; b) non-poled with titanium; c) poled + and d) poled + with titanium.

8.3.2 Contact angle measurements

The surface energy, which is intimately related to wettability, is one of the key factors governing biological interaction with a given material [23-25]. It is usually reported that biomaterial surfaces with moderate hydrophilicity show improved cell growth and higher biocompatibility [23].

The comparative wettability of the different PVDF samples was assessed by static contact angle measurements as shown in figure 8.3. It is observed that the contact angles of the different PVDF films are all below 90º and the "poled +" β-PVDF film is the most hydrophilic one, with a contact angle around 60º. When the β-PVDF films are poled by corona treatment their surface wettability increases, as shown in figure 8.3, due to the variations in the surface energy induced by the increased surface charge in the poled samples [26].

Comparing β-PVDF film with and without titanium, it is observed that surface wettability decreases with the titanium deposition. This can be ascribed to the roughness increase with the deposition of the thin titanium layer (figure 8.2): the roughness effect overshadows the influence of interfacial interactions and the contact angle value increases with increasing surface roughness [23, 27-28].

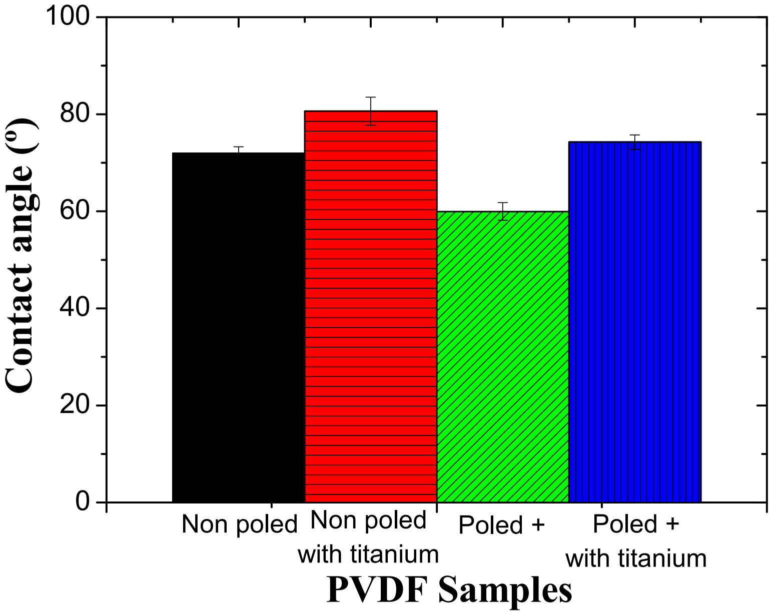

Figure 8.3 – Contact angle of the different PVDF films. Values are mean ± SD.

8.3.3 Cell viability and proliferation

The viability of MC-3T3-E1 osteoblasts was investigated by LIVE/DEAD assay, confirming the integrity of the cell membrane in all cases. Figure 8.4 shows that virtually no dead MC-3T3-E1 osteoblasts after observed 3 days after cell seeding on PVDF films.

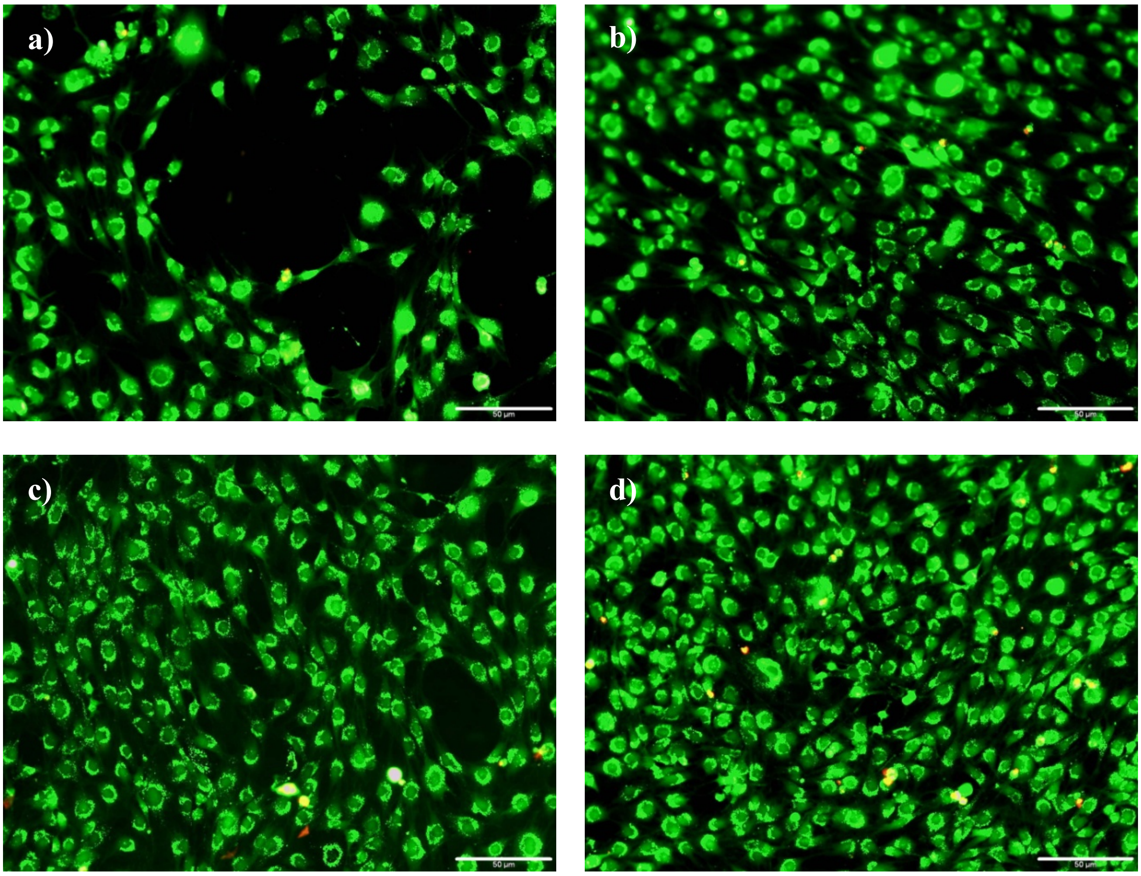

Figure 8.4 – LIVE/DEAD staining of MC-3T3-E1 osteoblasts a) PVDF non-poled and b) PVDF non-poled with titanium; c) PVDF poled + and d) PVDF poled + with titanium after cell culture for 3 days. The scale bar (50 µm) is valid for all the images.

The proliferation of the attached cells on the different PVDF films and TPCS throughout 5 days of culture under static and dynamic conditions is shown in figure 8.5. The absorbance (Abs) was measured at 570 nm for all the samples at each time.

At day 1, the cell proliferation on PVDF under static conditions was similar to the TPCS except for "poled +" β-PVDF with titanium that was higher. Comparing PVDF samples, non-poled β-PVDF shows the lowest cell proliferation and osteoblasts seem to prefer titanium surfaces. At day 3, "poled +" β-PVDF with titanium presents a higher cell proliferation.

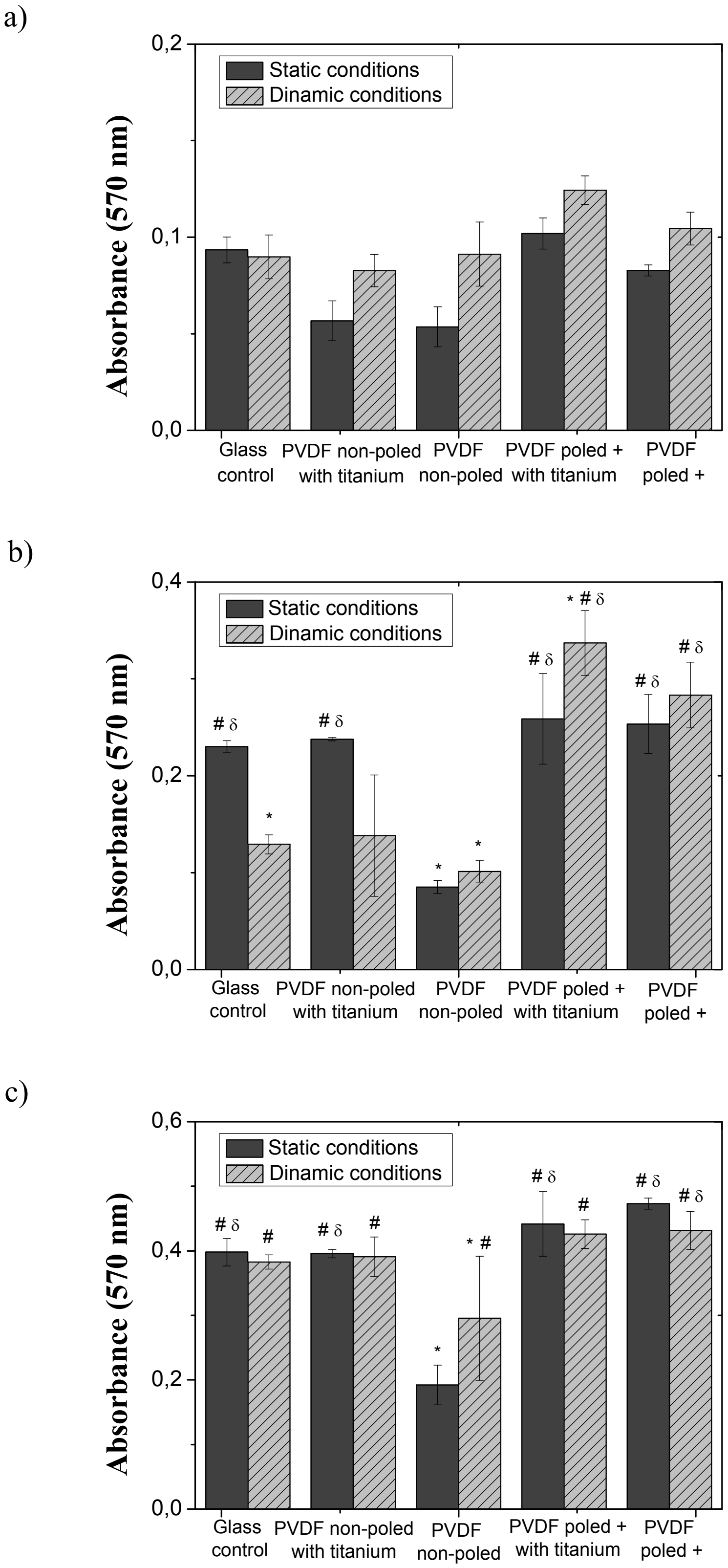

Figure 8.5 – MTT results from proliferation assays of MC-3T3 osteoblast seeded on different PVDF samples and on the control surface under static and dynamic conditions after a) 1 day, b) 3 days and c) 5 days. * $p \leq 0{,}05$ vs Glass control under static conditions; $^{\#}$ $p \leq 0{,}05$ vs PVDF non-poled under static conditions; $^{\delta}$ $p \leq 0{,}05$ vs PVDF non-poled under dynamic conditions.

The influence of a dynamic culture on cell proliferation in PVDF films was also studied (figure 8.5). It is observed than the dynamic culture improves the cell viability on the piezoelectric PVDF samples both with and without titanium coating.

After 5 days, both control TCPS and non-poled β-PVDF with titanium layer samples under static and dynamic culture yield the same results.

8.4 Discussion

Previous studies on the osteoblast-PVDF interactions showed that can be used clinically for promoting tissue growth [13]. The different types of β-PVDF films affect in a different way the adhesion and proliferation of osteoblasts, as the cell response to different surfaces primarily depend on the cell type [5]. Further, as mentioned before, surface topography [5, 29-30] and surface charge have deep influence in cell adhesion and proliferation [4, 11]. In particular, it has been shown that positive charged surfaces supported higher cell attachment than neutral ones [12] and induce cell adhesion and proliferation in a different way depending on the cell types [5, 13]. It was also observed that positively charged β-PVDF films promote higher osteoblast adhesion and proliferation. Thus, the combination of surface roughness and charge is a key point for promoting cell adhesion and proliferation on material surface.

The goal of this work was the assessment that dynamic mechanical stimulus of a flat surface with an electric charge distribution, and consequent effect on the response of pre-osteoblastic cells in monolayer culture. Electroactive β-PVDF has an all-trans planar "zig-zag" configuration and the unitary cell has a permanent dipolar moment. In non-poled polymer samples (samples non-poled β-PVDF or non-poled β-PVDF with titanium), dipoles are randomly oriented in the material and no net charge appear at the surface. In these samples, dynamic mechanical solicitations have no effect on electric charge distribution. Nevertheless, the same material present permanent surface distribution of positive charges once electrically poled (samples "poled +" β-PVDF or "poled +" β-PVDF with titanium), since polymer dipoles during the electrical poling process rotate and align in the direction of the applied electrical field, acquiring a net orientation in the space. When the polymer chains of these samples are dynamically deformed, the net surface charge oscillates with same frequency than the mechanical stimulus.

Regarding static and dynamic conditions, it is possible to observe than cell proliferation on "poled +" β-PVDF over 3 days is higher on dynamic conditions than on static conditions, suggesting that the mechanical stimulus improve the osteoblast growth. It is notice that this fact is not verified in the non-poled samples and therefore the observed effect is to be ascribed to the varying charge density due to the mechanical stimulation. These results suggest that surface charge is a relevant parameter to be considered in the design of proper scaffolds and membranes for specific tissue engineering applications, and piezoelectric materials may provide the necessary electrical stimulus for cell growth, especially under a mechanically stimulus environment.

Assessment of the effect of this dynamic electric stimulation is demonstrated by the higher proliferation observed in cell cultured on "poled +" β-PVDF under dynamic conditions than in static wells. Further, this is also proven by the fact that there is no significant difference (or even the opposite effect is found) between cells cultured on non-poled β-PVDF in static and dynamic conditions (figure 8.5), where the surface charge variations should be negligible. So, the effect of dynamic stimulation is not due to mechanical action itself but to the electrical stimulation induced by piezoelectric effect in the poled electroactive PVDF substrate. It is worth note that results corresponding to first days of culture must be considered since proliferation rate of these cells is high and culture reach confluence in short culture time (in just five days in poled PVDF substrates), thus, proliferation tends to be similar in all membranes and in all conditions after 5 days of growth. An interesting exception is non-coated and non-poled β-PVDF substrates in which proliferation is clearly slower than to the ones observed for the control samples, as seen in the fluorescence images like those shown in figure 8.4 and in MTT measurements (figure 8.5). This feature was already shown in our previous investigation [14] in which it was shown the significant difference between fibronectin adsorption on poled and non-poled substrates and significantly smaller cell numbers in non-poled β-PVDF with respect to both negatively or positively charged PVDF surfaces.

Titanium coated samples allows reaching the same conclusion. Titanium layer has a positive effect in poled samples which is significant in the first day although diminishes in longer culture periods. In the case of non-poled samples proliferation of the titanium coated samples, non-poled β-PVDF with titanium samples is like that of control TCPS wells, thus clearly improving proliferation with respect to non-coated samples. In the case of poled samples titanium layer increases roughness but also increases hydrophobicity, two factors that are expected to affect in opposite direction cell proliferation. But certainly the main effect of titanium coating in these samples is the charge surface distribution improvement.

8.5 Conclusions

Piezoelectric poly(vinylidene fluoride) has been studied as a suitable material for tissue engineering applications due to its piezoelectric effect. In order to isolate the piezoelectric effect on cell response, poled and non-poled material, as well as material coated with a thin titanium layer to get a more homogeneous charge distribution, has been tested in osteoblast under static and dynamic conditions. The polarization and titanium layer deposition modifies mean roughness of PVDF films surface and therefore cell adhesion and proliferation on the samples. Osteoblast adhesion and proliferation is different depending on the samples, being the first more influenced by the piezoelectric material. The positively charge of β-PVDF promotes higher adhesion and proliferation on osteoblast. Dynamic culture with MC3T3-E1 cells showed higher cell proliferation on "poled +" β-PVDF. In this way, these results demonstrated that varying surface electrical charge when a mechanical solicitation is applied influences cell response and confirms the electroactive polymers potential for cell culture and tissue engineering.

8.6 References

1. Anselme, K., *Osteoblast adhesion on biomaterials.* Biomaterials, 2000. **21**(7): p. 667-681.

2. Chen, Y., et al., *Morphology and adhesion of mesenchymal stem cells on PLLA, apatite and apatite/collagen surfaces.* Journal of Materials Science-Materials in Medicine, 2008. **19**(7): p. 2563-2567.

3. Lee, Y.-S. and T. Arinzeh, *The Influence of Piezoelectric Scaffolds on Neural Differentiation of Human Neural Stem/Progenitor Cells*. 2012.

4. Syed, T. and C. Royal Society of. *Biological interactions with surface charge in biomaterials*. 2012; Available from: http://dx.doi.org/10.1039/9781849733366.

5. Huag, H.-S., et al., *Formation of microporous poly(hydroxybutyric acid) membranes for culture of osteoblast and fibroblast.* Polymers for Advanced Technologies, 2009. **20**(12): p. 1082-1090.

6. Wang, H.-I.C.a.Y., *Cell Responses to Surface and Architecture of Tissue Engineering Scaffolds*, in *Regenerative Medicine and Tissue Engineering - Cells and Biomaterials*, D. Eberli, Editor. 2011, InTech.

7. Kunzler, T.P., et al., *Systematic study of osteoblast and fibroblast response to roughness by means of surface-morphology gradients.* Biomaterials, 2007. **28**(13): p. 2175-2182.

8. Kroeze, R.J., et al., *Biodegradable Polymers in Bone Tissue Engineering.* Materials, 2009. **2**(3): p. 833-856.

9. Weber, N., et al., *Characterization and in vitro cytocompatibility of piezoelectric electrospun scaffolds.* Acta Biomaterialia, 2010. **6**(9): p. 3550-3556.

10. Lovinger, A.J., *Developments in crystalline polymers*. Vol. vol. 1. 1982, London: Elsevier Applied Science.

11. Verma, D., K.S. Katti, and D.R. Katti, *Osteoblast adhesion, proliferation and growth on polyelectrolyte complex-hydroxyapatite nanocomposites.* Philosophical Transactions of the Royal Society a-Mathematical Physical and Engineering Sciences, 2010. **368**(1917): p. 2083-2097.

12. Amaral, I.F., et al., *Attachment, spreading and short-term proliferation of human osteoblastic cells cultured on chitosan films with different degrees of acetylation.* Journal of Biomaterials Science-Polymer Edition, 2007. **18**(4): p. 469-485.

13. Schneider, G.B., et al., *The effect of hydrogel charge density on cell attachment.* Biomaterials, 2004. **25**(15): p. 3023-3028.

14. Ribeiro, C., et al., *Fibronectin adsorption and cell response on electroactive poly(vinylidene fluoride) films.* Biomedical Materials, 2012. **7**(3): p. 035004.

15. Gomes, J. and et al., *Influence of the β-phase content and degree of crystallinity on the piezo- and ferroelectric properties of poly(vinylidene fluoride).* Smart Materials and Structures, 2010. **19**(6): p. 065010.

16. Nunes, J.S., et al., *Relationship between the microstructure and the microscopic piezoelectric response of the alpha- and beta-phases of poly(vinylidene fluoride).* Applied Physics a-Materials Science & Processing, 2009. **95**(3): p. 875-880.

17. Ribeiro, C., et al., *Influence of Processing Conditions on Polymorphism and Nanofiber Morphology of Electroactive Poly(vinylidene fluoride) Electrospun Membranes.* Soft Materials, 2010. **8**(3): p. 274-287.

18. California, A., et al., *Tailoring porous structure of ferroelectric poly(vinylidene fluoride-trifluoroethylene) by controlling solvent/polymer ratio and solvent evaporation rate.* European Polymer Journal, 2011. **47**(12): p. 2442-2450.

19. Nalwa, H.S., *Ferroelectric polymers: chemistry, physics and applications*. Vol. vol. 1. 1995, New York: Marcel Dekker, Inc.

20. Rodrigues, M.T., et al., *beta-PVDF Membranes Induce Cellular Proliferation and Differentiation in Static and Dynamic Conditions*, in *Advanced Materials Forum Iv*, A.T. Marques, et al., Editors. 2008, Trans Tech Publications Ltd: Stafa-Zurich. p. 72-76.

21. Branciforti, M.C., et al., *New technique of processing highly oriented poly(vinylidene fluoride) films exclusively in the beta phase.* Journal of Polymer Science Part B-Polymer Physics, 2007. **45**(19): p. 2793-2801.

22. Sencadas, V., R. Gregorio, and S. Lanceros-Mendez, *alpha to beta Phase Transformation and Microestructural Changes of PVDF Films Induced by Uniaxial Stretch.* Journal of Macromolecular Science Part B-Physics, 2009. **48**(3): p. 514-525.

23. Rosales-Leal, J.I., et al., *Effect of roughness, wettability and morphology of engineered titanium surfaces on osteoblast-like cell adhesion.* Colloids and Surfaces a-Physicochemical and Engineering Aspects, 2010. **365**(1-3): p. 222-229.

24. Sigal, G.B., M. Mrksich, and G.M. Whitesides, *Effect of surface wettability on the adsorption of proteins and detergents.* Journal of the American Chemical Society, 1998. **120**(14): p. 3464-3473.

25. Vanwachem, P.B., et al., *Interaction of cultured human-endothelial cells with polymeric surfaces of different wettabilities.* Biomaterials, 1985. **6**(6): p. 403-408.

26. Bodhak, S., S. Bose, and A. Bandyopadhyay, *Role of surface charge and wettability on early stage mineralization and bone cell–materials interactions of polarized hydroxyapatite.* Acta Biomaterialia, 2009. **5**(6): p. 2178-2188.

27. Wenzel, R.N., *Resistance of solid surfaces to wetting by water.* Industrial & Engineering Chemistry, 1936. **28**(8): p. 988-994.

28. Marshall, S.J., et al., *A review of adhesion science.* Dental Materials, 2010. **26**(2): p. E11-E16.

29. Wan, Y.Q., et al., *Adhesion and proliferation of OCT-1 osteoblast-like cells on micro- and nano-scale topography structured poly(L-lactide).* Biomaterials, 2005. **26**(21): p. 4453-4459.

30. Lord, M.S., M. Foss, and F. Besenbacher, *Influence of nanoscale surface topography on protein adsorption and cellular response.* Nano Today, 2010. **5**(1): p. 66-78.

9. Conclusions and future work

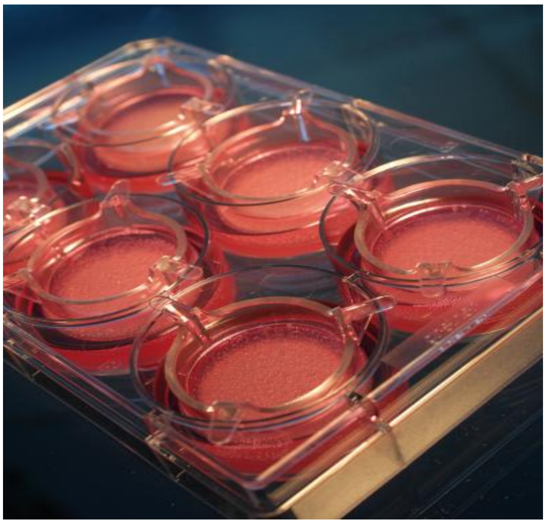

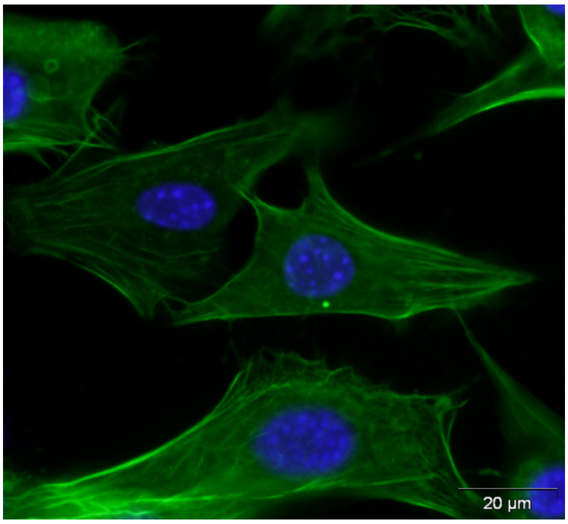

9.1 Conclusions

Attempts to find tissue engineering solutions to treat injuries and diseases have made necessary the development of polymers that meet a number of demanding requirements in order to be part of those solutions.

Most of the polymers studied for cell culture and tissue engineering applications are used in substrates liabilities. But, since it is well known that bone, cardiac and nervous cells react to electrical stimuli, the necessity of active substrates has emerged. In this way, electroactive polymers, particularly piezoelectric polymers, appear as interesting materials as they can produce electrical response when are mechanically deformed and vice-versa.

Thus, two piezoelectric polymers, PVDF and PLLA, were selected with this propose. PVDF was used due to its high piezoelectric response and the PLLA due to its biodegradability.

The processing of PVDF and PLLA in the form of films and fibers as well as their characterization were achieved. PVDF and PLLA electrospun fiber membranes morphology was controlled by changing process parameters such as applied voltage, feed rate and collector system. Random nanofibers were obtained on a plate collector, while oriented nanofibers were collected using a rotating drum. The piezoelectric response of both polymers has been proven and characterized by PFM with the study of local properties of individual electrospun fibers. In this way, these results have opened the possibility of these electrospun fibers be used in bio-electroactive applications.

With respect to the PLLA fibers, the optimum fiber alignment was observed for a rotation speed of 1000 rpm. It has been shown that the electrospinning processing conditions had no effect in the PLLA polymer phase and that the PLLA as electrospun membranes are nearly amorphous. Additionally, with annealing treatment, crystals rapidly grew and the crystallinity degree of electrospun fibers was tailored between 0%, i.e. amorphous fibers, and 50%. The PLLA fiber diameter obtained was around micrometers but this diameter can be reduced by the introduction of PEO polymer during the electrospinning process and further PEO removal. In this way, it was possible to obtain electrospun membranes with few hundreds of nanometers.

Concerning PVDF fibers, the optimum fiber alignment was also observed for a rotation speed of 1000 rpm. The different combination of processing parameters showed strong influence on the phase present in the fiber mats and therefore, its electroactivity. The obtained β-phase fraction ranged between 50% and 85%. Further, it was possible obtain fiber diameters with a few hundreds of nanometers to micrometers, the crystalline fraction depending only slightly on the electrospinning conditions.

PVDF is a non biodegradable polymer while PLLA can be degraded. So, the PLLA degradation was studied in contact to PBS up to 20 weeks and the main effect on the samples was only a slight decrease in the sample weight. So, the polymer is stable for applications up to 20 weeks.

After the processing and characterization of PVDF and PLLA membranes was achieved, the biological response was addressed. Human chondrocytes and MC3T3-E1 osteoblast were used in PLLA and PVDF membranes, respectively. This cell lines were chosen due to the fact that can react to electrical stimulus. In both cases, the surface properties of the polymers showed influence on the cell adhesion and proliferation.

In the case of PLLA electrospun membranes, adhesion, proliferation and differentiation of human chondrocytes was studied in aligned and non-aligned amorphous and semi-crystalline electrospun mats. It was verified that the proliferation of human chondrocytes in the monolayer substrates is similar on aligned and non-aligned amorphous mats. It was observed that proliferation was lower in the more crystalline samples than in the amorphous ones and the crystallization of aligned mats showed nearly suppresses proliferation. However, in the case of the differentiation rate, it was observed significant differences between non-aligned and aligned mats, being higher on the non-aligned ones with no significant differences between amorphous and crystalline mats.

The influence of PVDF films on biological response was also investigated. First, the FN conformation on poled and non-poled β-PVDF films was studied and was found that poled PVDF films adsorbed higher FN amounts than non-poled samples. In this way, it was verified that electrical surface charge density has modified the conformation of adsorbed FN on the substrate surface and cell adhesion on the FN-coated samples. As a consequence, cell number in the substrate was significantly higher in poled than in non-poled films. The osteoblast adhesion and proliferation under static and dynamic conditions was also studied in order to evaluate the piezoelectric effect on cell response. The osteoblast adhesion and proliferation was found to be different depending on the poling state of the samples and it was possible to conclude that poled β-PVDF promotes higher osteoblast adhesion and proliferation as well as that dynamic culture showed higher cell proliferation on "poled +" β-PVDF.

In this way, these results confirm the viability of the materials for the development of active substrates for cell culture and tissue engineering applications.

9.2 Future work

A number of valuable results were obtained in this research project which will be of utility for future investigations.

It was found that piezoelectric polymers materials were promising candidates regarding tissue engineering applications. However, it is important to continue the research on these polymer based piezoelectric materials. The effect of morphology (aligned and non aligned fibers) and polarization in the biological response was investigated separately to better understand each effect. However, in the future those effects should be properly combined in order optimize the biological response.

Following the same approaches, other morphologies than fibers, such as three dimensional scaffolds, microspheres and/or fiber suspensions should be developed in order to tailor biological response. Further, hybrid membranes and scaffolds can be further produced in which the piezoelectric polymers are combined with specific bioactive materials or drugs to target specific application goals.

Two cells types were used in this work. But, as it is know, cell types respond differently to different material surface, so other cell types should be studied in order to determine in which of them the electro-mechanical stimulus can be better taken to advantage for tissue regeneration. In particular, the study of how dynamic electro- mechanical stimuli affect mesenchymal stem cell differentiation seems to be an interesting challenge.

Each developed and optimized material should be also evaluated *in vivo* through the use of animal models. Essential parameters such as inflammation, cellular proliferation and differentiation must be investigated.